

**Numerical Study of Emission Control of Urban and Rural Kitchens for Healthy
Environment**

by

Md. Hamidur Rahman

A Thesis Submitted to the Board of Examiners in Partial Fulfillment of the
Requirements for the Degree of

DOCTOR OF PHILOSOPHY IN MECHANICAL ENGINEERING



**Department of Mechanical and Chemical Engineering
Islamic University of Technology (IUT), OIC
Gazipur, Bangladesh**

March 2016

The thesis titled *Numerical Study of Emission Control of Urban and Rural Kitchens for Healthy Environment* Submitted by Md. Hamidur Rahman St. No. 091701 of Academic Year 2015-2016 has been found as satisfactory and accepted as partial fulfillment of the requirement for the degree of Doctor of Philosophy on Mechanical Engineering.

Board of Examiners:

1.

Prof. Dr. A. K. M. Sadrul Islam
Professor, Dept. of MCE,
IUT, Board Bazar, Gazipur.

Chairman
(Supervisor)

2.

Prof. Dr. A. K. M. Sadrul Islam
Head, Dept. of MCE,
IUT, Board Bazar, Gazipur.

Member
(Ex-officio)

3.

Prof. Dr. M. Imtiaz Hussain
Vice-Chancellor,
IUT, Board Bazar, Gazipur.

Member

4.

Prof. Dr. Mohammad Ali
Professor & Head, Dept. of ME,
BUET, Dhaka.

Member

5.

Prof. Dr. Md. Anayet Ullah Patwari
Professor, Dept. of MCE,
IUT, Board Bazar, Gazipur.

Member

6.

Dr. R. G. M. Hasan
Senior Lecturer, Dept. of Mechanical and
Constructional Engg.,
Northumbria University, Newcastle, UK

Member
(External)

Declaration of Candidate

It is hereby declared that this thesis or any part of it has not been submitted elsewhere for the award of any Degree or Diploma.

Prof. Dr. A. K. M. Sadrul Islam

Head, Mechanical and Chemical Engineering
Islamic University of Technology (IUT), OIC
Gazipur.
Date: 28 March 2016

Md. Hamidur Rahman

Student No.: 091701
Academic Year: 2010-2016
Date: 28 March 2016

Dedication

To all my well-wishers who came forward and supported me and my family to overcome the crucial moment of my life while my lovely son Tahmid Rahman Jarif had been diagnosed Leukemia. I am sincerely grateful to my entire IUTians fellow for their continued support in this regard. Especially I cannot but to mention the name of Mr. Habibullah Amin Chowdhury, Dr. Shahadat Hussain, Mr. Saif Kabir, Mr. Abidur Rahman, Dr. Atiqur Rahman, Dr. Mohammed Shahidur Rahman and above all, my parents who have been so kind to me and generous from all aspects. There are many other dearest people who deserve special thanks in this regard.

Table of Contents

Declaration of Candidate	3
Dedication	4
List of Figures	8
List of Tables	13
Nomenclature	14
Acknowledgment	17
Abstract	18
1. Introduction	20
1.1.Thesis Organisation:.....	23
2. Literature Review	24
2.1.Urban Indoor Air Quality:.....	24
2.2.Rural Indoor Air Quality:.....	28
2.3.Objectives And Motivations	34
3. Problem Formulation and Methodology	36
3.1.Typical Model of a Urban Kitchen	37
3.2.Typical Model of a Rural Kitchen	37
3.3.Experimental Set-up.....	39
3.3.1.For Urban Kitchen.....	39
3.3.2.For Rural Kitchen.....	40
3.3.3.Temperature Measurement Instrument, Calibration and Uncertainty...	41
3.3.4.Emissions Instrument and Uncertainty	43
3.4.Numerical Method	47
3.4.1.Transport Equations	48
3.4.2.Turbulence Model	50
3.4.2.1.The k-epsilon Model	50
3.4.2.2.Buoyancy Turbulence	51

3.4.3.Combustion Model.....	52
3.4.3.1.Species Transport Equation for Source.....	53
3.5.Grid Independence Test	54
4. Study of Urban Kitchen	56
4.1.Measurement of Temperature and Emission.....	56
4.2.Numerical study of Urban Kitchen	58
4.2.1.Code Validation	62
4.2.2.Velocity and Temperature Field.....	64
4.2.3.Kitchen Indoor Emission.....	72
4.2.3.1.Without Ventilation.....	72
4.2.3.2.Natural Ventilation.....	77
4.2.3.3.Forced Ventilation without Hood	80
4.2.3.4.Forced Ventilation with Hood.....	83
4.3.Summary	91
5. Study of Rural Kitchen	94
5.1.Estimation of Source Concentration	95
5.1.1.CO at source:.....	96
5.1.2.CO ₂ at source:	98
5.1.3.PM at source:	99
5.2.Measurement of Temperature and Emission.....	101
5.3.Numerical study of Rural Kitchen	108
5.3.1.Numerical grid and code validation.....	110
5.3.2.Without Ventilation.....	112
5.3.3.With Natural Ventilation.....	116
5.3.4.Natural Ventilation with Hood.....	121
5.4.Summary	125

6. Conclusions and Future Recommendations.....	128
References	131
Appendix I	136
Arduino Microcontroller and Circuit Diagram.....	136
Appendix II.....	137
Uncertainty analysis	137
Appendix III	139
Calibration Certificate	139
Appendix IV.....	141
Simulation Process Flow Diagram	141
Appendix V	142
Typical Analysis of Biomass	142
Appendix VI.....	143
List of Published Papers	143

N.B. A CD containing the whole thesis is provided in the pocket of the back cover.

List of Figures

Fig. 1.1: Flow diagram of Urban and Rural kitchen.	20
Fig. 3.1: Computational model with two burners, a) with front wall vent, b) with commercial hood (c) typical kitchen layout showing plane A and plane B.	37
Fig. 3.2: Computational domain of the rural kitchen.	38
Fig. 3.3: Experimental setup for typical (a) urban kitchen 1 and (b) urban kitchen 2, and (c) schematic diagram for temperature and CO ₂ measurement.	40
Fig. 3.4: (a) A typical rural kitchen at Tangail with (b) a conventional soil stove and (c) schematic diagram for CO, CO ₂ , PM and Temperature measurement.	40
Fig. 3.5: (a) Temperature sensor (b) Calibration test of laboratory built multiprobe temperature device.	42
Fig. 3.6: (a) CO ₂ meter (Brand EXTECH, USA) (b) CO meter (Brand EXTECH, USA) (c) PM meter (Brand TSI, USA).	43
Fig. 3.7: Pressure distributions for grid independency test (a) for domain without hood and (b) for domain with hood.	54
Fig. 3.8: Temperature distributions for grid independency test at (a) for domain without hood and (b) for domain with hood.	55
Fig. 3.9: Grid independence test for the rural kitchen model (a) temperature profile b) velocity profile.	55
Fig. 4.1: Temperature profiles at five locations on a vertical line passing the breathing point (a) for urban kitchen 1 and (b) for rural kitchen 2.	57
Fig. 4.2: CO ₂ profile at the breathing point for urban kitchen 1.	57
Fig. 4.3: CO ₂ profile at the breathing point urban kitchen 2.	58
Fig. 4.4: Computational domain with boundary for (a) typical vent (Case 1, Case 2 and Case 3), (b) kitchen hood (Case 4), (c) front vent (Case 5) and (d) base vent (Case 6).	60
Fig. 4.5: Computational grid of the model at (a) plain A (b) plain B.	61
Fig. 4.6: Computational grid of the model (a) at plain A (b) isometric.	62
Fig. 4.7: Computational grids of two burners.	62
Fig. 4.8: Comparison between numerical and experiment a) axial velocity distributions and b) v-velocity distributions.	63

Fig. 4.9: Locations of the investigated plane and lines.	65
Fig. 4.10: 3-D velocity distributions at the investigated plane of a) Case 1, b) Case 2, c) Case 3 and d) Case 4.	66
Fig. 4.11: a) Wall Temperature distributions, and b) velocity of flow close to wall surface, for Case 1.	67
Fig. 4.12: Temperature distributions at plane 1 of a) Case 1 and b) Case 3.	68
Fig. 4.13: (a) Wall Temperature distributions for Case 4, and (b) Temperature at the plane for Case 4 and (c) Wall Temperature distributions for Case 1.	69
Fig. 4.14: U-velocity distributions along Line 1.	70
Fig. 4.15: V-velocity distributions along Line 2.	70
Fig. 4.16: Temperature distributions along Line 1.	71
Fig. 4.17: Temperature distributions along Line 2.	72
Fig. 4.18: Locations of the investigated plane and lines. (all dimension are in m).	73
Fig. 4.19: Locations of the investigated plane and lines.	73
Fig. 4.20: Temperature variations at X-Y & Z breath lines for Case 1 (closed vent).	74
Fig. 4.21: CO ₂ concentration contour at YZ-breath plane. Close vent (Case1).	75
Fig. 4.22: CO ₂ variations at X-Y & Z breath lines for Case 1 (closed vent).	76
Fig. 4.23: Temperature variations at X-Y & Z breath lines for Case 2 (natural ventilation).	77
Fig. 4.24: CO ₂ concentration contour at YZ-breath plane. Open vent (Case 2).	78
Fig. 4.25: CO ₂ variations at X-Y & Z breath lines for Case 2 (natural ventilation).	79
Fig. 4.26: Temperature variations at X-Y & Z breath lines for Case 3 (forced ventilation without hood).	80
Fig. 4.27: CO ₂ concentration contour at Y-breath plane. 1.5 m/s vent (Case 3).	81
Fig. 4.28: CO ₂ variations at X-Y & Z breath lines for Case 3 (forced ventilation without hood).	82
Fig. 4.29: Temperature variations at X-Y & Z breath lines for Case 4 (forced ventilation with hood).	83
Fig. 4.30: CO ₂ concentration contour at Y-breath plane. 1.5 m/s with hood (Case 4).	84
Fig. 4.31: CO ₂ variations at X-Y & Z breath lines for Case 4 (forced ventilation with hood).	85

Fig. 4.32: Temperature variations at X-Y & Z breath lines for Case 5 (forced ventilation with front vent).	86
Fig. 4.33: CO ₂ concentration contour at Y-breath plane. Front vent (Case 5).....	87
Fig. 4.34: CO ₂ variations at X-Y & Z breath lines for Case 5 (forced ventilation with front vent).	88
Fig. 4.35: Temperature variations at X-Y & Z breath lines for Case 6 (forced ventilation with base vent).....	89
Fig. 4.36: 12 CO ₂ concentration contour at Y-breath plane. Base vent (Case 6).....	90
Fig. 4.37: CO ₂ variations at X-Y & Z breath lines for Case 6 (forced ventilation with base vent).....	91
Fig. 4.38: CO ₂ concentration at the breathing zone (a) Case 1, (b) Case 4, (c) Case 5 and (d) Case 6.	92
Fig. 5.1: (a) Digital CO / CO ₂ meter at the breathing zone, (b) Traditional kitchen for experiment.	95
Fig. 5.2: Experimental setup at IUT Campus a) stove with duct and b) position of the measuring devices.....	96
Fig. 5.3: CO concentration at source for (a) Cowdung and (b) Cowdung-Rice husk.....	97
Fig. 5.4: CO concentration at source for (a) Firewood and Cowdung and (b) Firewood.....	97
Fig. 5.5: CO ₂ concentration at source for (a) Cowdung and (b) Cowdung and Rice husk.....	98
Fig. 5.6: CO ₂ concentration at source for (a) Firewood and Cowdung and (b) Firewood.....	98
Fig. 5.7: Experiment of PM source concentration measurement.	99
Fig. 5.8: Different data set of PM concentration at source of rural kitchen stove.	100
Fig. 5.9: Temperature profile with time along Z direction for rural kitchen 1 at (a) probe 1, (b) probe 2, (c) probe 3 and (d) probe 4.	101
Fig. 5.10: Temperature profile with time along Z direction for rural kitchen 1 at (a) probe 1, (b) probe 2, (c) probe 3 and (d) probe 4.	102
Fig. 5.11: Temperature profile with time along Z direction for rural kitchen 2 at (a) probe 1, (b) probe 2, (c) probe 3 and (d) probe 4.	103

Fig. 5.12: CO ₂ profile with time at the breathing point for rural kitchen 1 (a) data set 1 and (b) data set 2.....	104
Fig. 5.13: CO ₂ profile with time at the breathing point for rural kitchen 2 (a) data set 1 and (b) data set 2.....	104
Fig. 5.14: CO concentration with time at the breathing point for rural kitchen 2.....	105
Fig. 5.15: PM concentration with time at the breathing point for rural kitchen 1.	106
Fig. 5.16: PM concentration with time at the breathing point for rural kitchen 2.	108
Fig. 5.17: Kitchen model with different planes and line.....	109
Fig. 5.18: Computational domain with boundary conditions (a) without vent (b) vent without hood and (c) vent with suction hood diameter 2D. (All dimensions are in m).....	109
Fig. 5.19: Computational grid at X-Z and Y-Z plane.	110
Fig. 5.20: Computational grid at Y-Z plane with Chimney.	111
Fig. 5.21: Comparisons between Experiment and Prediction.	111
Fig. 5.22: Carbon Monoxide concentration (source 338 PPM) at (a) longitudinal plane, (b) lateral plane and (c) breathing plane with close vent.	112
Fig. 5.23: CO concentration at a line passing the breathing point for source 338 PPM.	113
Fig. 5.24: Carbon Dioxide concentration (source 7100 PPM) at (a) longitudinal plane, (b) lateral plane and (c) breathing plane with close vent.	113
Fig. 5.25: CO ₂ concentration at a line passing the breathing point for source 7100 PPM.	114
Fig. 5.26: Particulate Matter concentration (source 2867 µg/m ³) at (a) longitudinal plane, (b) lateral plane and (c) breathing plane with close vent.	115
Fig. 5.27: Particulate Matter concentration at a line passing the breathing point for source of 2867 µg/m ³	115
Fig. 5.28: Carbon Monoxide concentration (source 338 PPM) at (a) longitudinal plane, (b) lateral plane and (c) breathing plane with open vent.	117
Fig. 5.29: CO concentration at a line passing the breathing point for source of 338 PPM.	117
Fig. 5.30: Carbon Dioxide concentration (source 7100 PPM) at (a) longitudinal plane, (b) lateral plane and (c) breathing plane with open vent.	118

Fig. 5.31: CO ₂ concentration at a line passing the breathing point for source of 7100 PPM.	119
Fig. 5.32: Particulate Matter concentration (source 2867 µg/m ³) at (a) longitudinal plane, (b) lateral plane and (c) breathing plane with open vent.	120
Fig. 5.33: Particulate Matter concentration at a line passing the breathing point for source of 2867 µg/m ³	120
Fig. 5.34: CO concentration (source 338 PPM) at (a) longitudinal plane, (b) lateral plane and (c) breathing plane with open hood.	121
Fig. 5.35: CO concentration at a line passing the breathing point with open hood for source of 338 PPM.	122
Fig. 5.36: CO ₂ concentration (source 7100 PPM) at (a) longitudinal plane, (b) lateral plane and (c) breathing plane with open hood.	123
Fig. 5.37: CO ₂ concentration at a line passing the breathing point with open hood for source 7100 PPM.	124
Fig. 5.38: Particulate Matter concentration (source 2867 µg/m ³) at (a) longitudinal plane, (b) lateral plane and (c) breathing plane with open hood.	124
Fig. 5.39: Particulate Matter concentration at a line passing the breathing point for source of 2867 µg/m ³	125
Fig. 5.40: Comparison between average experimental and numerical concentrations for (a) without vent (b) vent without hood and (c) vent with suction hood diameter 2D.	126

List of Tables

Table 3.1: Test Cases of urban and rural kitchen.....	36
Table 3.2: Calibration test results for multi probe thermometer.....	42
Table 3.3: Uncertainty of Temperature Measurement.....	43
Table 3.4: Uncertainty of CO ₂ Measurement.....	44
Table 3.5: Uncertainty of CO Measurement.....	45
Table 3.6: Standard Uncertainty and Deviation of PM Meter.....	47
Table 3.7: Uncertainty of PM Measurement.....	47
Table 4.1: Details of Boundary Conditions.....	59
Table 4.2: Different cases of Urban Kitchen Study.....	60
Table 4.3: Comparison between Numerical and Experimental Data for urban kitchen 1.....	64
Table 4.4: Comparison between Numerical and Experimental Data for urban kitchen 2.....	64
Table 4.5: Findings of breathing point CO ₂ concentration in connection with the possible health hazards.....	93
Table 5.1: CO and CO ₂ emission concentration.....	95
Table 5.2: Findings of breathing point concentrations of different contaminants in connection with the possible health hazards.....	127

Nomenclature

h	Static enthalpy, $\left(\frac{J}{kg}\right)$
I	molar concentration of component
k	Turbulent kinetic energy $\left(= \frac{\overline{u'^2} + \overline{v'^2} + \overline{w'^2}}{2}\right)$, $\left(\frac{m^2}{s^2}\right)$
P_k	turbulence production due to viscous forces
P_{kb}	Buoyancy production term
p	Absolute Pressure, (Pa)
S_M	Sum of body forces
S	Strain rate $\left(= \frac{1}{2}\left(\frac{\partial U_i}{\partial x_j} + \frac{\partial U_j}{\partial x_i}\right)\right)$, (s^{-1})
T	Static temperature, (K)
t	Time, (s)
\vec{U}	Velocity vector (x,y,z) , (m/s)
u	u-component of velocity in x direction, (m/s)
v	v-component of velocity in y direction, (m/s)
w	w-component of velocity in z direction, (m/s)
x	X axis coordinate, (m)
y	Y axis coordinate, (m)
z	Z axis coordinate, (m)

Greek symbols

σ_ρ	Turbulence Schmidt Number
σ_{xx}	Stress component in x direction on a face normal to x, (Pa)
σ_{xy}	Stress component in y direction on a face normal to x, (Pa)
σ_{xz}	Stress component in z direction on a face normal to x, (Pa)
σ_{yx}	Stress component in x direction on a face normal to y, (Pa)
σ_{yy}	Stress component in y direction on a face normal to y, (Pa)
σ_{yz}	Stress component in z direction on a face normal to y, (Pa)
σ_{zx}	Stress component in x direction on a face normal to z, (Pa)
σ_{zy}	Stress component in y direction on a face normal to z, (Pa)
σ_{zz}	Stress component in z direction on a face normal to z, (Pa)
μ	Dynamic viscosity, $\left(\frac{kg}{m \cdot s}\right)$
μ_{eff}	Effective turbulence viscosity, $\left(\frac{kg}{m \cdot s}\right)$
μ_t	Turbulent dynamic viscosity, $\left(\frac{kg}{m \cdot s}\right)$
ρ	Fluid's density, (kg/m^3)
Φ	Dissipation function
ε	Turbulent dissipation rate $\left(= \rho C_\varepsilon \frac{k^2}{\mu_t}\right), \left(\frac{m^2}{s^3}\right)$
λ	Thermal conductivity of the fluid, $\left(\frac{W}{m \cdot K}\right)$

Abbreviations

Acute Lower Respiratory Infection	ALRI
Acute Respiratory Infection	ARI
Chinese National Standard	CNS
Commercial Kitchen Ventilation	CKV
Computational Fluid Dynamics	CFD
Forced expiratory flow	FEF
Forced Vital Capacity	FVC
Indoor Air Pollution	IAP
Indoor Air Quality	IAQ
International Society for Augmentative and Alternative Communication	ISAAC
Liquid Petroleum Gas	LPG
National Institute of Standards and Technology	NIST
Peak Expiratory Flow Rate	PEFR
Peak expiratory flow,	PEF
Portable Power Generators	PPG
Slow Vital Capacity	SVC
Suspended Particulate Matter	SPM
Upper Respiratory Tract Infection	URTI
Volatile Organic Compounds	VOC's
World Health Organization	WHO

Acknowledgment

Praise be to ALLAH (SWT), who gave me the success in this endeavor.

I would like to express my sincere thanks and gratitude to Prof. Dr. A. K. M. Sadrul Islam, my research advisor, for his consistent support, guidance and encouragement throughout this research period. I would also like to thank Prof. Dr. M Ruhul Amin, Professor of Montana State University, USA, for sharing his thoughts and ideas to enrich the technical content of this thesis.

I am also grateful to my parents, my brother for their encouragement and love. I would like to thank my wife, Sara Afroz, for her endless support and my lovely son, Tahmid Rahman and daughter Zakia Taskin who have been the source of my inspirations and success.

A special thanks to all my dearest colleagues, especially Prof. Dr. Md. Ashraful Haque, Prof. Dr. Md Zahid Hussain, Prof. Dr. Anayet Ullah Patwari and last but not the least all my fellow IUTians colleagues. Their endless cooperation, support, advice, comments are greatly acknowledged.

Abstract

Lack of proper ventilation of exhaust fumes from gas and biomass fired stoves in both urban and rural residential kitchens are a major health concern for majority populations. It could even cause destruction of property, reduced quality of life and lifespan. In this research, a typical urban kitchen with a standard dimension of $2.13\text{m} \times 2.43\text{m} \times 3.05\text{m}$ was modeled with single open door exit. Two heat sources were used to resemble the double burner gas stove of an urban residential kitchen. On the other hand, a single burner traditional soil stove was used for the model of a rural kitchen with dimension of $3.50\text{ m} \times 2.20\text{ m} \times 1.85\text{ m}$. In both cases, steady state simulations were performed using a three dimensional CFD code with appropriate boundary conditions. The present numerical method for urban kitchen was validated by comparing with the experimental data and showed very reasonable agreement. A grid independence test was also performed to determine the optimum grid resolution reflecting the accuracy of the numerical solution.

For urban kitchen, the results are presented for temperature field and velocity field, and CO_2 concentration and discussed under both natural forced ventilation systems. For the gas stoves located in the kitchen corner, the flow tends to shift towards the corner side wall and exhibits high temperature zone all above the burners. A comparative analysis between the ventilation (natural and forced) and no ventilation conditions are reported. Very high concentration (above 5000 PPM) of carbon dioxide gas was observed at the plane passing the breathing zone. Exposure to this environment for longer time may cause serious health damage of the occupants. A kitchen hood system has been simulated for both thermal comfort and carbon dioxide gas emission for the kitchen. It has been observed that the carbon dioxide gas concentration significantly reduced within the breathing zone due to use of kitchen hood system. In the breathing zone, the CO_2 concentration is only about 500 PPM which is 10 times lower than the close vent case. Two other positions of the kitchen hood suction have been studied for the effect of thermal distribution and emission rate. It has been observed that both front and base extraction method

reduces the emissions significantly to well below the safe limit. They also can maintain thermal comfort quite well inside the kitchen space.

For the rural kitchen study, varying intensity of emissions of CO, CO₂ and Particulate Matter (PM) from different kinds of Bio-fuels burning have been investigated. Dispersions of these pollutants in the kitchen space have been investigated for without ventilation and natural ventilation without hood and with hood systems. It has been observed that at unventilated condition, CO, CO₂ and PM concentration exceeds safe standard value. Even the natural ventilation condition fails to keep the concentration below the safe limit. However, a significant improvement can be observed for the kitchen with hood under natural ventilation.

Chapter 1

1. Introduction

Indoor air quality and thermal comfort are the important health and safety measures for room occupants. It is a common problem in the majority of the urban residential buildings in the country like Bangladesh due to poor architectural design of the living spaces, specially the kitchen, which is not properly followed by the optimum code of design for comfort ventilation and has not been paid appropriate attention yet by the researchers. Insufficient ventilation of exhaust fumes produced from gas or biomass fired stoves in both urban and rural residential kitchens could cause destruction of property, reduced quality of life and lifespan. Exposure to high CO₂ concentration for longer time may cause serious health damage of the occupants [2]. As per Wisconsin Department of Health Services of USA [2], over 5,000 PPM exposures to CO₂ lead to serious oxygen deficit resulting in permanent brain damage, coma and even death. Apart from that, exposure to certain ranges of CO₂ concentrations may cause minor to severe health related problems.

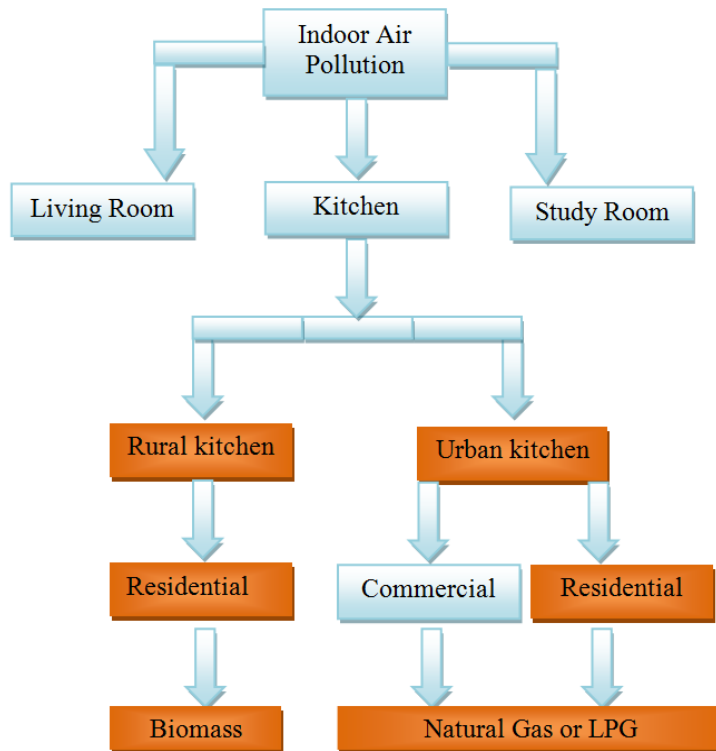


Fig. 1.1: Flow diagram of Urban and Rural kitchen.

Indoor Air Pollution (IAP) is mainly studied for living room, study room, kitchen etc. Among these kitchens is the most vulnerable indoor place where emissions occur due to fuel burning. As shown in the Fig. 1.1, kitchens may be studied at both rural and urban areas. In this research, residential rural kitchen has been studied with bio-fuel burning. On the other hand, residential urban kitchen has been studied for conventional natural gas burning.

In the rural areas emissions from biomass stove have always been ignored by the researchers and environmentalists in spite of their dire consequences when left uncontrolled and unattended. In the rural areas of the developing countries where kitchen receives the least amount of attention from the family members, the health risk is unimaginable. Occupants of the house are being exposed to serious pollution caused by the flue gases emitted when various conventional bio-fuels are burnt. The emission of CO₂, CO and PM can reduce the quality and span of life in a surprising manner. In rural areas, practically little attention is provided to the structure of the kitchen, exhaust system or the serious health threats to which the cook is exposed.

Exposure to CO₂ can produce a variety of health effects. These may include headaches, dizziness, restlessness, a tingling or pins or needles feeling, difficulty in breathing, sweating, tiredness, increased heart rate, elevated blood pressure and even coma. The levels of CO₂ in the air and potential health problems are [2]:

- 250 - 350 PPM – background (normal) outdoor air level
- 350- 1,000 PPM - typical level found in occupied spaces with good air exchange.
- 1,000 – 2,000 PPM - level associated with complaints of drowsiness and poor air.
- 2,000 – 5,000 PPM – level associated with headaches, sleepiness, and stagnant, stale, stuffy air. Poor concentration, loss of attention, increased heart rate and slight nausea may also be present.
- >5,000 PPM – Exposure may lead to serious oxygen deprivation resulting in permanent brain damage, coma and even death.

Exposure to low levels of carbon monoxide can produce the following symptoms like throbbing headache, dizziness, fatigue, and shortness of breath. Exposure to high levels can result in severe headache, weakness, dizziness and nausea, irregular heartbeat and unconsciousness. Occasionally, these symptoms may be confused with symptoms of the flu. Exposure to high levels can also result in seizures, coma, respiratory failure, and death. Exposure to high carbon monoxide levels during pregnancy is associated with birth defects and fetal death. In addition to the toxic effects of carbon monoxide, the gas is very flammable and at high concentrations it may be explosive.

When low grade bio-fuels such as wood, animal dung or others are burned, air becomes polluted that may cause acute respiratory infections (ARI), and results in premature death of young individuals. The most critical ARI disease called Acute Lower Respiratory Infection (ALRI) is associated with pneumonia [4]. Annually about 20% of the children's death less than five years and about 10% of perinatal deaths [5; 6] are caused due to ALRI. Regional percentage of mortality due to ALRI in Asia is 42% and in Africa 28% [7]. IAP is responsible for 2 million deaths per year in poor families over which 1 million are children [8; 9]. World Bank and other international development organization have considered the impact of IAP as an important issue for the coming decades.

Computational simulation has been attracting the attention in the past recent years, due to its cost effectiveness and high accuracy predictions. It becomes an important tool in engineering application, in particular, in the field of fluid mechanics in order to predict highly three dimensional complex flow structures and associated dispersion of the transport species such as contaminants (CO, CO₂, PM etc.). Moreover, the commercial computational tools allow modeling of the combustion chemical reactions with a very reasonable accuracy. Therefore, CFD has become an invaluable tool for Indoor Air Quality simulation for green building study.

1.1. Thesis Organisation:

This numerical study will be presented in the following manner. First, a detailed literature review of the earlier studies, selected from the relevant field, more particularly, indoor air quality, kitchen ventilation, emission dispersions and associated health hazards will be presented in Chapter 2. Specific objectives and motivation of the current study and a brief introduction on the different test cases (test matrix) will be given in chapter 3 in order to clarify the key objectives of this study. Following these, a numerical approach along with the detailed description of the experimental instrumentations, uncertainty, numerical model, governing equations, boundary conditions, grid independency test, CFD validations will be discussed in Chapter 4. In Chapter 5, numerical results followed by experimental results for validations will be presented for urban kitchen for four different cases such as (a) effects of ventilation Systems on temperature distributions, (b) Carbon Dioxide gas emission from double burner gas stove, (c) effects of kitchen hood system and (d) effects of the position of kitchen vent suction in urban residential kitchen. In Chapter 6, results of experimental and numerical study of CO, CO₂ and PM emissions from rural kitchen will be investigated and discussed. Finally, conclusions and specific contributions, from the current study, will be drawn in the subsequent chapters, as well as computational challenges and future directions that are required for further study of kitchen indoor air quality modeling.

Chapter 2

2. Literature Review

In the recent studies, Indoor Air Quality (IAQ) has been given importance for green building design in order to achieve comfort and healthy environment for the room occupants. There are few experimental as well as numerical studies in the past years, conducted with least attention to the indoor air pollution in particular in the developing countries. In this section, a chronological review of these studies will be presented in two subsections. All studies that include both experimental and numerical works for urban IAQ will be summarized in the first subsection, while the second subsection will cover the rural IAQ. Then all these studies will be summarized at the end of this chapter and the objectives and motivations of this present study will be presented in the next chapter.

2.1. Urban Indoor Air Quality:

Awbi et al. [10] presented a single zone ventilation model to estimate the ventilation rate required to maintain a specific relative humidity in a dwelling for the purpose of reducing large scale surface condensation of water vapour in water. Using field data of temperature and relative humidity, air supply and extract rates for individual rooms are estimated by applying this model.

Kondo et al. [11] conducted a numerical simulation of ventilation efficiency in commercial kitchen. The airflow and temperature distributions in a commercial kitchen were simulated based on the k- ϵ turbulence model. QUICK scheme was used in calculating the convective term of momentum equation in CFD and the shape factor was calculated by the Monte-Carlo method. The ventilation efficiency was investigated for three types of ventilation systems. A kitchen model of 3.0m x 1.5m x 2.2 m size was used. They found that keeping the hot outdoor air supply position near the lower face of the hood or the upper face of the cooking equipment results in a more comfortable working environment. Moreover, the local ventilation was found

more effective when the outdoor air supply outlet was positioned on the upper face of the cooking equipment.

Park et al. [12] studied the air flow and contaminant distribution in a full-scale kitchen opened to a living room, ventilated by an exhaust hood using commercial CFD program, PHOENICS. The locations of the gas range and the window were chosen as the parameters to investigate the indoor environment. The values of the contaminant index for several layouts of the gas range and the window were calculated and compared. Their results revealed that when the gas range is installed along the wall with specified window location, its position in relation to the wall has unnoticed effect on contaminant index. However, for a fixed gas range location, the indoor air quality deteriorates by the proximity of the window to the gas range.

Chi-ming et al. [13] conducted experiment to study the efficient side exhaust system for residential urban kitchens in Taiwan. They designed the exhaust in three ways namely single slot, twin slot and fence slot systems. The experiment was conducted with different configurations by varying the heights. They concluded that the side exhaust systems installed close to the pot rims performed well in smoke control at the same exhaust flow rate ($7.4 \text{ m}^3/\text{min}$) which is lower than the $11.6 \text{ m}^3/\text{min}$ required by Chinese national standard 3805 (CNS-3805).

Nantka [14] investigated indoor conditions in Silesian Buildings with natural ventilation. Results were obtained by questionnaires, measurements and simulations of ventilation processes in typical blocks of flats and office buildings in Silesia. The effects of airtightness, natural ventilation and some pollutants on the indoor environment were discussed. To determine the air leakage values for windows and doors, the pressurization tests were conducted with the use of a plastic cover tightly taped to the window and door frame (the small-scale tests). There were also large-scale pressurization tests applied in selected rooms, flats and offices. Two types of stands and two methods were used. They found that the indoor air quality depends

on the air change rates and the natural ventilation rate depends on airtightness of external walls and especially windows.

Kajtar and Leitnar [15] studied CFD modeling of indoor air quality and thermal comfort. CFD modeling was made by FLOVENT. Well established $k - \varepsilon$ turbulence model was used for turbulence capture. Numbers of cases have been investigated in regard to the amount of air removed by kitchen hood. Supply air has been provided with air terminal devices installed above the windows. Each diffuser (4 x 50cm, with 50% free area ratio) was placed above the windows. The study concluded that the minimum safe carbon-dioxide concentration can be attained at 160 m³/h exhaust airflow, and to meet IAQ requirements considerably higher ventilation rate should be provided. According to calculated results, approximately 4.7 m³/h airflow is sufficient to ensure complete burning process of natural gas.

Odunze et al. [16] studied the CFD analysis of the effects of the size and location of an air-inlet in domestic kitchen extraction. A model kitchen including a gas range cooker and an extraction hood was constructed and the cooking process was simulated. The flow field during the cooking process in the kitchen was modeled using FLUENT Airpak 3.0.12. They concluded that air-inlet location effects both local (cooking zone) and global extraction (breathing and room zones). Depending on the location of the air-inlet, incomplete room air mixing of contaminants can occur.

Panagopoulos et al. [17] performed an indoor air quality case study in an apartment complex. Using CFD techniques they predicted air flow, VOCs and formaldehyde contaminant distributions in the apartment comprised of a kitchen, ventilated by an exhaust hood. The CFD methodology developed can be employed to improve indoor pollution and ventilation techniques, namely focusing on the optimum sizing and siting of ventilation schemes and provision of practical suggestions as a part of an Indoor Pollution Management System.

Villi et al. [18] investigated the computational aspects of modeling different strategies for kitchen ventilation. Their paper dealt with the evaluation of different simulation approaches to kitchen ventilation modeling. Multi-zone, CFD and zonal approach are discussed. Results illustrated the important influence of proper ventilation for kitchen IAQ. Their study demonstrated the applicability of the zonal approach for predicting pollutant indoor concentration with a level of accuracy comparable to CFD predictions.

Zhou et al. [19] conducted a research on indoor CO₂ concentration distributions in an apartment using CFD code Fluent 6.3 for solving governing equations by means of finite volume methods. They investigated on flow field, temperature distributions and CO₂ concentration distributions under six different cases in an apartment. Their design comprised of a living room, a kitchen equipped with hood & smart-fan along with an inlet air flow passage. Their results indicated that range hood has great influence on temperature distributions and CO₂ concentrations only during the cooking period.

Mohammed [20] conducted a numerical investigation of Indoor Air Quality and thermal comfort in a ventilated room. He investigated airflow characteristics, indoor air quality (IAQ), and the thermal comfort with a displacement ventilation system using three dimensional CFD code [Air Pak 2.0.6]. After validation of the code, a numerical study was executed for a typical room with dimensions of 5m x 3m x 3m according to a variety of supply air velocities, supply air temperature and supply air relative humidity. He found that temperature and velocity fields are affected by buoyancy force and supply air velocity have no effect on the trend of relative humidity profiles. In the displacement ventilation system, the thermal comfort depended on the supply air temperature and the air velocity, while the inlet relative humidity showed negligible effects.

Brohard et al. [21] investigated performance and energy efficiency of CKV systems by performing flow-visualization research and publishing design guidelines for the food service community. Three hood systems were tested. Those are wall

mounted canopy, island mounted canopy and proximity (Back shelf). Charbroilers and griddles, representing heavy duty and medium duty appliances respectively, were tested. In their study idle and emulated cooking conditions were also tested. The influence of air mass disturbances (drafts) and tapered side panels was also investigated. They have introduced replacement or makeup air that significantly impact on hood performance and recommended as a key factor in the design of kitchen ventilation systems. This makeup air close to the hood's created local air velocities and turbulence that resulted in periodic or sustained failures in thermal plume capture and containment.

2.2. Rural Indoor Air Quality:

Pandey et al. [22] performed a study at a rural community of the hill region of Nepal to find out if there is any association between domestic smoke pollution and ARI in infants and children younger than two years of age. This preliminary study showed that episodes of moderate and severe ARI (Acute Respiratory Infections) increased with increasing level of exposure to domestic smoke pollution, thus suggesting domestic smoke pollution to be an important, preventable risk factor of ARI.

Albalak et al. [23] undertook a study to examine the association between exposure to air pollution from domestic biomass fuel combustion and chronic bronchitis in two rural Bolivian highland villages. In one village the cooking is done exclusively at indoors where in other village the cooking is done primarily at outdoors. The results of this study suggested an association between chronic bronchitis and exposure to domestic biomass fuel combustion. However, further large scale studies from other areas of the developing world are needed to confirm the association.

Zhang and Smith [24] researched on emission of Carbonyl compounds from rural cooking stoves in China. They presented a new database of carbonyl emission factors for commonly used cooking stoves in China. Experiment was conducted on

22 types of fuel/stove combination. Experiments revealed that all the tested cooking stoves produced Formaldehyde and Acetaldehyde and that the vast majority of the biomass stoves produced additional Carbonyl compounds. Their study revealed that cleaner fuels like LPG produces far lesser Carbonyl compounds than biomass fuels. Considering varying stove types while fuel type was constant, they observed that improved stoves emits more Carbonyl compounds which imply that stove improvement when only energy efficiency is considered may cause higher air pollution.

Ravi et al. [25] carried out CFD simulations of the flow, heat transfer, pyrolysis and combustion in the configuration of a simple sawdust stove to develop simple algebraic equations that describe individual phenomena. Such equations are needed in the field for performance analysis and prediction, and could also be used for the performance optimization of stove geometry.

Vinod Mishra [26] studied biomass for cooking and heating. Many women and young children in developing countries exposed to high levels of air pollution at indoors. He investigated the association between household uses of biomass fuels and acute respiratory infections in young children under two years in less developed countries. Wood, crop residues, animal dung were used in their study as these fuels are used in more than two fifths of the world's households. He found very strong health risk condition for the exposing people especially the children who spend large amount of time with their mother.

Schei et al. [27] investigated the prevalence of asthma with different degrees of indoor wood smoke pollution among an indigenous population in Latin America. Their study singled out the use of open fire for cooking as an important risk factor for asthma symptoms and severity compared to other cooking technologies.

Dasgupta et al. [28] provided a detailed analysis of the implications for indoor air pollution, 24 hr monitoring data for PM_{10} , with a particular focus on cooking location, structural materials, and ventilation practices. Household-specific factors apparently matter more than fuel choice in determining PM_{10} concentrations.

In some biomass-burning households, concentrations are barely higher than in households that use natural gas. Experimentally a large variation of PM₁₀ was found in higher concentrations.

K. R. Smith [29] investigated indoor air pollution from household cooking and space heating that apparently causes substantial illness in developing countries where mostly used solid fuels are biomass, crop residues, cow dung etc. He investigated on three areas such as 1) epidemiology: case control studies for tuberculosis, cardiovascular disease, acute respiratory disease and pregnancy outcomes. 2) exposure assessment, 3) interventions-engineering and dissemination approaches for improved stoves to reduce green house gas emissions from household stoves.

Kilabuko et al. [30] performed a study to characterize the levels of pollutants in biomass fuel using at homes and examined the association between biomass fuel smoke exposure and Acute Respiratory Infection (ARI) disease in Nianjema village in Bagamoyo, Tanzania. Results of this study suggested an association between respiratory diseases and exposure to domestic biomass fuel smoke, although similar studies are recommended by the authors to confirm this involvement.

Kumar et al. [31] undertook a study about the effects of indoor air pollutants like SO₂, NO₂ and SPM generated from fuels used in cooking stoves. A total of 3,456 children were examined (59.2% male and 40.8% female). Among them, 31.2% of the children's families were using biomass fuels for cooking and 68.8% were using Liquefied Petroleum (LP) gas. Levels of indoor SO₂, NO₂ and SPM were measured using a Handy Air Sampler. The study revealed that the mean level of indoor SO₂ was significantly higher in case of families using biomass fuels for cooking as compared to families using LP gas. The mean level of indoor NO₂ and indoor SPM for families using biomass fuels for cooking was significantly higher when compared to families using LP gas. This study suggested that biomass fuels increase the concentrations of indoor air pollutants that cause asthma, rhinitis and URTI in children. LP gas smoke was also associated with respiratory allergy.

Padhi et al. [32] conducted research on impact of domestic fuels used in typical Indian rural kitchen on children's health. Moderate scale survey was done on 750 households considering air quality parameters like CO₂, CO, NO₂, NO, SO₂, O₃, SPM, temperature and humidity. Questionnaire was developed on the pattern of ISAAC. Some lung function parameters like PEF, FVC, FEF and SVC were examined on an electronic spirometer. Logistic regression estimated the odds of suffering from respiratory infections in the households using biomass fuels relative to that of those who use LPG. The study concluded that exposure to cooking smoke from biomass combustion is significantly associated with decline in lung function and prevalence of doctor-diagnosed asthma and other respiratory diseases.

Gurley et al. [33] studied the evaluation of the health effects of a pilot indoor air pollution intrusion in rural and peri-urban Bangladesh. Their studies planned to measure improvements in IAP levels from improved cookstoves. Measurements included acute episodes of illness, especially acute respiratory illnesses and pneumonia in children under 5 years old. They also used some intermediate health indicators such as oxygen saturation in children, maternal blood pressure, and amount of CO in breath. Toxins and pollutants in the air which have been linked with poor health outcomes were also measured, such as particulate matter and CO.

Kao et al. [34] numerically investigated the airflow characteristics and particulate matter (PM) transport for different natural ventilation patterns with the same air change rate. Four typical natural ventilation patterns (full-open, pass-through, right short-circuit and left short-circuit), representing the ratios of the outlet-to-inlet opening size ranging from 1.67 to 0.17, were considered to study airflow characteristics. The results showed that although the air change rate is the same, airflow characteristics and PM transport behaviors are quite different for various ventilation patterns. The removal efficiencies of PM₁₀ for the four ventilation patterns are all found to be much better than those of PM_{2.5} and PM₁. Particle escape is the major mechanism to remove PM for rooms with double-sided ventilation, whereas particle deposition is important for single-sided ventilation rooms.

Kumie et al. [35] measured the levels of indoor NO₂ concentration in homes with under-five years of aged children in rural Ethiopia. Wood, crop residues and animal dung were the main household fuels. The mean 24-hrs concentration of NO₂ was 97 µg/m³. Highland households showed significantly higher indoor NO₂ concentration. Their study demonstrated high levels of indoor NO₂ in rural homes of Ethiopia. The major limitation of their study was the use of NO₂ as the sole indicator of indoor air pollution from biomass fuels. They recommended a possible approach for model calculations based on literature data in relations between the concentrations of NO₂ and of other pollutants such as particulate matter, whether measured as PM₁₀ or as other fractions of suspended particles.

Khalequzzaman et al. [36] compared indoor air pollution levels and incidence of symptoms in children between biomass and fossil fuel. They conducted a study among biomass (n=42) and fossil fuel (n=60) users having age of less than 5 years. Mean concentration of dust particles and geometric mean concentrations of VOCs such as Benzene, Xylene, levels of CO and CO₂ which are significantly higher in biomass than fossil fuel users' kitchen. The measured pollutants are CO, CO₂, NO₂, SO₂, VOCs. Their study suggested that the measured pollutants did not directly result in prevalence symptoms among the children and thus other factors might be involved.

Adefeso et al. [37] determined the emission factors of CO from gasoline-powered Portable Power Generators (PPG). They evaluated the effects of the CO influx on the indoor air quality and identified appropriate ways of maintaining the ambient concentrations below the safe level. They showed that high air exchange rate allowed CO concentrations to decay fast while low air exchange rates lead to CO accumulation at indoor. They recommended that a PPG should not be placed at least 10 meters from the building.

Grabow et al. [38] conducted a research on indoor air pollution in a test kitchen from biomass cooking-stoves used in rural areas. They investigated the effect

of increasing air exchange rates in a test Kitchen. All emissions data were acquired using the Aprovecho Research Center manufactured Indoor Air Pollution Meter (IAP Meter) and were analyzed using Statistical Analysis Systems (SAS®), version 9.2. Tests were performed in the 24.6 m³ Aprovecho Research Center Test Kitchen. Three stoves were tested namely three stone fire (TSF), rocket stove, and top-lit updraft (TLUD) stove. Their results showed that increasing ventilation dramatically decreases the levels of CO and PM. The cleaner combustion in the TLUD along with increasing ventilation resulted in 90% reduction of IAP which is the requirement currently set by the Department of Energy of the United States.

Agarwal et al. [39] conducted a community based cross-sectional study in 760 non-smoking rural women involved in household cooking with four types of cooking fuels i.e. Biomass, Kerosene stove, Liquid Petroleum Gas (LPG) and Mixed(combination of two and more cooking fuels). In case of Peak Expiratory Flow Rate (PEFR), less than 80% of the predicted was considered as abnormal PEFR. The overall prevalence of abnormal PEFR was found to be 29.1% with greater predominance among biomass fuel users (43.3%) with high risk ratio (1.86) as compared to kerosene (0.63), LPG (0.75) and mixed (0.66) fuel users. Overall results indicated that prolonged exposure to cooking fuels particularly biomass fuels as a source of cooking adversely affects PEFR in nonsmoking rural women.

The sources of all diseases at indoors are mainly caused by inadequate ventilation, chemical contaminants from indoor or outdoor sources, and/or biological contaminants. Many volatile organic compounds (VOC's) can also be the reason for acute effects on the occupants of a building. In poor quality indoors all kinds of biological contaminants such bacteria, molds, pollen, and viruses are fast growing and cause health related problems for the room occupants. These situations are commonly referred to the term named as sick building syndrome (SBS). It is applied to the cases where the occupants are experienced acute health- or comfort-related effects. S M Joshi [40] investigated signs and symptoms of SBS as well as the chemical and biological contaminants responsible for different diseases. The health related symptoms are headache, dizziness, nausea, eye, nose or throat irritation, dry

cough, dry or itching skin, difficulty in concentration, fatigue, sensitivity to odours, hoarseness of voice, allergies, cold, flu-like symptoms, increased incidence of asthma attacks and personality changes.

From the above literature study, it is apparent that a number of investigations have been devoted to both urban and rural kitchens to account the indoor air pollution and dispersions within the kitchen space. Some efforts have been made for emission control. However, their study failed to explain details of contaminants dispersion characteristics with or without ventilation systems. Moreover, a real combustion heat sources in the cooking bench have not been taken into account in any of the numerical studies. Therefore, this paper aims to investigate the indoor air contamination and temperature comfort under natural, forced and no ventilated conditions.

2.3. Objectives And Motivations

This research has presented the evidence of health risk contaminants such as CO₂ in urban kitchen and CO, CO₂ and Particulate Matter (PM) concentrations in rural kitchens of the developing countries and their impact on the human health.

The specific objectives of this research are:

1. To investigate the indoor air contamination and temperature distributions under natural, forced and no ventilation conditions for urban kitchen.
2. To investigate the indoor air contamination and temperature distributions for rural kitchen under natural ventilation system.
3. To study numerically the dispersion characteristics of combustion by-products mainly CO and CO₂ for both urban and rural kitchen.
4. To measure the CO and CO₂ emission in urban and rural kitchen and then compare the numerical results with the experimental data in order to obtain numerical validations.
5. To measure PM concentration in rural kitchen for comparing the numerical results.

6. To establish control strategy for the kitchen to keep the pollutants concentration lower.

In this research, the effective way of predicting contaminants concentrations and dispersions within the kitchen space and their impact on human health will be focused. This study can help to adopt some strategic design guidelines for controlling hazardous components emission and to keep them below the safe threshold. Moreover, findings of this research can be used as comprehensive tool for designing and constructing an architectural green building. Therefore, it will certainly improve the quality of life of the occupant and ensure the existence of healthy living environment.

Chapter 3

3. Problem Formulation and Methodology

In this section details of the experimental and numerical methods have been discussed with necessary figures. At the beginning of the subsection, a typical model of the urban kitchen has been presented with the imposed boundary conditions and test conditions. The next part is associated with the discussion of the computational grid for urban kitchen. Followed by this section the part of the experimental methods have been discussed that includes description of the typical kitchen, experimental setup, and use of different instruments such as CO meter, CO₂ meter and PM meter along with the uncertainty study of the instruments and laboratory calibration of the multi-probe thermometer.

The contents of this thesis have been illustrated in Table 3.1. There are four different studies for urban kitchen named as TU1, TU2, TU3 and TU4. On the other hand, rural kitchen has been focused on three different types of study namely TR1, TR2 and TR3. Test conditions of the variables are also presented in the same table. It gives a complete manifestation to the reader about the scope and key objectives of this research.

Table 3.1: Test Cases of urban and rural kitchen

Kitchen Type	Test Types	Test Details	Test Cases with Variables		
			Test Cases	Test Variable	Ventilation types
Urban	TU1	Effect of Ventilation system on temperature distribution (Numerical)	Validation	Posner et al. [10]	---
	TU2	Effect of Ventilation system on CO ₂ distribution (Numerical)	Case 1	Close vent	No ventilation
	TU3	Effect of kitchen hood on temperature and CO ₂ distribution (Numerical)	Case 2	Open vent	Natural ventilation
			Case 3	1.5 m/s vent	Forced ventilation
	TU4	Effect of position of the kitchen vent suction on temperature and CO ₂ distribution (Numerical)	Case 4	1.5 m/s kitchen hood	Forced ventilation
			Case 5	Front vent 0.5 m/s	Forced ventilation
			Case 6	Base vent 0.5 m/s	Forced ventilation
Rural	TR1	Source concentration of different biomass fuel (Experimental)	CO and CO ₂ concentration for cow-dung, cow-dung/rice-husk, firewood/cow-dung, firewood		
	TR2	Comparison of breathing point concentrations for firewood burning in the traditional hard soil stove. Experimental at two different rural kitchen	Temperature, CO, CO ₂ and PM		
	TR3	Effect of roof top ventilation systems on CO, CO ₂ and PM ₁₀ concentration (Numerical)	Test Cases	Pollutants	Ventilation types
			Case 1	CO	No vent
			Case 2	CO	Natural ventilation
			Case 3	CO	Natural ventilation with hood
			Case 4	CO ₂	No vent
			Case 5	CO ₂	Natural ventilation
			Case 6	CO ₂	Natural ventilation with hood
			Case 7	PM ₁₀	No vent
		Case 8	PM ₁₀	Natural ventilation	
		Case 9	PM ₁₀	Natural ventilation with hood	

3.1. Typical Model of a Urban Kitchen

In the present study, a typical urban kitchen is modeled and simulated using three dimensional CFD (Computational Fluid Dynamics) code ANSYS CFX-12.1 [3]. The computational domain comprises of double stove burners as the heat and emission source, one open door and a vent as shown in Fig. 3.1a.

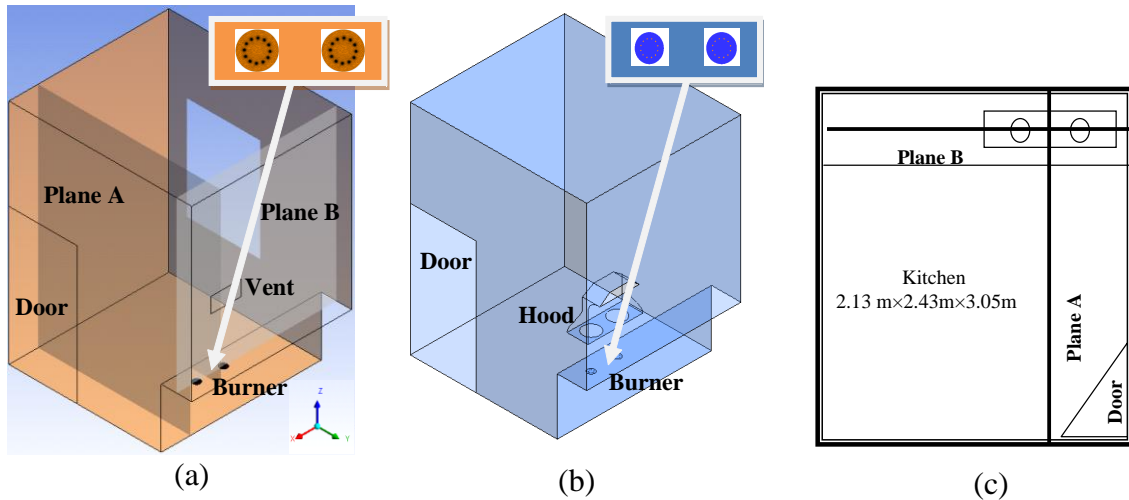


Fig. 3.1: Computational model with two burners, a) with front wall vent, b) with commercial hood (c) typical kitchen layout showing plane A and plane B.

A same model with a hood system is also simulated as seen in Fig. 3.1b. Standard kitchen floor area with dimensions can also be seen in Fig. 3.1c. Two planes A and B as shown in Fig. 3.1c are used for grid structure and results presentation.

3.2. Typical Model of a Rural Kitchen

A conventional rural kitchen used in developing countries is also modeled in this study. The computational domain consists of one heat source resembling single stove, closed walls at three sides and a front side open to the atmosphere, as shown in Fig. 3.2.

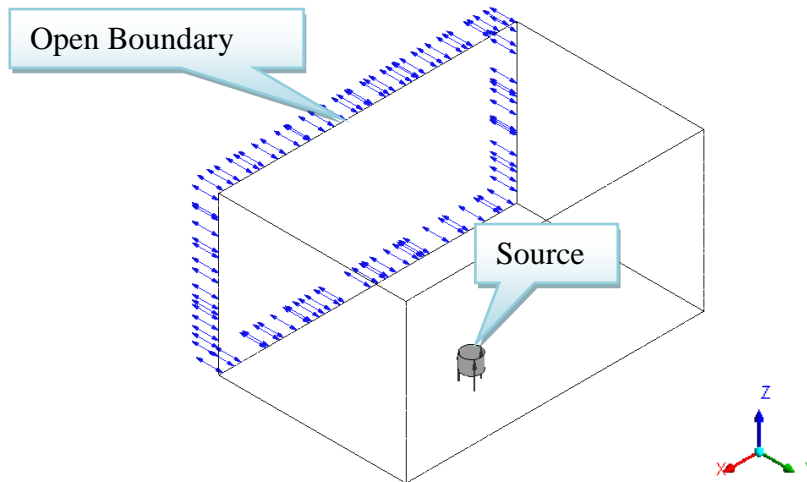


Fig. 3.2: Computational domain of the rural kitchen.

A commercial CFD code ANSYS CFX-12.1 [3] was employed to simulate the model in different conditions. ANSYS CFX software provides complete mesh flexibility, including the ability to solve flow problems using unstructured mesh with reasonable accuracy. The geometry of the typical rural kitchen was adopted for the model. The $k-\epsilon$ turbulence model was used as per the studies of Posner et al. [1] and Kajtar et al [15]. Comparison between RNG $k-\epsilon$ turbulence model and standard $k-\epsilon$ turbulence model were made by Posner et al. [1]. The rural kitchen space is provided with air as the working medium and single stove is added to the model for different kinds of bio-fuels emissions. The combustion model could not be used as the commercial code has no such module.. The measured source concentration of CO, CO₂ and PM were directly given as input to the stove. The kitchen is also employed with a duct with and without hood that are placed directly on the roof above the stove. There are nine cases investigated based on different exhaust conditions as illustrated in Table 3.1. In case 1, 4 and 7, the duct is completely closed meaning pollutants are accumulated under the roof just above the stove, case 2, 5 and 8 are of open type vent through which the contaminants leaves the kitchen naturally and in case 3, 6 and 9, the pollutants are leaving the exhaust system naturally through the hood. Therefore, all cases allow us to understand the effect of the duct installed with and without hood system under natural ventilation and thus the results are compared with the space of having no duct in the roof (no ventilation).

3.3. Experimental Set-up

In this study, few experiments were conducted at both urban and rural kitchens of standard living apartment of urban city and villages respectively. Two kitchens were randomly chosen in two different urban locations. One is named here as urban kitchen 1 and the other is urban kitchen 2. On the other hand, two rural kitchens were selected for experimentation in the rural areas of Gazipur and Tangail districts.

3.3.1. For Urban Kitchen

Experimental setup of urban kitchen 1 and 2 can be seen in Fig. 3.3. The net area of urban kitchen 1 and 2 are respectively 4.65 m^2 and 5.20 m^2 . Kitchen 1 has two doors and one window without any ventilating facilities. However, kitchen 2 has exhaust fan at the upper right corner but has an open door facing to the living room. It is also associated with single window at the left side of the stove. For measuring temperature a vertical stand was used as seen in Fig. 3.3, with five temperature sensors located at every 0.093m distance from the bottom sensor. Schematic diagram in the Figure 3.3c, illustrates the relative positions of the temperature sensors. The CO_2 meter was attached with the stand at the breathing zone as indicated in the Fig. 3.3c, at a distance of 1.372 m from the floor. Measurements for CO were ignored for gas combustion as it is recorded negligible emission concentration. This is a true possible state for the place where the natural gas combustion occurs in the presence of sufficient air. In all sets of readings the data were recorded with a computer integrated data acquisition system. Thus it allowed measurement to take as time dependent.

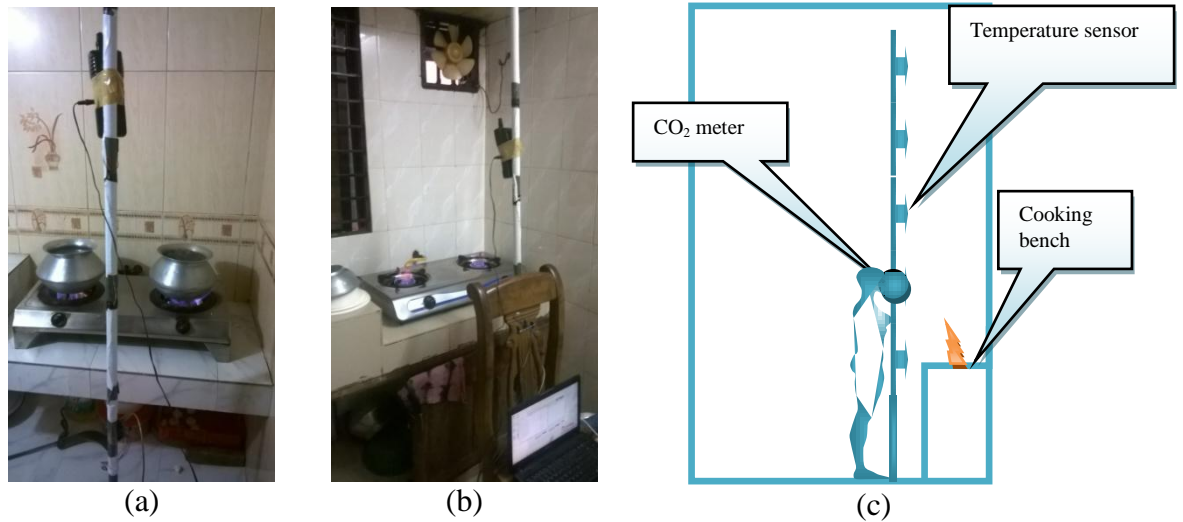


Fig. 3.3: Experimental setup for typical (a) urban kitchen 1 and (b) urban kitchen 2, and (c) schematic diagram for temperature and CO₂ measurement.

3.3.2. For Rural Kitchen

The experiments were conducted at a village for the rural kitchen using conventional stove. Poor people living in the rural areas are using biomass (which is cheap but produces higher emission) that can lead to long term health related consequences.

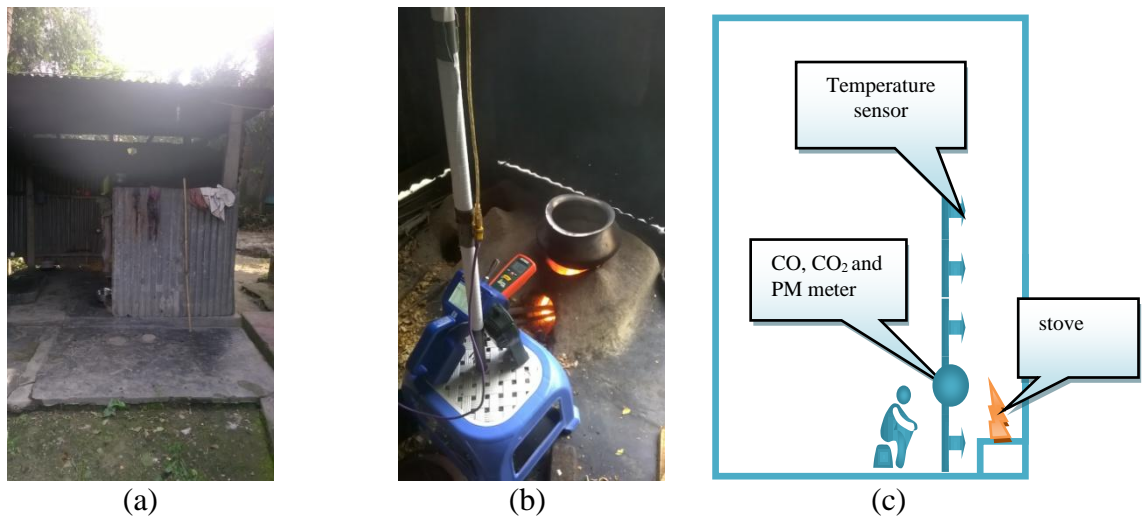


Fig. 3.4: (a) A typical rural kitchen at Tangail with (b) a conventional soil stove and (c) schematic diagram for CO, CO₂, PM and Temperature measurement.

Figure 3.4a shows a typical kitchen of usual size and construction selected randomly in rural areas for pollutants monitoring. Only single stove traditional

kitchen was considered for experiment on rural kitchen as seen in Fig. 3.4b. The traditional kitchen stove was made of mud soil and the measurements were carried out for CO₂, CO and Particulate Matter (PM) concentrations. Relative positions of all emission measuring devices and temperature sensors can be seen in Fig. 3.4c. In this figure position of the second sensor from the bottom is indicated as the breathing point where all the devices are attached.

3.3.3. Temperature Measurement Instrument, Calibration and Uncertainty

A microcontroller based five point temperature measuring device shown in Fig. 3.5a was constructed to facilitate vigorous measurement of the temperature field inside the kitchen. The temperature module featured with LM35 temperature sensor with necessary pin out terminals. The LM35 series are precision integrated-circuit temperature sensors, whose output voltage is linearly proportional to the Celsius (Centigrade) temperature. The power supply pins (VCC) and the ground (GND) pins of the temperature sensors are connected with VCC and GND of the microcontroller circuit and it measures the voltage from the out pin to see the variation of temperature. Arduino Duemilanove microcontroller board based on the ATmega328 was used as the acquisition circuit (see Appendix I for Circuit Diagram). This model has 14 digital input/output pins (of which 6 can be used as PWM outputs), 6 analog inputs, a 16 MHz crystal oscillator, a USB connection, a power jack, an ICSP header, and a reset button. The microcontroller can simply be connected to a computer with a USB cable and data recorded instantly by using the open source code.

In order to ensure accurate reading a standard calibration procedure was conducted which is shown in Fig. 3.5. Initially all digital thermometers available at the laboratory were checked for 0°C reading by dipping the thermocouple in to the ice. The best functioning digital thermometer was then selected for calibration as standard instrument. During the calibration process each sensors were placed in a hot stream flow maintained by an electric blower (see Fig. 3.5b). Thermocouple of standard thermometer and the temperature sensors were set at proximity to each other to ensure measurement at identical local point (see Fig. 3.5a).

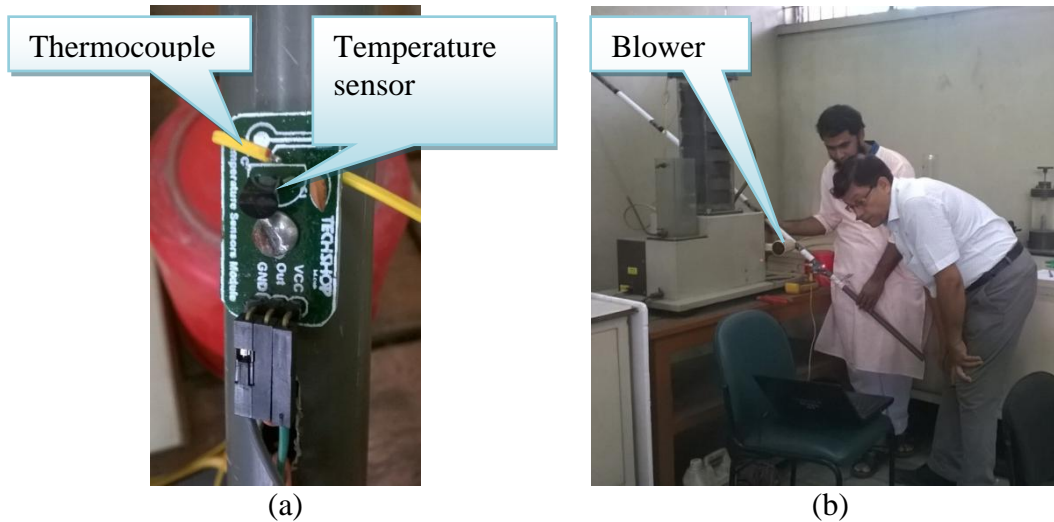


Fig. 3.5: (a) Temperature sensor (b) Calibration test of laboratory built multiprobe temperature device.

Table 3.2: Calibration test results for multi probe thermometer			
(Laboratory built device)			
Temperature Probe	Standard Temperature, °C	Measured Temperature, °C	% of Error
T1	59.90	60.10	0.33
T2	59.80	60.10	0.49
T3	63.40	63.40	0
T4	62.40	62.40	0
T5	64.45	64.45	0

Calibration data for all five sensors (T1, T2, T3, T4, and T5) are presented in Table 3.2. Standard and measured temperature showed very negligible differences. A maximum % of error was assessed to be 0.49%. Therefore, the instrument was found satisfactory for performing the experiment.

On the basis of experimental data as shown in Table 3.3 and available standard equations (see Appendix II), the standard uncertainty of the temperature measurement is calculated as ± 0.798 °C and the expanded uncertainty is ± 0.19 at 95% confidence level with coverage factor of $k=2$ (see Appendix II for the correction factor). So it implies that the true value lies within the acceptable measurement range.

Table 3.3: Uncertainty of Temperature Measurement (Laboratory built device)			
Temperature, °C	Residuals, °C	Residuals ² , (°C) ²	Calculations
47.85	-0.343	0.117649	Average Temperature 48.19 °C
47.85	-0.343	0.117649	
46.88	-1.313	1.723969	Variance 0.64 (°C) ²
48.34	0.147	0.021609	
48.83	0.637	0.405769	Standard Deviation 0.798 °C
47.85	-0.343	0.117649	
49.80	1.607	2.582449	Standard Uncertainty ±0.798 °C
48.83	0.637	0.405769	
47.85	-0.343	0.117649	Expanded Uncertainty ±(2×1.16×0.798/10)= ±0.19
47.85	-0.343	0.117649	

3.3.4. Emissions Instrument and Uncertainty

In this part specifications and the accuracy of experimental instruments are discussed as follows.



Fig. 3.6: (a) CO₂ meter (Brand EXTECH, USA) (b) CO meter (Brand EXTECH, USA) (c) PM meter (Brand TSI, USA).

CO₂ Meter:

CO₂ meter was imported from famous brand name Extech of United States of America (USA) and is shown in Fig. 3.6a. The meter is calibrated to a standard 400

PPM CO₂ concentration at the factory. It was received with following major specifications:

Function Range 0 to 9999 PPM

Resolution 1 PPM

Accuracy \pm (%5rdg + 50 PPM)

Pressure dependence: +1.6% reading per kPa deviation from normal pressure, 100 kPa

Sensor Type NDIR (non-dispersive infrared) technology

Operating Conditions 0 to 50°C

This meter has measurement limit of maximum 9999 PPM. However the measurement accuracy is reasonable within the limit of 5000 PPM. For instance, if the recorded value is 5000 PPM then the accuracy range is within 5000 \pm 300 PPM. Conversely, the concentration accuracy of CO₂ above 5000 PPM is not specified by the company.

Uncertainty analysis of CO₂ measurement revealed that the measured value lies within standard uncertainty of \pm 262 PPM. However, after deploying the correction factors, the expanded uncertainty estimated as \pm 60.78 PPM which again falls in 1.1% of the average concentration.

Table 3.4: Uncertainty of CO ₂ Measurement			
Concentration PPM	Residuals, PPM	Residuals ² , (PPM ²)	Calculations
5410	-20.7	428	Average Concentration 5430 PPM
5360	-70.7	4998	
5491	60.3	3636	Variance 68710 (PPM ²)
5302	-128.7	16563	
5047	-383.7	147225	Standard Deviation 262 PPM
5340	-90.7	8226	
5564	133.3	17768	Standard Uncertainty \pm 262 PPM
5763	332.3	110423	
5899	468.3	219304	Expanded Uncertainty $\pm(2 \times 1.16 \times 262 / 10) = \pm 60.78$ PPM
5131	-299.7	89820	

CO Meter:

CO meter shown in Fig. 3.6b was also imported from Extech of USA. The meter is calibrated to a standard CO concentration at the factory. It was received with following major specifications:

Measurement range 0-1000 PPM

Resolution 1 PPM

Accuracy $\pm 5\%$ or ± 10 PPM (whichever is greater)

Sensor Type Stabilized electrochemical Gas-specific (CO)

This meter can read maximum up to 1000 PPM CO concentration. The measurement accuracy is also quite reasonable within this limit. For instance, if the recorded value is 1000 PPM then the accuracy range is contained by 1000 ± 60 PPM.

Uncertainty analysis for CO measurement shows that the measured values are falling within standard uncertainty of ± 24 PPM. On the other hand, after corrections the estimated expanded uncertainty is calculated as ± 5.6 PPM which is within 1.6% of the mean value. So the measured data shows very insignificant discrepancies than that of the true value.

Table 3.5: Uncertainty of CO Measurement

Concentration	Residuals, PPM	Residuals ² , (PPM) ²	Calculations
351	16.1	259.21	Average Concentration 335 PPM
344	9.1	82.81	
352	17.1	292.41	Variance 574.10 PPM
361	26.1	681.21	
346	11.1	123.21	Standard Deviation 23.96 PPM
297	-37.9	1436.41	
305	-29.9	894.01	Standard Uncertainty ± 24 .
361	26.1	681.21	
315	-19.9	396.01	Expanded Uncertainty $\pm (2 \times 1.16 \times 24 / 10) = \pm 5.6$ PPM
317	-17.9	320.41	

PM meter:

A Particulate Matter (PM) counter shown in Fig. 3.6c was procured for measuring smoke emissions from biomass burning in the rural kitchen having particle sizes ranging from 0.3 to 10 μm . The model name of the PM meter is AEROTRAK™ Handheld Particle Counter Model 9306 and the origin is from the brand TSI of USA. It offers the most features and flexibility for versatile handheld particle contamination monitoring. This model complies with all the stringent requirements set forth in ISO 21501-4 calibrated at 0.3, 0.5, 1.0, 3.0, 5.0, 10.0 μm size channels in the TSI factory with NIST traceable PSL spheres. It can handle the six particle sizes of 0.3, 0.5, 1.0, 3.0, 5.0, 10.0 μm with following specifications:

Size Resolution <15% @ 0.5 μm (per ISO 21501-4 requirements)

Counting Efficiency 50% at 0.3 μm ; 100% for particles >0.45 μm

Concentration limit > 706,29,400 particles/ m^3 at 5% coincidence loss

Zero Count <1 count per 5 minutes (per ISO 21501-4 and JIS B9921)

Flow Rate 0.1 CFM (2.83 L/min) with $\pm 5\%$ accuracy

This device can capture data up to limit of 706,29,400 particles/ m^3 with 5% coincidence loss. Coincidence Loss is an error inherent to all light scattering technology. However the device accuracy is mainly configured with its particle counting efficiency. At a size of 0.3 μm this device can perform with 50% counting efficiency. However, it performs much better at >0.45 μm with 100% counting efficiency.

Certificate of the calibration was provided by the TSI, USA (see Appendix III). Calibrations were completed in the factory bench for known particle sizes of 0.296 μm , 0.498 μm , 0.994 μm , 3.06 μm , 5.02 μm and 10.2 μm . Following Table 3.6 shows standard uncertainty and standard deviations of the equipment. It is seen that % of deviations are quite sensible at all particle sizes. However, a maximum deviation of 2% is seen at a larger size of 10 μm and in the midrange it is even less than 1%.

Table 3.6: Standard Uncertainty and Deviation of PM Meter

Particle Sizes	Standard Uncertainty, μm	Standard deviation, μm	% deviation (approx.)
0.296	0.003	0.0053	1.7
0.498	0.0045	0.0079	1.6
0.994	0.0075	0.010	1.0
3.06	0.01	0.030	0.9
5.02	0.015	0.060	1.2
10.2	0.05	0.200	2

Uncertainty analysis of PM measurement is found to be very reasonable as presented in Table 3.7. The standard uncertainty falls within $\pm 89 \mu\text{g}/\text{m}^3$ and the expanded uncertainty is calculated as $\pm 20.7 \mu\text{g}/\text{m}^3$ which is convincingly within 3.7% of the average concentration.

Table 3.7: Uncertainty of PM Measurement

Concentration $\mu\text{g}/\text{m}^3$	Residuals, $\mu\text{g}/\text{m}^3$	Residuals ² , $(\mu\text{g}/\text{m}^3)^2$	
726	176.8	31258	Average Concentration 549 $\mu\text{g}/\text{m}^3$
675	125.8	15825	
573	23.8	566	Variance 7942 $(\mu\text{g}/\text{m}^3)^2$
538	-11.2	125	
556	6.8	46	Standard Deviation 89 $\mu\text{g}/\text{m}^3$
500	-49.2	2420	
456	-93.2	8686	Standard Uncertainty $\pm 89 \mu\text{g}/\text{m}^3$ Expanded Uncertainty $\pm(2 \times 1.16 \times 89/10) = \pm 20.7 \mu\text{g}/\text{m}^3$
472	-77.2	5959	
524	-25.2	635	
472	-77.2	5959	

3.4. Numerical Method

The purpose of this numerical study is to investigate the emission dispersion in both urban and rural kitchen of the developing countries like Bangladesh. Inside the kitchen space the flow has low velocity and pressure field and is moderately turbulent. The temperature variations of air will also occur due to advancement of the heat of combustion of the natural gas and temperature source of the biomass stove into the kitchen space. Therefore, the choice of an appropriate model is important for accurate and reliable predictions.

3.4.1. Transport Equations

In this section, the governing equations of mass, momentum, and energy conservation are presented. For this numerical study, the flow inside the kitchen space was considered as three dimensional, turbulent and incompressible. Air was used as a working fluid. The differential form of conservation equations for flow and heat transfer can be written as:

Conservation of Mass:

The general compact form of the continuity equation is

$$\frac{\partial}{\partial t}(\rho) + \nabla \cdot (\rho \vec{U}) = 0 \quad (3.1)$$

This equation can be expressed using the components of the velocity in three directions as follows,

$$\frac{\partial}{\partial t}(\rho) + \frac{\partial}{\partial x}(\rho u) + \frac{\partial}{\partial y}(\rho v) + \frac{\partial}{\partial z}(\rho w) = 0 \quad (3.2)$$

For steady,

$$\frac{\partial}{\partial x}(\rho u) + \frac{\partial}{\partial y}(\rho v) + \frac{\partial}{\partial z}(\rho w) = 0 \quad (3.3)$$

Conservation of Momentum:

The general compact form of the momentum equation can expressed as

$$\frac{D}{Dt}(\rho \vec{U}) = \nabla \cdot \sigma_{ij} + \rho g \quad (3.4)$$

Where the substantial derivative is, $\frac{D}{Dt}(\) = \frac{\partial}{\partial t}(\) + u \frac{\partial}{\partial x}(\) + v \frac{\partial}{\partial y}(\) + w \frac{\partial}{\partial z}(\)$.

The momentum equation can be expressed in words as

Density × (Local acceleration + convective acceleration) = Pressure force per unit volume + viscous force per unit volume.

The following are the momentum equations by component,

X – Momentum,

$$\left(\frac{\partial}{\partial t}(\rho u) + u \frac{\partial}{\partial x}(\rho u) + v \frac{\partial}{\partial y}(\rho u) + w \frac{\partial}{\partial z}(\rho u) \right) = \left(\frac{\partial}{\partial x}(\sigma_{xx}) + \frac{\partial}{\partial y}(\sigma_{yx}) + \frac{\partial}{\partial z}(\sigma_{zx}) \right) \quad (3.5)$$

Y – Momentum,

$$\left(\frac{\partial}{\partial t}(\rho v) + u \frac{\partial}{\partial x}(\rho v) + v \frac{\partial}{\partial y}(\rho v) + w \frac{\partial}{\partial z}(\rho v) \right) = \left(\frac{\partial}{\partial x}(\sigma_{xy}) + \frac{\partial}{\partial y}(\sigma_{yy}) + \frac{\partial}{\partial z}(\sigma_{zy}) \right) \quad (3.6)$$

Z- Momentum,

$$\left(\frac{\partial}{\partial t}(\rho w) + u \frac{\partial}{\partial x}(\rho w) + v \frac{\partial}{\partial y}(\rho w) + w \frac{\partial}{\partial z}(\rho w) \right) = \left(\frac{\partial}{\partial x}(\sigma_{xz}) + \frac{\partial}{\partial y}(\sigma_{yz}) + \frac{\partial}{\partial z}(\sigma_{zz}) \right) \quad (3.7)$$

$$\text{Where, } \sigma_{xx} = -p - \frac{2}{3} \mu (\nabla \cdot \vec{U}) + 2\mu \frac{\partial}{\partial x}(u); \quad \sigma_{yy} = -p - \frac{2}{3} \mu (\nabla \cdot \vec{U}) + 2\mu \frac{\partial}{\partial y}(v);$$

$$\sigma_{zz} = -p - \frac{2}{3} \mu (\nabla \cdot \vec{U}) + 2\mu \frac{\partial}{\partial z}(w)$$

$$\sigma_{xy} = \sigma_{yx} = \mu \left(\frac{\partial}{\partial y}(u) + \frac{\partial}{\partial x}(v) \right); \quad \sigma_{xz} = \sigma_{zx} = \mu \left(\frac{\partial}{\partial x}(w) + \frac{\partial}{\partial z}(u) \right);$$

$$\sigma_{yz} = \sigma_{zy} = \mu \left(\frac{\partial}{\partial z}(v) + \frac{\partial}{\partial y}(w) \right)$$

Conservation of Energy:

$$\rho \frac{D}{Dt}(h) = \frac{D}{Dt}(p) + \nabla \cdot (\lambda \nabla T) + \Phi \quad (3.8)$$

Change of enthalpy of the system = work due to change of fluid volume + heat influx through the surroundings + mechanical energy dissipation.

Representation of Energy equation by components,

$$\begin{aligned} \frac{\partial}{\partial t}(\rho h) + u \frac{\partial}{\partial x}(\rho h) + v \frac{\partial}{\partial y}(\rho h) + w \frac{\partial}{\partial z}(\rho h) &= \left(\frac{\partial}{\partial t}(p) + u \frac{\partial}{\partial x}(p) + v \frac{\partial}{\partial y}(p) + w \frac{\partial}{\partial z}(p) \right) + \\ &\left(\frac{\partial}{\partial x} \left(\lambda \frac{\partial}{\partial x}(T) \right) + \frac{\partial}{\partial y} \left(\lambda \frac{\partial}{\partial y}(T) \right) + \frac{\partial}{\partial z} \left(\lambda \frac{\partial}{\partial z}(T) \right) \right) + \Phi \end{aligned} \quad (3.9)$$

Where,

$$\Phi = \mu \left[\begin{aligned} &2 \left(\frac{\partial u}{\partial x} \right)^2 + 2 \left(\frac{\partial v}{\partial y} \right)^2 + 2 \left(\frac{\partial w}{\partial z} \right)^2 + \left(\frac{\partial v}{\partial x} + \frac{\partial u}{\partial y} \right)^2 + \left(\frac{\partial w}{\partial y} + \frac{\partial v}{\partial z} \right)^2 + \left(\frac{\partial u}{\partial z} + \frac{\partial w}{\partial x} \right)^2 \\ &- \frac{2}{3} \left(\frac{\partial u}{\partial x} + \frac{\partial v}{\partial y} + \frac{\partial w}{\partial z} \right)^2 \end{aligned} \right]$$

3.4.2. Turbulence Model

3.4.2.1. The k-epsilon Model

The turbulence kinetic energy (k) is the variance of the fluctuations in velocity. It has dimensions of ($L^2 T^{-2}$); for example, m^2/s^2 . The turbulence eddy dissipation (ε) is the rate at which the velocity fluctuations dissipate, and has dimensions of k per unit time ($L^2 T^{-3}$); for example, m^2/s^3 .

The $k - \varepsilon$ model introduces two new variables into the system of equations. The continuity equation is then,

$$\frac{\partial}{\partial t}(\rho) + \frac{\partial}{\partial x_j}(\rho U_j) = 0 \quad (3.10)$$

and the momentum equation becomes:

$$\frac{\partial}{\partial t}(\rho U_i) + \frac{\partial}{\partial x_j}(\rho U_j U_i) = -\frac{\partial}{\partial x_i} P' + \frac{\partial}{\partial x_j} \left[\mu_{eff} \left(\frac{\partial U_i}{\partial x_j} + \frac{\partial U_j}{\partial x_i} \right) \right] + S_M \quad (3.11)$$

where S_M is the sum of body forces, μ_{eff} is the effective viscosity accounting for turbulence, and P' is the modified pressure.

The $k - \varepsilon$ model, like the zero equation model, is based on the eddy viscosity concept. So the effective viscosity can be written as

$$\mu_{eff} = \mu + \mu_t$$

where μ_t is the turbulence viscosity. The $k - \varepsilon$ model assumes that the turbulence viscosity is linked to the turbulence kinetic energy and dissipation via the relation:

$$\mu_t = C_\mu \rho \frac{k^2}{\varepsilon}$$

where C_μ is a constant.

The values of k and ε come directly from the differential transport equations for the turbulence kinetic energy and turbulence dissipation rate:

$$\frac{\partial}{\partial t}(\rho k) + \frac{\partial}{\partial x_j}(\rho U_j k) = \frac{\partial}{\partial x_j} \left[\left(\mu + \frac{\mu_t}{\sigma_k} \right) \frac{\partial k}{\partial x_j} \right] + P_k - \rho \varepsilon + P_{kb} \quad (3.12)$$

$$\frac{\partial}{\partial t}(\rho \varepsilon) + \frac{\partial}{\partial x_j}(\rho U_j \varepsilon) = \frac{\partial}{\partial x_j} \left[\left(\mu + \frac{\mu_t}{\sigma_\varepsilon} \right) \frac{\partial \varepsilon}{\partial x_j} \right] + \frac{\varepsilon}{k} (C_{\varepsilon 1} P_k - C_{\varepsilon 2} \rho \varepsilon + C_{\varepsilon 1} P_{\varepsilon b}) \quad (3.13)$$

where $C_{\varepsilon 1}$, $C_{\varepsilon 2}$, σ_k and σ_ε are constants.

P_{kb} and $P_{\varepsilon b}$ represents the influence of the buoyancy forces. P_k is the turbulence production due to viscous forces, which is modeled using:

$$P_k = \mu_t \left(\frac{\partial U_i}{\partial x_j} + \frac{\partial U_j}{\partial x_i} \right) \frac{\partial U_i}{\partial x_j} - \frac{2}{3} \frac{\partial U_k}{\partial x_k} \left(3\mu_t \frac{\partial U_k}{\partial x_k} + \rho k \right) \quad (3.14)$$

For incompressible flow, $\frac{\partial U_k}{\partial x_k}$ is small and the second term on the right hand

side of the equation 4.14 does not contribute significantly to the production. In order to avoid the build-up of turbulent kinetic energy in stagnation regions, two production limiters are available.

3.4.2.2. Buoyancy Turbulence

Full buoyancy model is being used where the buoyancy production term P_{kb} is modeled as:

$$P_{kb} = - \frac{\mu_t}{\rho \sigma_\rho} g_i \frac{\partial \rho}{\partial x_i} \quad (3.15)$$

This buoyancy production term is associated with the k and ε equation. P_{eb} is assumed to be proportional to P_{kb} and must be positive, therefore it is modeled as:

$$P_{eb} = C_3 \cdot \max(0, P_{kb})$$

For the directional option, P_{eb} is modified by a factor accounting for the angle φ between velocity and gravity vectors:

$$P_{eb} = C_3 \cdot \max(0, P_{kb}) \cdot \sin \varphi$$

Default model constants are given by:

- $\sigma_\rho = 1$ for full buoyancy model and Dissipation Coefficient, $C_3 = 1$.

3.4.3. Combustion Model

This model works based on the turbulent mixing rate, Ri for the mean reaction rate of species i . It assumes that chemical reactions occur much faster than turbulence can mix reactants and heat into the reaction region. This assumption fits well with the combustion as the fuel burns at a faster rate. For fast reactions the reaction rate is limited by the turbulent mixing rate. The turbulent mixing rate is assumed to be related to the timescale of turbulent eddies that are present in the flow. This concept is originally introduced by Spalding (1971) and later generalized by Magnussen and Hjertager (1976). The timescale used for this purpose is the so-called eddy lifetime, $\tau = k/\varepsilon$, with k being the turbulent kinetic energy and ε the turbulent dissipation rate. Chemistry typically described by relatively simple single or two step mechanism.

The net rate of production of species i due to reaction r , $R_{i,r}$ is given by the smaller (i.e. limiting value) of the two expressions below.

Based on mass fraction of reactants:

$$R_{i,r} = \nu'_{i,r} M_{w,i} A \rho \frac{\epsilon}{k} \min \left(\frac{Y_{\mathcal{R}}}{\nu'_{\mathcal{R},r} M_{w,\mathcal{R}}} \right) \quad (3.16)$$

Based on mass fraction of products:

$$P_{i,r} = \nu'_{i,r} M_{w,i} A B \rho \frac{\epsilon}{k} \frac{\sum_P Y_P}{\sum_j^N \nu''_{j,r} M_{w,j}} \quad (3.17)$$

Where

- k - turbulence kinetic energy
- ϵ - turbulence dissipation rate
- Y_P, Y_R - mass fraction of species
- A - Magnussen constant for reactants (default 4.0)
- B - Magnussen constant for products (default 0.5)
- $M_{w,i}$ - molecular weight
- $(R), (P)$ - reactants, products

The Eddy Dissipation model is the best applied to turbulent flows when the chemical reaction rate is fast relative to the transport processes in the flow. There is no kinetic control of the reaction process. For the Eddy Dissipation model it is sufficient that fuel and oxidant be available in the control volume for combustion to occur.

3.4.3.1. Species Transport Equation for Source

The i^{th} species mass fraction transport equation is given by the following equation

$$\frac{\partial}{\partial t}(\rho Y_i) + \frac{\partial}{\partial x_j}(\rho u_j Y_i) = \frac{\partial}{\partial x_j} \left(\rho D_i \frac{\partial Y_i}{\partial x_j} \right) + R_i + S_i \quad (3.18)$$

Where,

- Y_i - The mass fraction of chemical species i
- D_i - Diffusion coefficient
- R_i - Reaction source term. Chemical reactions are modeled as source terms in the species transport equation.
- S_i - includes all other sources.

The differential form of the species transport equation (3.18) is simultaneously solved for all species in the rural kitchen as well such as CO₂, CO, PM dispersion.

3.5. Grid Independence Test

Grid independence test of the numerical solutions is a must needed step for achieving accuracy of the predictions. The numerical approach remains imperfect unless the solutions are tested for independency on the computational grid. However, optimization of the total number of cells and nodes within the domain is an essential part of the numerical study to attain least use of time and computational resources.

For the grid independence test of the urban kitchen, three computational grid systems with 0.3, 0.7 and 1.3 million cells, respectively, were adopted for comparison. The pressure (Fig. 3.7) and temperature profiles (Fig. 3.8) are compared for all three different grid systems for the model without (Fig. 3.7a and Fig 3.8a) and with hood system (Fig. 3.7b and Fig. 3.8b). The results are plotted along the vertical line (along Z direction) at the middle of the investigated plane (breathing plane). Based on these comparisons it was concluded that the converged solution can be obtained for both models with a grid system of about 1.3 million cells for the entire domain in order to facilitate computational effort with reasonable accuracy.

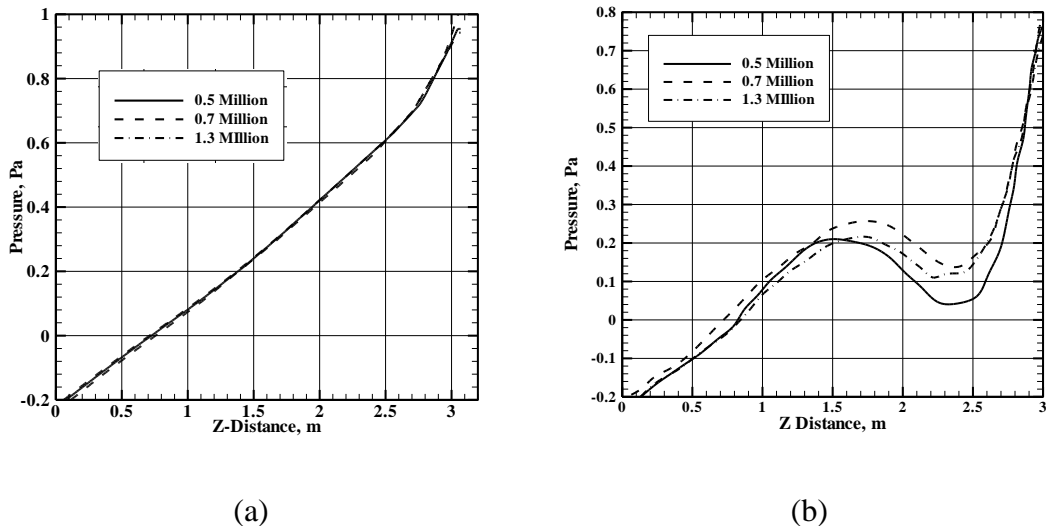


Fig. 3.7: Pressure distributions for grid independency test (a) for domain without hood and (b) for domain with hood.

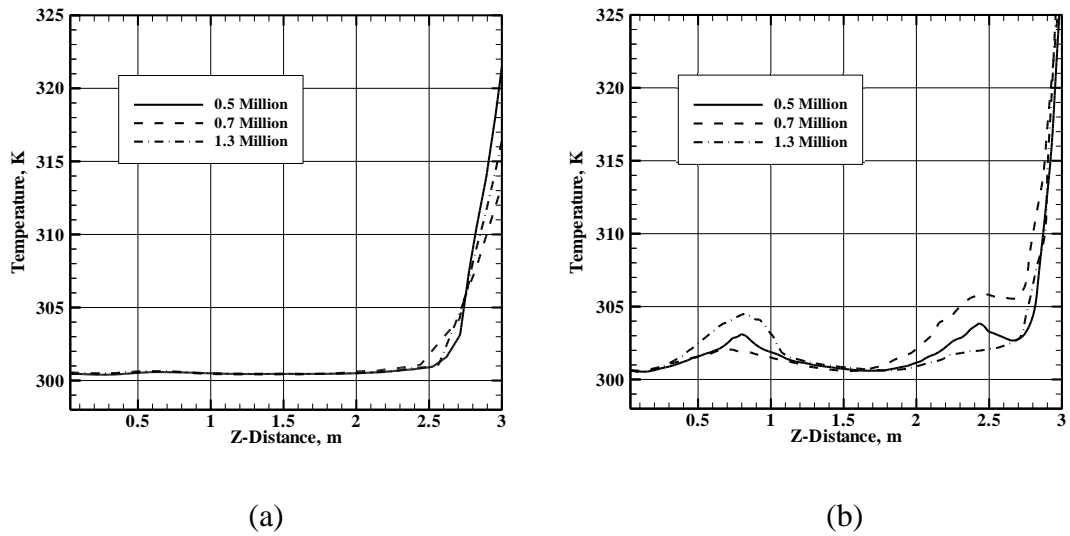


Fig. 3.8: Temperature distributions for grid independency test at (a) for domain without hood and (b) for domain with hood.

On the other hand, for the grid independence test of the rural kitchen model, three different computational grids comprising of 1.06, 1.29 and 2 million cells were used. The resulting temperature and velocity profiles were compared for these three different grid system and shown in Fig.3.9 a and b, respectively. Based on comparisons, 2 million cells for the whole domain were adopted.

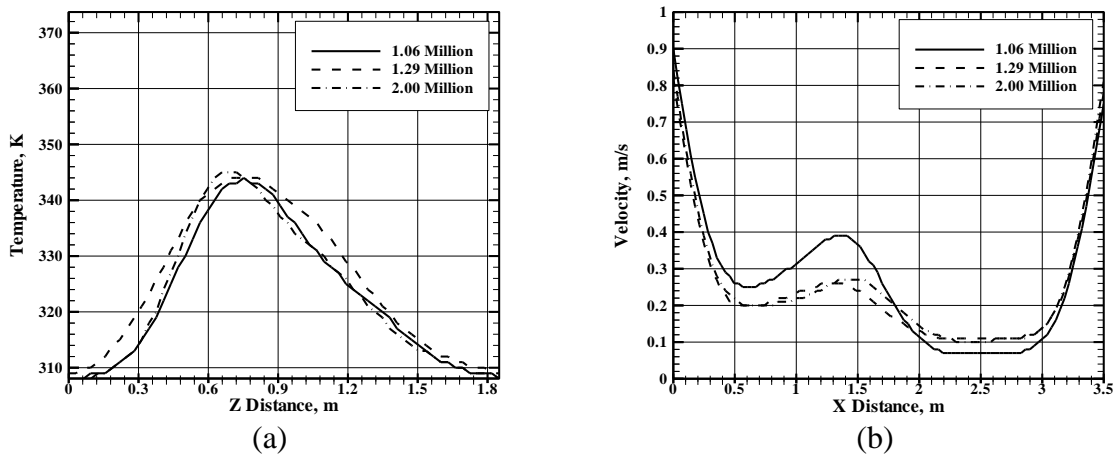


Fig. 3.9: Grid independence test for the rural kitchen model (a) temperature profile (b) velocity profile.

Chapter 4

4. Study of Urban Kitchen

In this section, both experimental and numerical results of urban kitchen have been analyzed for different conditions. There are two kitchens preferred for the experiment in Uttara and Kolabagan area of Dhaka city, the capital of Bangladesh. The urban kitchen 1 at Uttara comprised of one open door, one window, one small exhaust fan and two burners stove where the urban kitchen 2 at Kolabagan consisted of single door (open or close), one close window, two burners stove and without exhaust systems. The experiments were carried out for temperature and emissions of the pollutant in particular CO₂. Later section covers analyses of numerical results of a typical kitchen model followed by discussions of different test cases, grid systems, code validation etc.

4.1. Measurement of Temperature and Emission

Figure 4.1 is presented for temperature profiles in urban kitchen 1 and 2. Temperature was recorded at five distinct positions in a vertical line passing the breathing point. Probe 1 and probe 5 measured temperatures near the floor and the roof, respectively. The breathing point temperature is recorded by the probe 2 in both cases. It is seen that the temperature is significantly higher near the roof and increases gradually with time to reach steady at around 1500 seconds of time elapsed. Flat distributions are observed for urban kitchen 1 where the fresh air influx takes place through the door. On the other hand stepper distributions are recorded for closed urban kitchen 2. The temperature near the roof reaches maximum 74°C where kitchen 1 shows 56 °C. At the breathing point kitchen 1 shows 36 °C and kitchen 2 shows 48°C that are well beyond the comfort limit of room temperature (see Fig. 10 a and b).

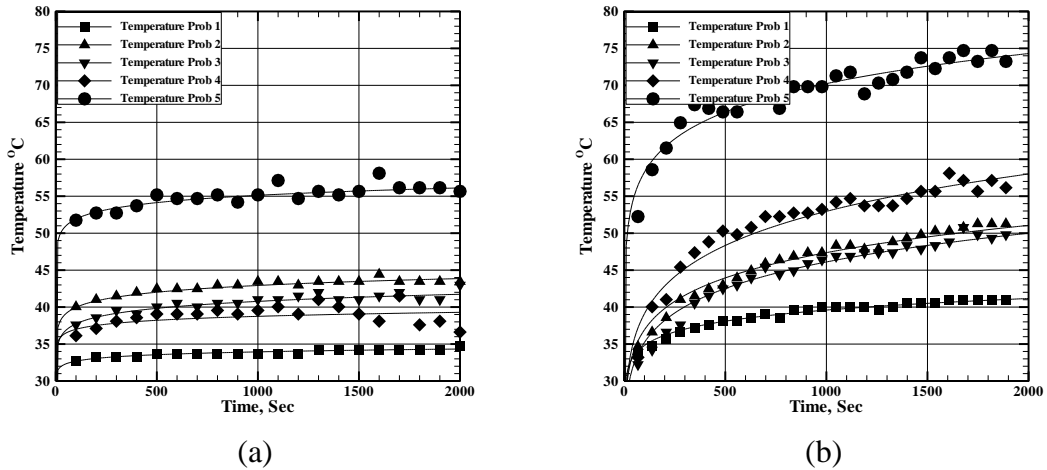


Fig. 4.1: Temperature profiles at five locations on a vertical line passing the breathing point (a) for urban kitchen 1 and (b) for rural kitchen 2.

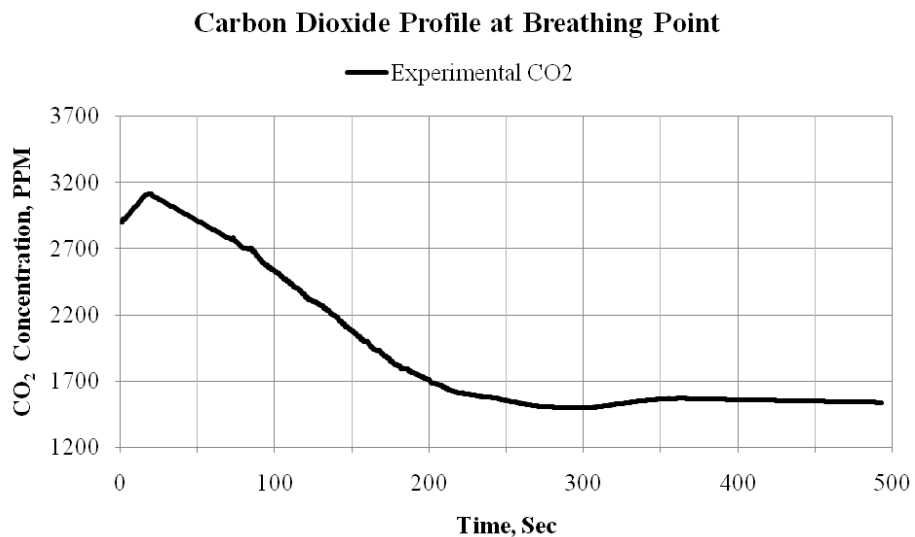


Fig. 4.2: CO₂ profile at the breathing point for urban kitchen 1.

Both kitchens consisted of two burners stove and natural gas was the burning fuel. In the presence of sufficient air when combustion take place CO₂, water and trivial amount of the other constituents are produced. Therefore, it is to be verified how clean the air is after natural gas burning and the level of CO₂ concentration in the kitchen more particularly at the breathing zone. Fig. 4.2 is presented for CO₂ concentration variations over the time at the breathing point of urban kitchen 1. It shows that the concentration increases to about 1600 PPM and then decreases to 1400 PPM. All these time dependent data signify that the dispersion of emission and

dissipation of heat are highly unsteady in nature. For urban kitchen 2 (see Fig. 4.3), it is observed that the concentration increases from 3600 PPM to 4500 PPM. At such a high level of concentration headache, loss of attention, loss of consciousness, increased heart rate may occur at long term exposure.

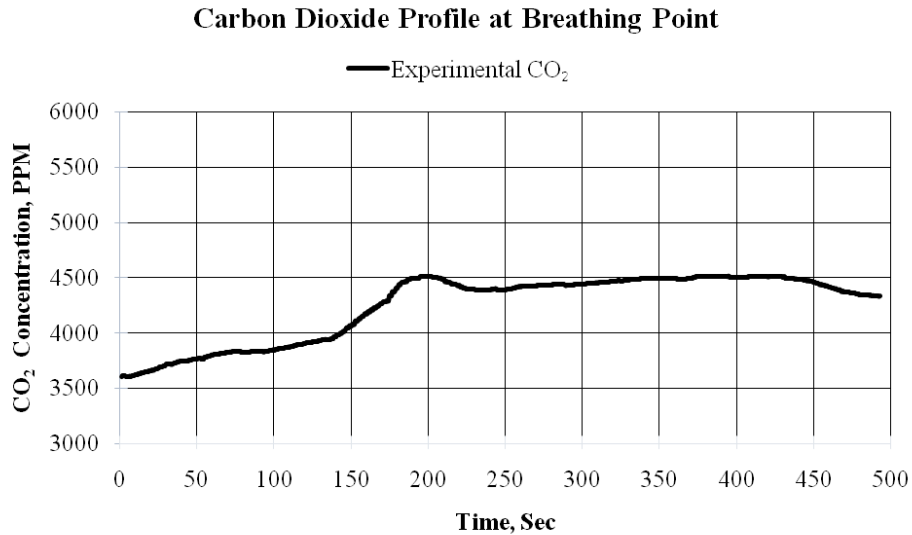


Fig. 4.3: CO₂ profile at the breathing point urban kitchen 2.

4.2. Numerical study of Urban Kitchen

A numerical model has also been developed for urban kitchen Indoor Air Quality (IAQ) study. In the present study, one typical urban kitchen was modeled and simulated using three dimensional CFD code ANSYS CFX-12.1 [3]. The Computational Fluid Dynamics (CFD) model integrates the effects of airflow and thermal characteristics and associated emissions to understand the detailed distributions of concentrations, airflow, and temperature inside the kitchen. Different steps of computational processes are illustrated in Appendix IV.

The computational domain consisted of heat sources resembling as burners, door, wall boundaries and exhaust systems. High resolution second order accurate advection scheme was used to discretize the equations for the flow, turbulent kinetic energy, and turbulence eddy dissipation. The $k-\varepsilon$ turbulence model was adopted for the turbulence closure as it was employed by Kajtar and Leitner [15] in their

simulation work. Table 4.1 shows details of the boundary conditions. The kitchen space is filled with air in the model and the combustion of natural gas occurs in the burners in all cases of urban kitchen. In CFX, Eddy Dissipation Model (EDM) is used for combustion simulation. Combustions take place in the presence of air while the fuel is leaving the burner at a rate of 0.5 m/s. Table 4.2 illustrates six different cases with different exhaust conditions. Case 1 is designated for the study of without ventilated condition. An open vent is introduced at the wall in Case 2 for the effect of natural ventilation where Case 3 is designed for the study of the effect of forced ventilated condition. Case 4 is a case of forced ventilation and is designed for kitchen hood system with an exhaust velocity of 1.5 m/s. On the other hand Case 5 and Case 6 are designated for the study of the position of the vent at the front and base of the stove. Therefore, all cases have been organized in such a way that the effects of different ventilated conditions under both natural as well as force can be well understood. It also allows comparing the results with the space of having no ventilation.

Table 4.1: Details of Boundary Conditions

Table 4.1: Details of Boundary Conditions		
Boundary Conditions	Validation Case Posner et al. [1]	Test Cases
Inlet	0.235 m/s normal speed	Fuel 0.5 m/s Door open-1 atm
Outlet	1 atmospheric pressure	Vent close open-1atm 1.5 m/s 0.5 m/s Hood 1.5 m/s
Turbulence Intensity	1%	1%
Working Fluid	Air at 25 ⁰ C	Methane Air Mixture
Buoyancy Effect	No	Yes
Turbulence Model	k-ε	k-ε
Combustion model	No	Eddy Dissipation Model
Wall	Adiabatic, no slip	Adiabatic, no slip
Advection Scheme	High Resolution (2 nd order)	High Resolution (2 nd order)

Table 4.2: Different cases of Urban Kitchen Study

Test Cases	Test Variable	Ventilation types
Validation	Posner et al. [1]	---
Case 1	Close vent	No ventilation
Case 2	Open vent	Natural ventilation
Case 3	1.5 m/s vent	Forced ventilation
Case 4	1.5 m/s kitchen hood	Forced ventilation
Case 5	Front vent 0.5 m/s	Forced ventilation
Case 6	Base vent 0.5 m/s	Forced ventilation

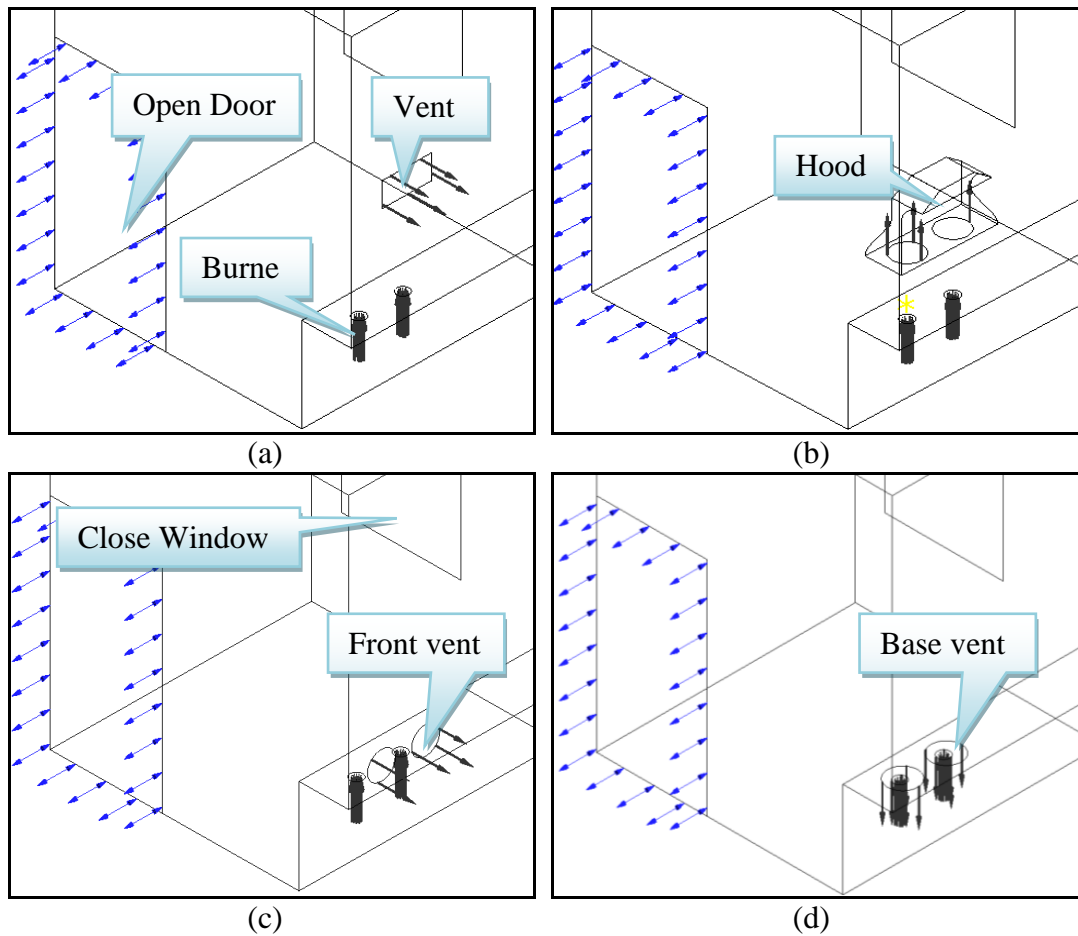


Fig.4.4: Computational domain with boundary for (a) typical vent (Case 1, Case 2 and Case 3), (b) kitchen hood (Case 4), (c) front vent (Case 5) and (d) base vent (Case 6).

All the cases of urban kitchen have been illustrated with Fig. 4.4. The common domain shown in Fig. 4.4a is used for Case 1, Case 2 and Case 3 by only varying the boundary conditions at the vent. Figure 4.4b shows domain for Case 4

(with kitchen hood), whereas Fig. 4.4c and 4.4d shows position of the front vent and base vent, respectively. All the cases have a single door where open type boundary condition was imposed. Though there was a provision for window in the kitchen however for simulation the window was considered close following the usual scenario of majority of residential kitchen. The position of the double burner source is identical in all cases.

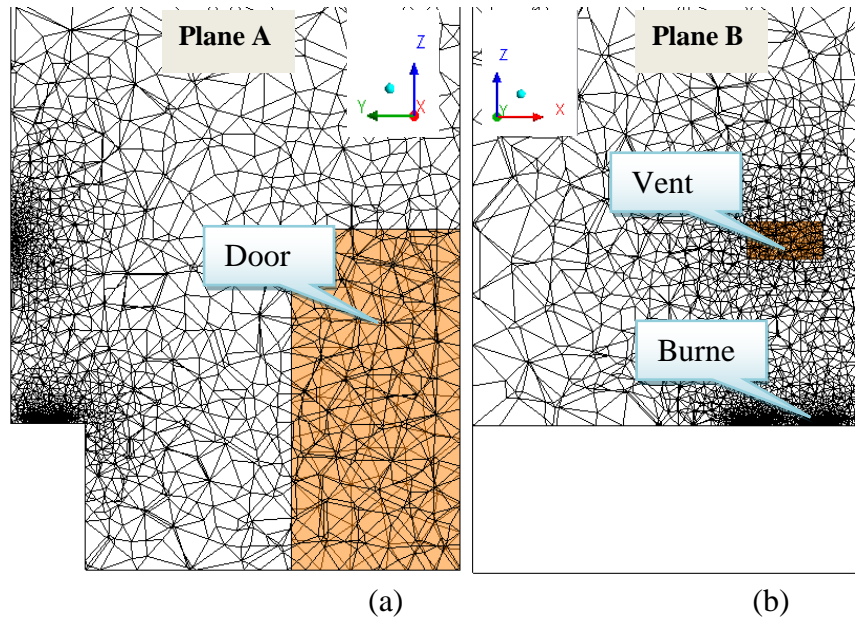


Fig. 4.5: Computational grid of the model at (a) plain A (b) plain B.

An unstructured tetrahedral grid was adopted for the entire domain and is shown in Fig. 4.5 at different cross-sectional planes, named as Plane A and Plane B. Appropriate attention was given in the combustion zone where gradient of the flow variables are expected to be significant. Since the real combustion is modeled and heat is convecting into the space due to burning of the natural gas, a very smooth grid transition from finer to coarser was maintained so that the information can be transmitted between the cells with reasonable accuracy. This can be further illustrated with Fig. 4.6. Few regions are given more importance while generating computational grids. Among them burners and vents (Fig. 4.5a) and hoods (Fig. 4.6b) are the regions of importance. The grids are refined enough in these two regions. In burner region, high degree of grid resolutions were maintained as the combustion is happening. Figure 4.7 shows the grid generated for the burners and burner's holes. It can be seen that, the transition from fine to coarse grid is very smooth and sufficient

number of cells are allocated in the burner holes that ensures both grid independency and solution accuracy.

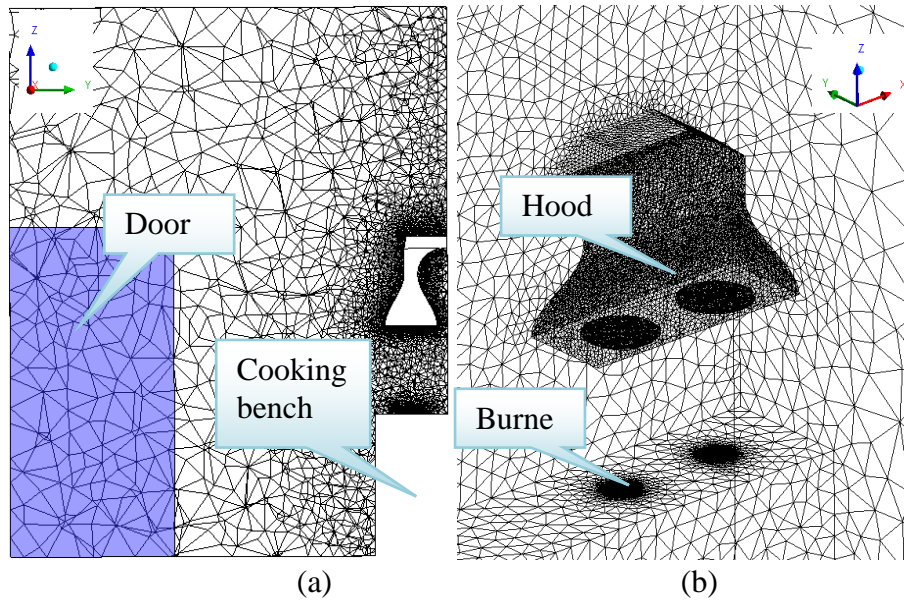


Fig. 4.6: Computational grid of the model (a) at plain A (b) isometric.

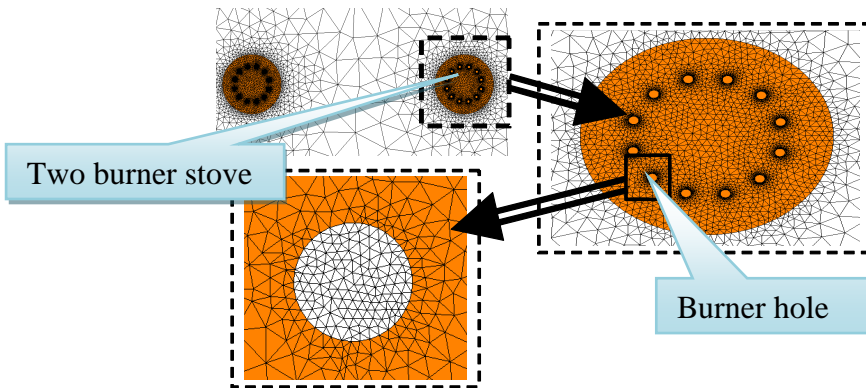


Fig. 4.7: Computational grids of two burners.

4.2.1. Code Validation

For any numerical study in particular to engineering applications, it is a common practice to achieve grid independency of the solution and convincing comparison between the experimental and numerical data. In doing so, the experimental work of Posner et al. [1] was considered for validation of the present study. In the work of Posner et al. [1], measurements were carried out for indoor air flow inside the model room. In their study conventional numerical results have been compared with the experimental results obtained by Laser Doppler Anemometry (LDA) and Particle Image Velocimetry (PIV). In the numerical part, they have used

k- ϵ turbulence model for the air flow simulation. Their experimental test conditions were imposed to simulate same model room as a validation case of the present study. Details of boundary conditions can be seen in Table 4.1 for the validation case. In their study, experimental data for only two parameters namely, axial velocity and v-velocity were available. Therefore, only these two sets of data were used for the validation in this present study.

A steady state simulation was performed with adiabatic wall condition to compare the numerical results with the experimental data. The numerically calculated values of axial velocity and v-velocity were compared with the corresponding experimental data and shown in Figs. 4.8 a and b, respectively. The comparisons with reasonable agreement build the confidence that the current numerical method can be adopted for the kitchen ventilation simulation to study air flow characteristics within the modeled space.

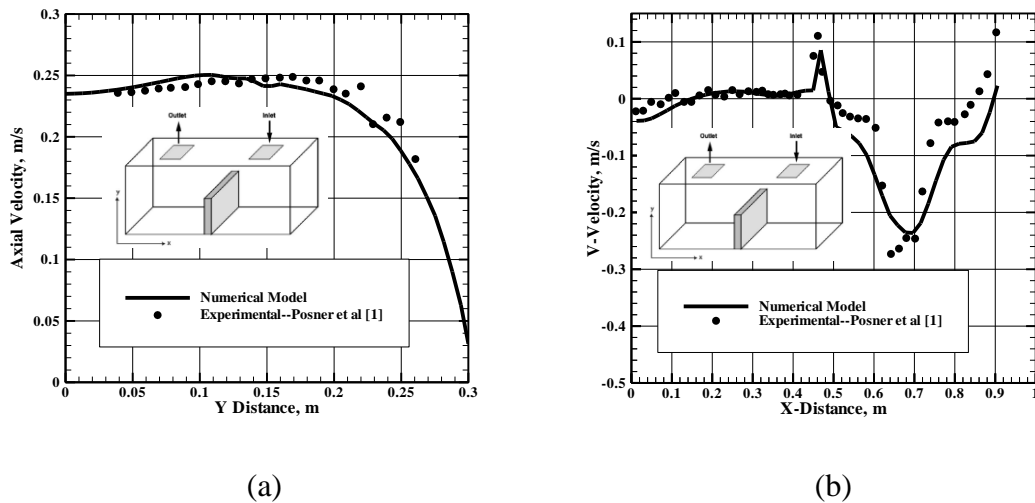


Fig. 4.8: Comparison between numerical and experiment a) axial velocity distributions and b) v-velocity distributions.

In order for compelling assessments, further experiments and simulations were conducted for the current study and the results are presented in Table 4.3 and 4.4. Table 4.3 shows comparison between numerical and experimental data for urban kitchen 1. It is seen that at the breathing point both temperature and concentration differed by 6% and 4.7% respectively. At the breathing point of urban kitchen 1, the

average experimental and numerical results are 1434 PPM and 1505 PPM respectively and the urban kitchen 2 showed 4246 PPM and 4720 PPM respectively (see Table 4.3 and 4.4). In both cases the concentrations are within 10% discrepancies and the temperatures are within 6%. Therefore it seems that the steady state simulations can well capture the flow and dispersion phenomenon of the pollutants.

Table 4.3: Comparison between Numerical and Experimental Data for urban kitchen 1

Test Cases	Avg. Experimental	Avg. Numerical	% of Difference
Temperature at Breath point	33 ⁰ C	31 ⁰ C	6%
CO ₂ at Breath Point	1434 PPM	1505 PPM	4.7%

Table 4.4: Comparison between Numerical and Experimental Data for urban kitchen 2

Test Cases	Avg. Experimental	Avg. Numerical	% of Difference
Temperature at Breath point	37 ⁰ C	35 ⁰ C	5.4%
CO ₂ at Breath Point	4246 PPM	4720 PPM	10%

4.2.2. Velocity and Temperature Field

In the following section, detailed investigations have been made on the nature of the velocity and temperature field inside the kitchen. In order to have discussions more compelling, a comparative study among the cases are presented at three critical locations. Those are Line 1, Line 2 and Breathing plane as shown in Fig. 4.9. Line 1 is located near the door to assess the nature of the air circulations through the door and Line 2 is located above the cooking bench in front of the vent to investigate nature of the exhaust flow. The only plane is selected at a section where the critical flow field characteristics around the burner, portion of the vent and vent wall, and 3-dimensional nature of the air circulations through the door can be well demonstrated and understood.

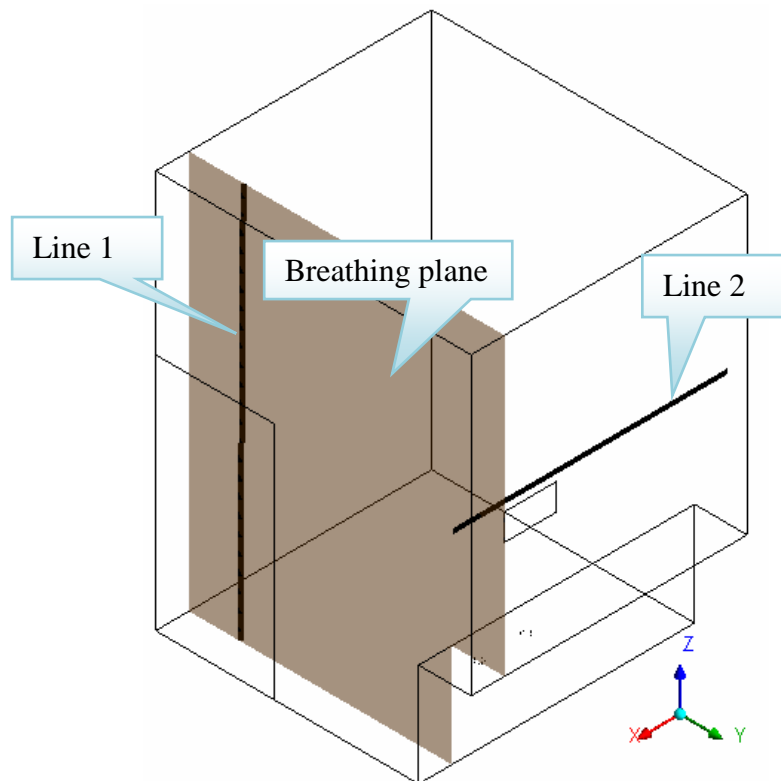


Fig. 4.9: Locations of the investigated plane and lines.

Figure 4.10 shows velocity distributions at the breath-plane section (shown in Fig. 4.9). The u -velocity ranges from -0.5 m/s to 0.4 m/s in the direction normal to the plane. The velocity vectors are normalized and showing the flow in y and z directions. As seen in the Fig. 4.10, the flow patterns are almost identical in all cases. However, the magnitudes are varying in all directions. The region E is marked as the breathing zone. It is observed that this zone is acting like a source from which the flow is spreading in all directions. In contrary, for Case 4 the flow pattern is completely different than the other cases. Here the source point does not appear and also the air turbulence is more around the hood system. The air circulations through the door can be illustrated with the u -velocity contour. Air is entering through upper section of the door and leaving through the lower section. It can be seen that strong air circulations occur for Case 1, in absence of ventilation (A of Fig. 4.10a). The strength of circulations gradually reduces from Case 2 (B of Fig. 4.10b) to Case 3 (C of Fig. 4.10c). The strength of circulations reduces in Case 4 after using the hood system (Fig. 4.10d). The outflow area coverage at the lower section of the door for both Cases 1 and 2 is greater as compared to Case 4.

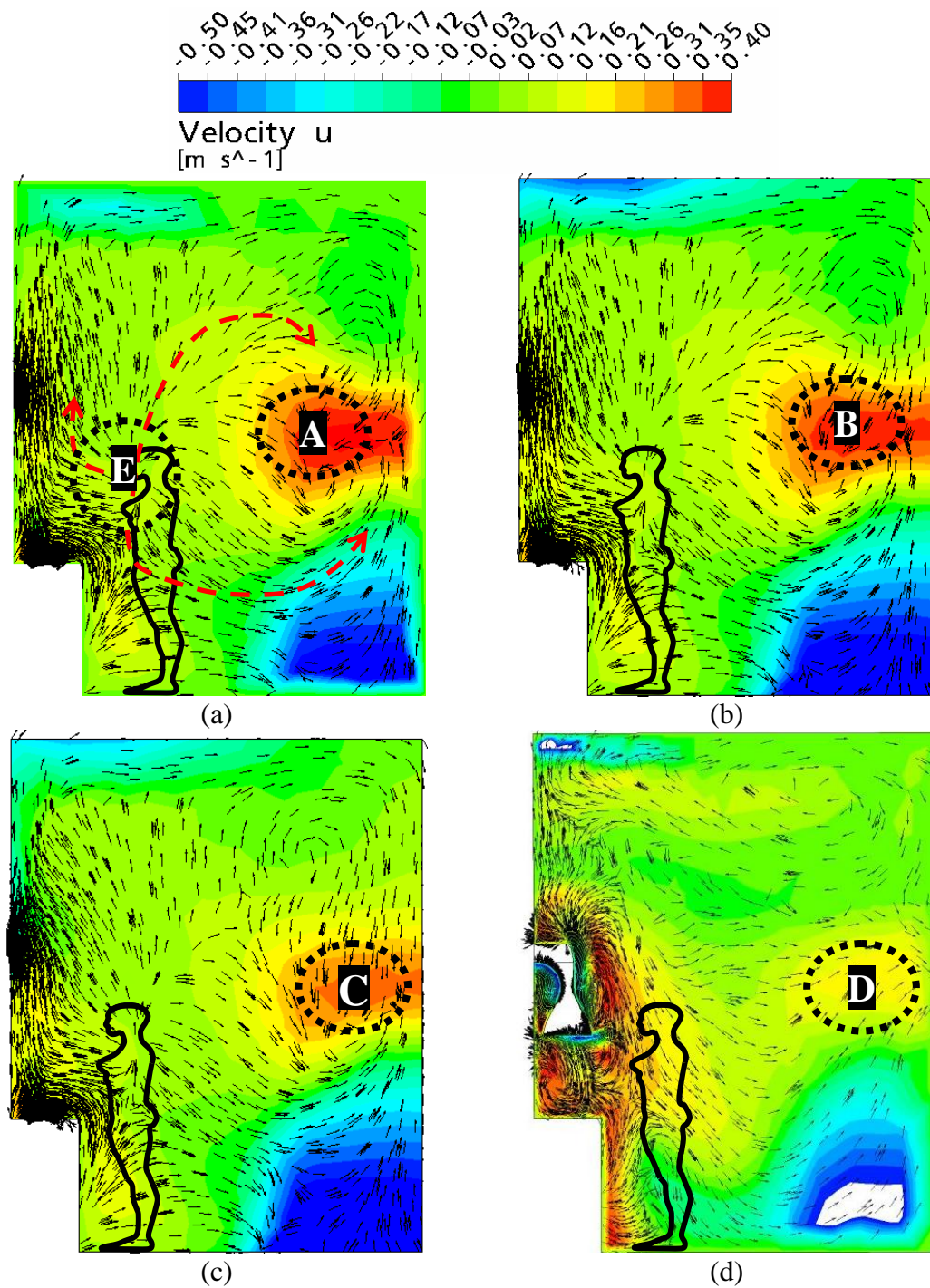


Fig. 4.10: 3-D velocity distributions at the investigated plane of a) Case 1, b) Case 2, c) Case 3 and d) Case 4.

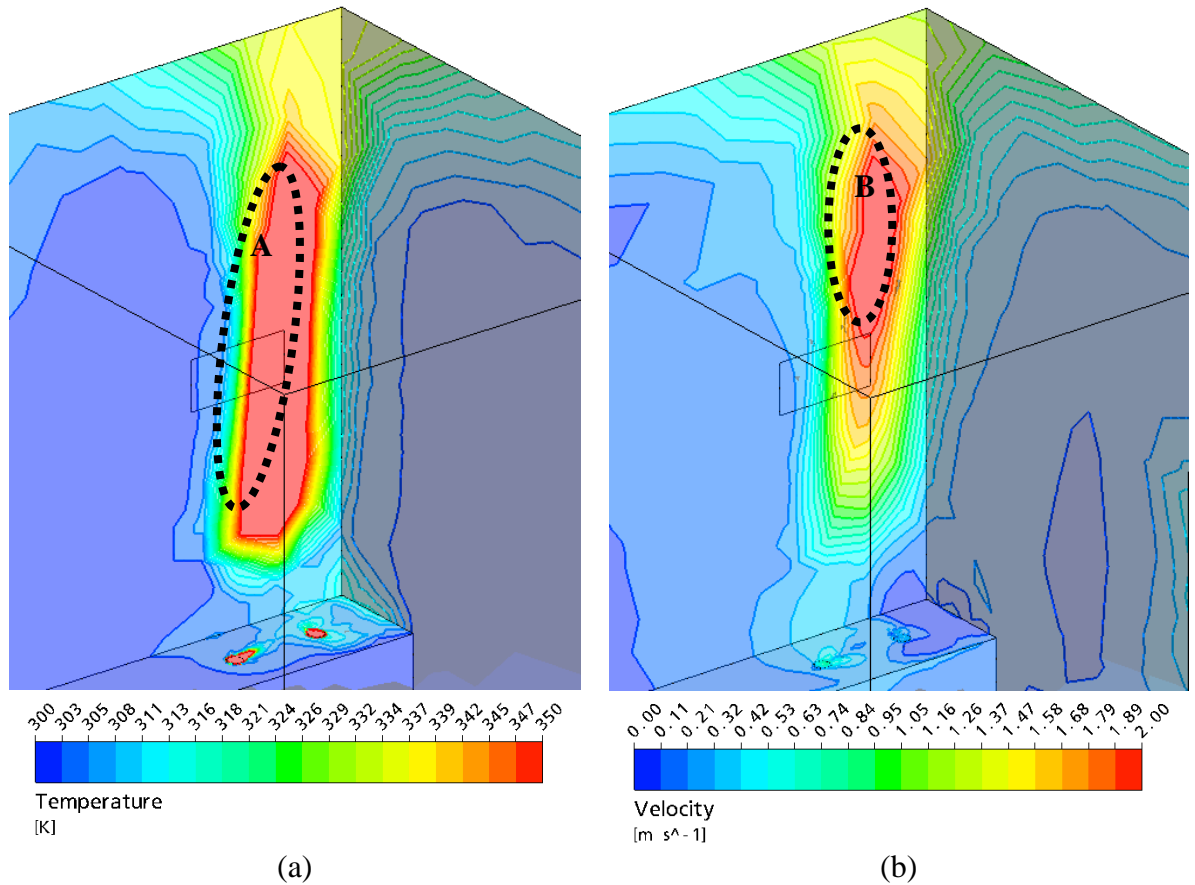


Fig. 4.11: a) Wall Temperature distributions, and b) velocity of flow close to wall surface, for Case 1.

Figure 4.11 is presented for Case 1, the most extreme condition in which there is no ventilation system. It can be seen from Fig. 4.11a that high temperature region (A) is covering about 40% of the vent area. This is because of the shift of high temperature flow towards the kitchen corner. As a whole, the region all above the burners is highly critical due to higher temperature distributions. The cook might be in a safer position because of standing a little far from the burners. However, the cooking zone still remains uncomfortable since the temperature is always seen higher than the comfort temperature. On the other hand, it can be seen from Fig. 4.11b that the velocity is significantly higher right above the vent corner region (B). Within this region, the maximum velocity is around 2 m/s. Therefore, the exhaust system should be designed and located in such a manner that it could work efficiently to blow out high temperature flow stream from the space continuously.

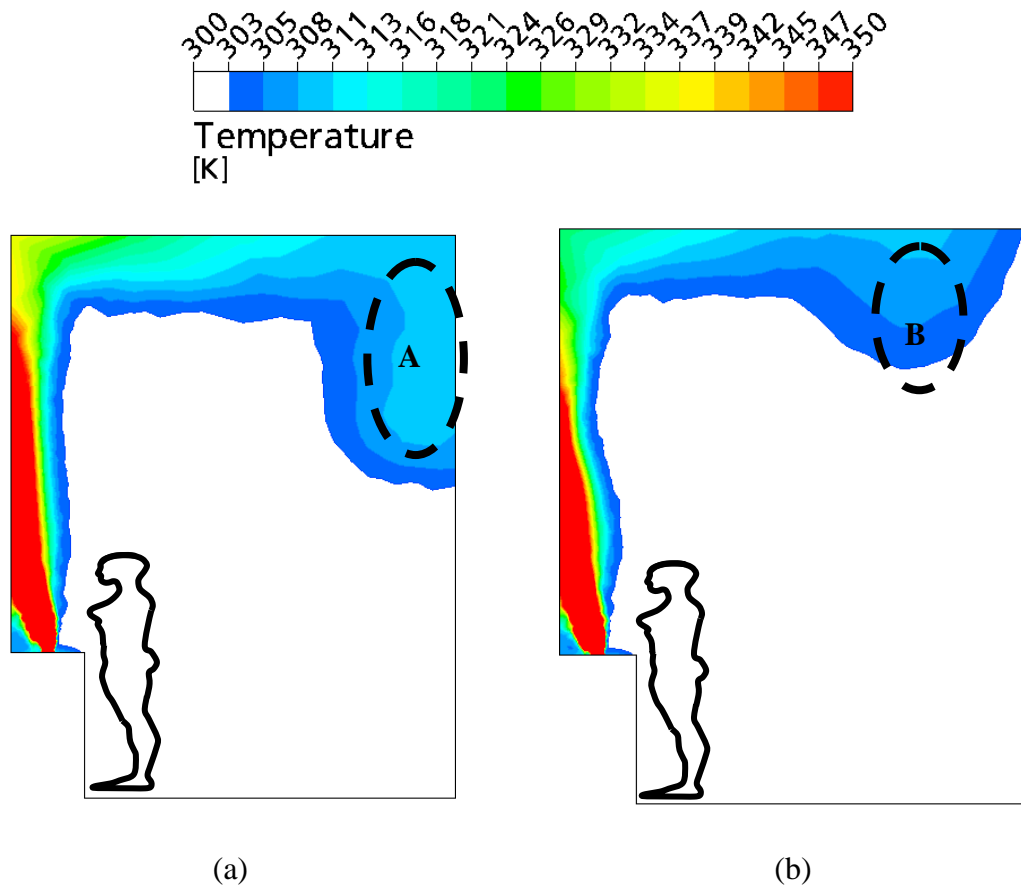


Fig. 4.12: Temperature distributions at plane 1 of a) Case 1 and b) Case 3.

Temperature distributions in the investigated plane are presented in Fig. 4.12 for Case 1 and Case 3. It is seen that, the temperature is always higher above the cooking bench and spreads vertically towards the roof. Zone B in Case 3, shows relatively low temperature in comparison to Case 1 because high temperature flow stream is forced out of the space through the vent. On the other hand, far from the cooking bench on the door side upper section the temperature seems relatively higher for Case 1 as compared to Case 3. This might be the cause of high temperature stream spreads more under no ventilated condition and thereby, increase the rate of inflow and outflow of air through the door as seen in Fig. 4.10 a and c.

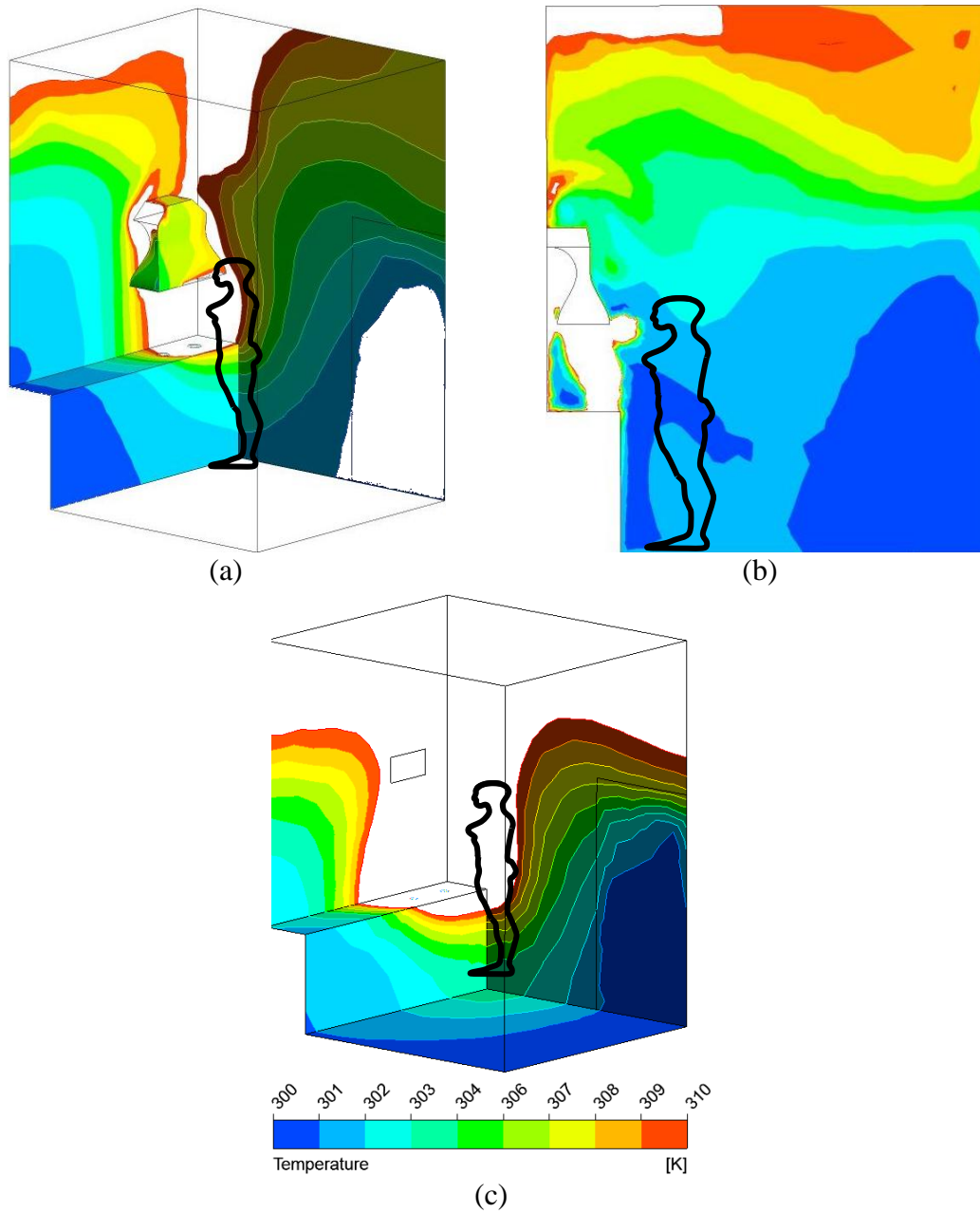


Fig. 4.13: (a) Wall Temperature distributions for Case 4, and (b) Temperature at the plane for Case 4 and (c) Wall Temperature distributions for Case 1.

Fig. 4.13 shows temperature distributions on the wall surfaces for the Case 4 with kitchen hood system and Case 1. It can be seen from Fig. 4.13a that high temperature zone still remains in the corner. However it spreads less than the Case 1. This is because of the exhaust system efficiently blows out high temperature flow

stream from the space continuously and replaces hot air with the fresh air. So the region all above the burner shows to higher temperature distributions.

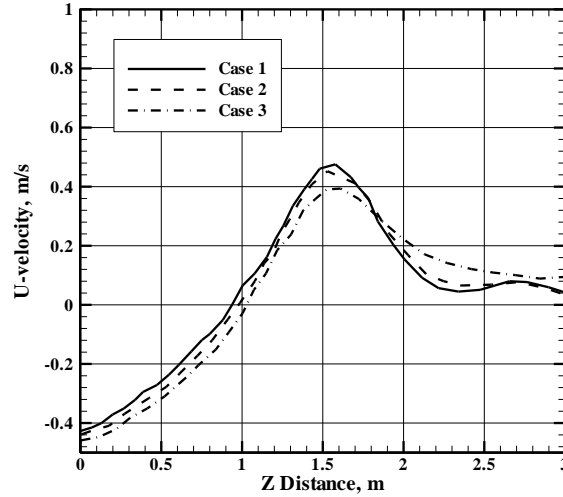


Fig. 4.14: U-velocity distributions along Line 1.

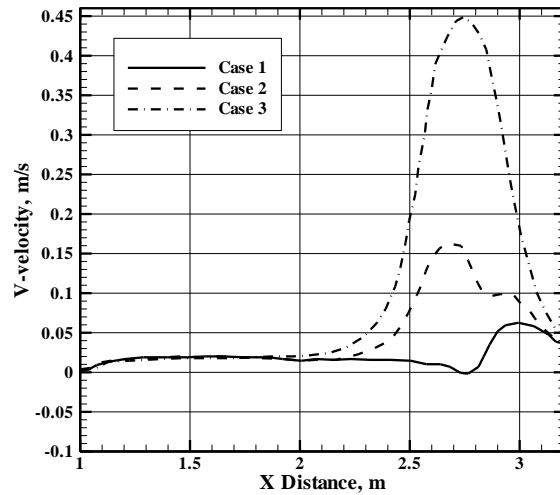


Fig. 4.15: V-velocity distributions along Line 2.

In order to quantify the results obtained from the simulations, Line 1 and Line 2 are selected to present the local velocity and temperature distributions and make comparisons among the cases. The u-velocity distributions are presented in Fig.4.14 along the vertical line 1. The flow for all cases follows similar trend but has differences in magnitudes. The air circulates through the door at a velocity of -0.6

m/s to 0.4 m/s in the normal direction. The effect of ventilation can be illustrated using V-velocity distribution (Fig. 4.15) which is essentially in the direction of the vent along the line 2. A significant difference of velocity is observed between Case 2 and Case 3 in the ventilation zone. Natural ventilation induces maximum of 0.16 m/s of flow in the y-direction in compared to Case 1. This is, however, increased to 0.44 m/s for Case 3.

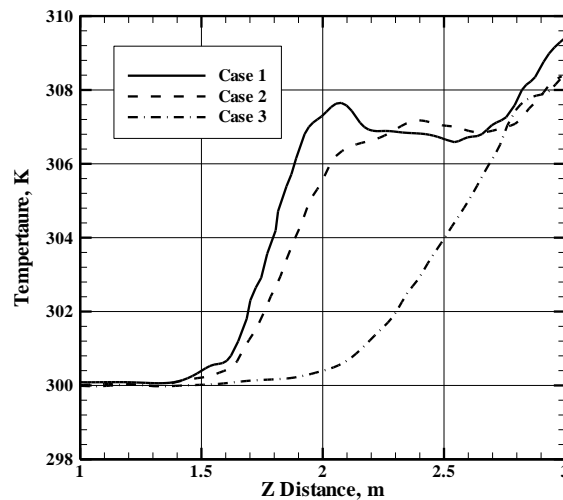


Fig. 4.16: Temperature distributions along Line 1.

Fig. 4.16 shows temperature distributions along the Line 1. It is seen that the temperature remains constant until 0.4 m height from the floor and then a significant discrepancies are observed. The reason for constant temperature over the length of 0.4 m is the mixing of outdoor fresh air with the indoor air. The mixing occurs in this region so effectively that the temperature does not increase even by one degree. Above this height, the temperature trend is seen similar between Case 1 and 2. However, through introducing the force ventilation system, the temperature can be lowered by 8°C at 1 m distance from the floor. The effect of ventilation on temperature is shown in Fig. 4.17 along the line 2. It is seen that the peak temperature for Case 3 is lowered by 12 °C in compared to Case 1 and 8 °C in compared to Case 2.

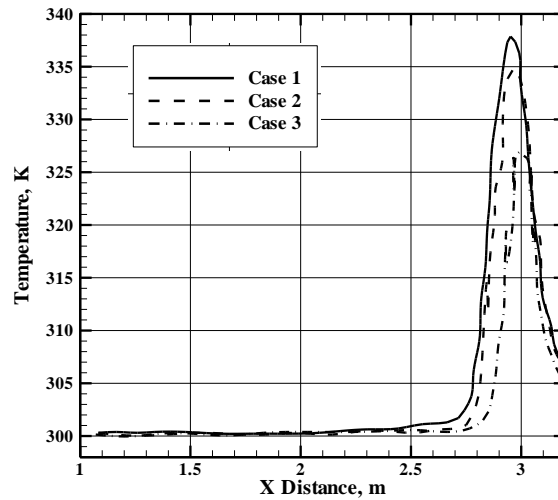


Fig. 4.17: Temperature distributions along Line 2.

4.2.3. Kitchen Indoor Emission

4.2.3.1. Without Ventilation

The numerical results for different cases of without ventilation at locations namely X-breath, Y-breath and Z-breath, shown in Fig. 4.18, are presented in this section. The X-breath is located close to the cooking bench and assessed the nature of the air circulations and CO₂ concentrations in lateral direction. Y-breath is located on the breath-plane in longitudinal direction and Z-breath is a vertical line on the breath-plane. As shown in Fig. 4.18, all these lines are passing through the breathing point. The position of the breathing point is $x=2.75\text{m}$, $y=2.3\text{m}$ and $z=1.37$. For completeness of this study and to have more effective analyses of the results, all these three lines are considered for X-Y plotting. For comprehensive demonstration and understanding of the critical flow field characteristics around the burner, around the kitchen hood system, and 3-dimensional nature of the air circulations, a breathing plane is preferred [see Fig. 4.18]. Figure 4.19 demonstrates the presentation of numerical data for kitchen with hood system.

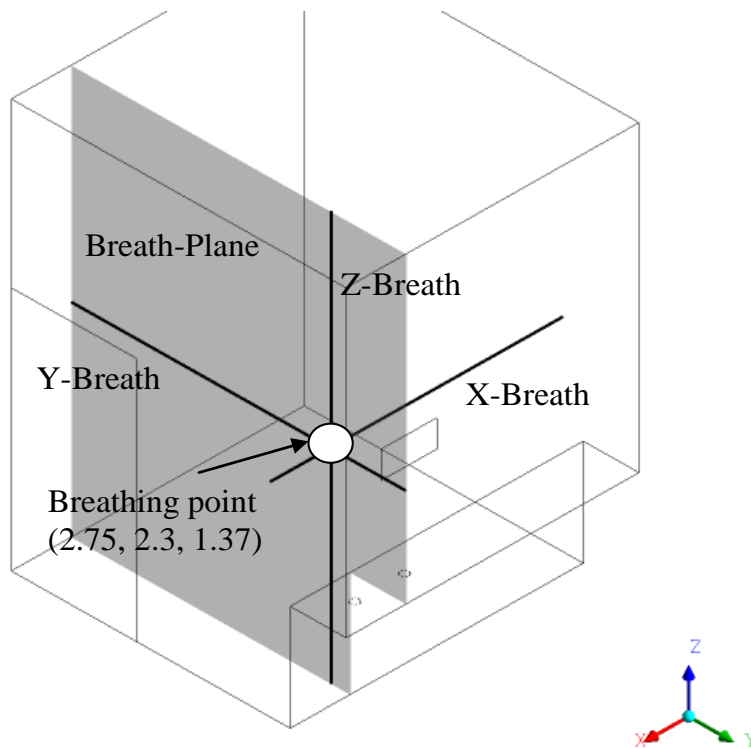


Fig. 4.18: Locations of the investigated plane and lines. (all dimension are in m)

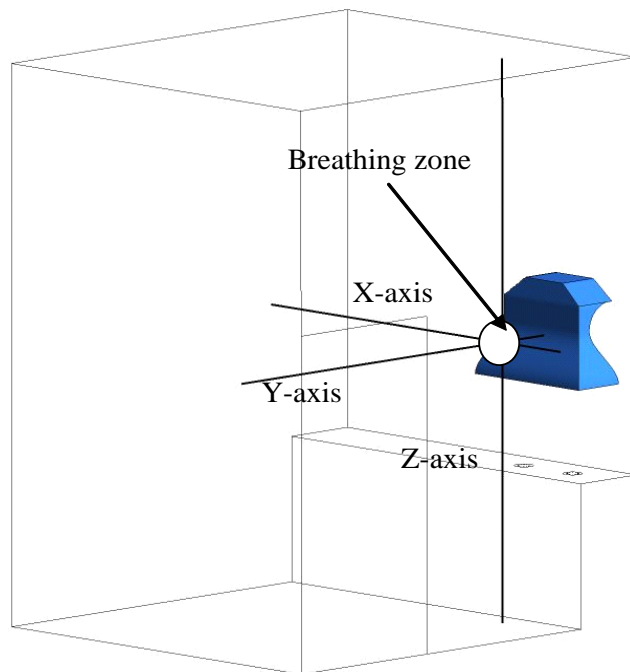


Fig. 4.19: Locations of the investigated plane and lines.

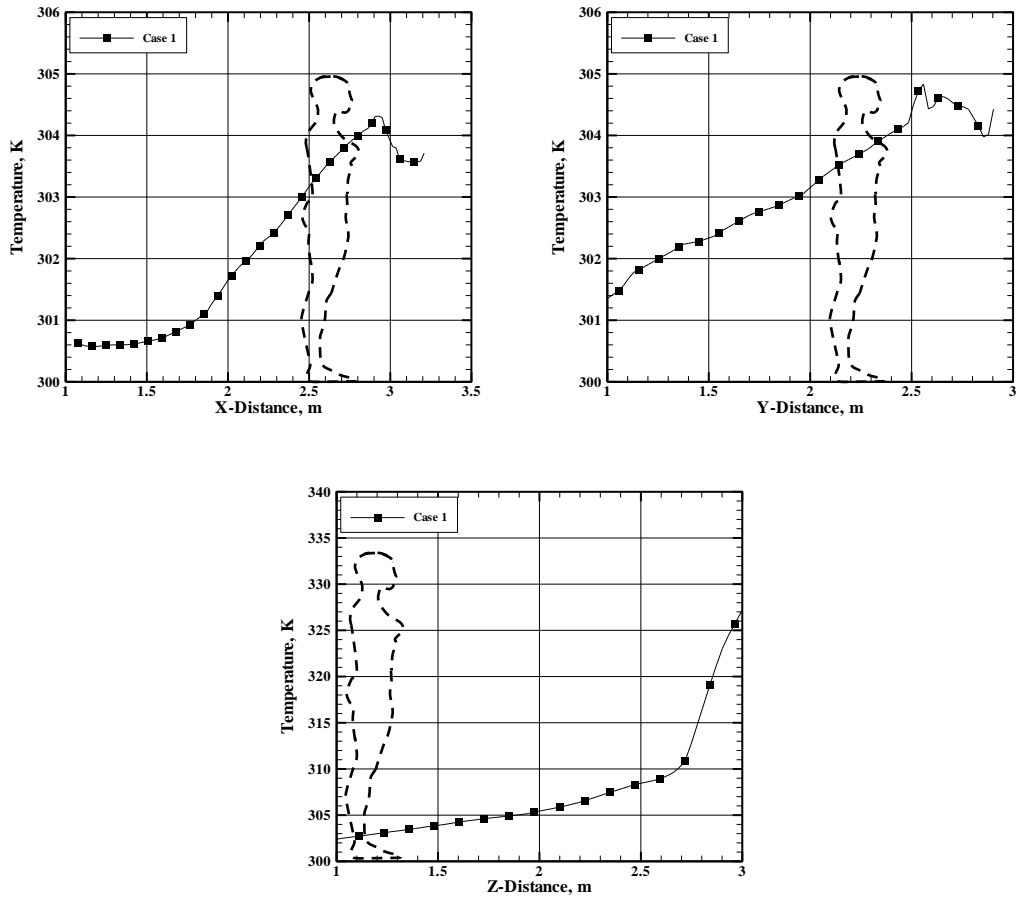


Fig. 4.20: Temperature variations at X-Y & Z breath lines for Case 1 (closed vent).

It is an absolute human desire to live in a healthy and comfortable environment. Apart from the emission issues, room temperature is also a key factor to accommodate thermal comfort. In this study it was also intended to check the thermal comfort level in the kitchen. To examine the temperature field for the kitchen without ventilation (Case 1) Fig. 20 is presented. Temperature variations can be seen along X, Y and Z breath lines. At the ambient temperature of 27°C , the difference of temperature ranges from 0.6°C to 4.4°C in lateral direction (X-breath line from left to right relative to the cook facing front), 1.4°C to 4.8°C in the longitudinal direction (Y-breath line from left to right relative to the cook) and 2.5°C to 54°C in the vertical direction (Z breath line from floor to the roof). The upper portion of the room (above 2.5 m) was identified as the heat accumulation zone where the temperature reached much beyond the room comfort temperature.

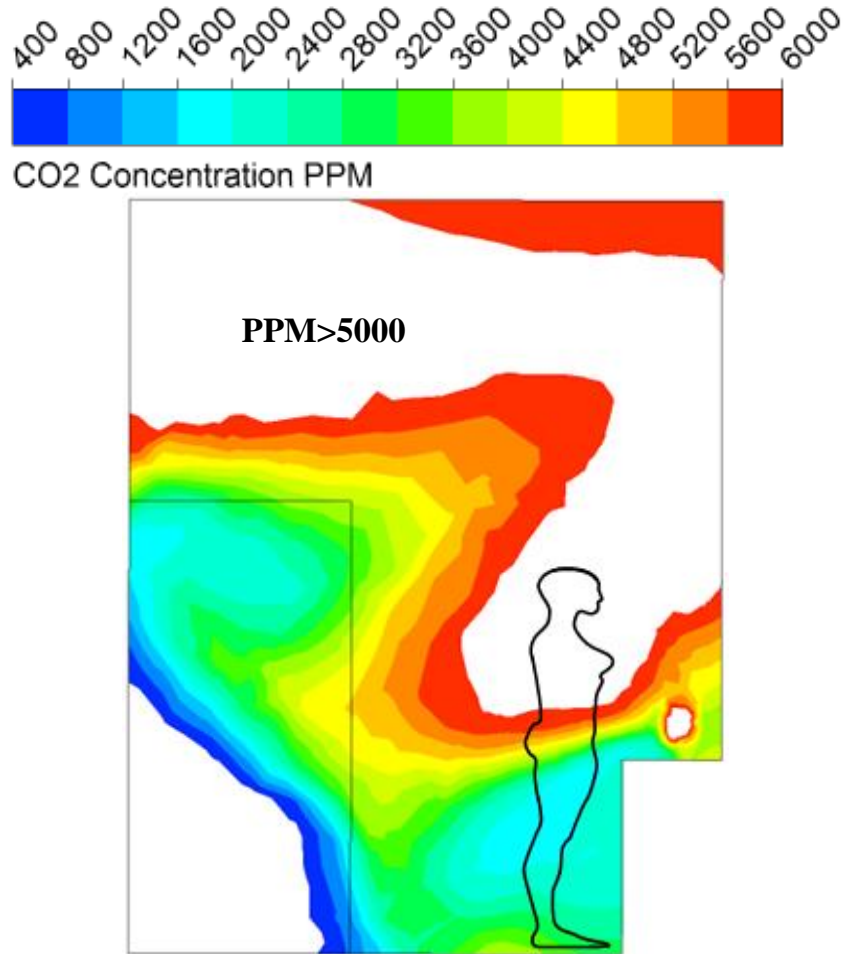


Fig. 4.21: CO₂ concentration contour at YZ-breath plane. Close vent (Case1).

As the natural gas is burned, CO₂ concentration in the kitchen space increases significantly over time if the room is not adequately ventilated. Fig. 4.21 is presented to understand CO₂ distributions in a plane passing the breathing zone at Y-Z plane (see Fig. 4.18). ANSYS CFX can predict CO₂ mass concentration in kg/m³ which was then converted to PPM using formula in UDF function of CFX and is given by

$$X_{PPM} = \frac{Y(\text{mg} / \text{m}^3) \times 24.45}{\text{Molecular weight}} \quad (4.1)$$

It was observed that a very high CO₂ level exists in almost 90% of the area of the plane for without ventilation case (Case 1) where major portion of the cook is surrounded by air of having CO₂ greater than 5000 PPM. Longer exposure to this high CO₂ level may cause health problem and in extreme case may result in permanent brain damage or immature death [2].

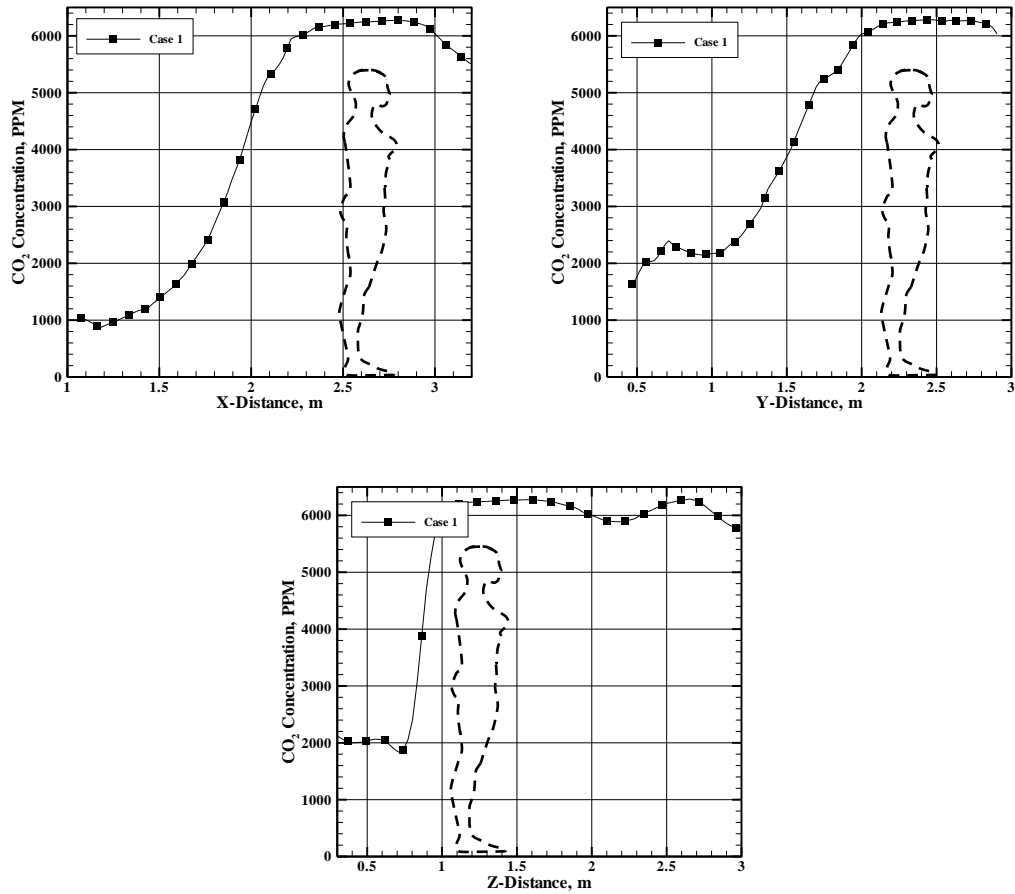


Fig. 4.22: CO₂ variations at X-Y & Z breath lines for Case 1 (closed vent).

Fig. 4.22 shows concentration of CO₂ distributions at three different lines passing through the breathing point (shown in Fig. 4.18). It is seen that for a close vent case (Case 1), at the breathing point, the CO₂ concentration is 6300 PPM which is over three times the limiting value. Along the X-breath line, CO₂ concentration is considerably increasing from 1000 PPM to 6300 PPM at all the way from left to right. At a close ventilated condition, half of the space is covered by the CO₂ over 4000 PPM. It is also noticeable from the Fig. 4.22 that along the Y-breath line CO₂ level remains over 4000 PPM at the right halfway distance. It means that quarter part of the kitchen area at the XY plane passing the breathing zone shows high level of CO₂ concentration. Fig. 4.22 also shows CO₂ distributions along Z-breath direction. From the height of 1m and above, the concentrations can be seen over 6000 PPM.

4.2.3.2. Natural Ventilation

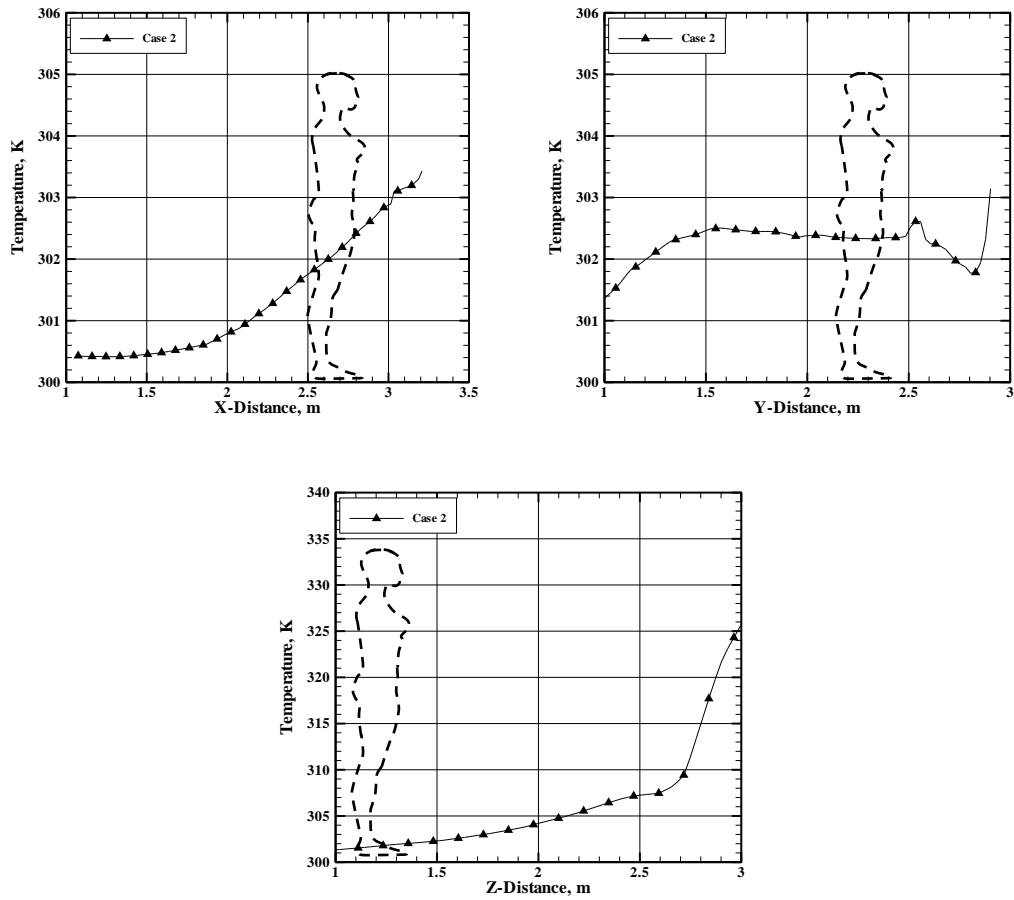


Fig. 4.23: Temperature variations at X-Y & Z breath lines for Case 2 (natural ventilation).

Temperature variations along the X Y and Z breath lines can be seen in Fig. 4.23 for Case 2 (natural ventilated condition). In the x direction, the temperature increases by 3°C from 1m distance. A steady distribution can be seen along y direction up to a length of 1.5m after which it decreases by at least 1°C. The reason could be the effect of natural flow through the vent. On the other hand the slope for increasing temperature is seen quite reasonable up to the height of 1.5 m along the Z direction (see Fig. 4.23). High heat accumulation is also evident at the upper zone of the kitchen where the temperature reaches as high as 52 °C.

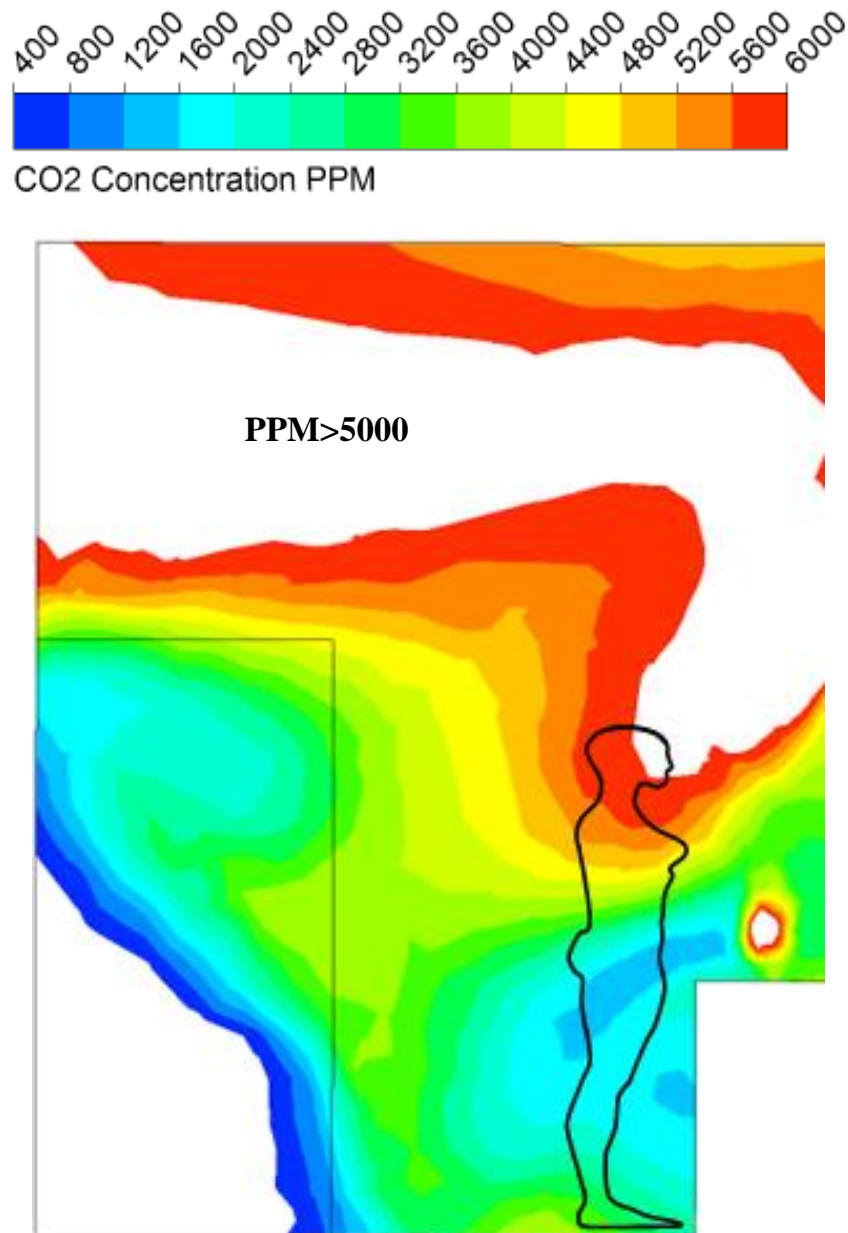


Fig. 4.24: CO₂ concentration contour at YZ-breath plane. Open vent (Case 2).

Figure 4.24 shows CO₂ contour at the YZ breathing plane for natural ventilated case (Case 2). The distribution pattern is almost identical with that of the closed vent condition (Case 1, see Fig. 4.21). The situation is slightly better in this case as the upper middle portion of the cook is exposed to relatively lower level emission. However, the cook still inhales air from high emission zone where CO₂ is over 6000 PPM.

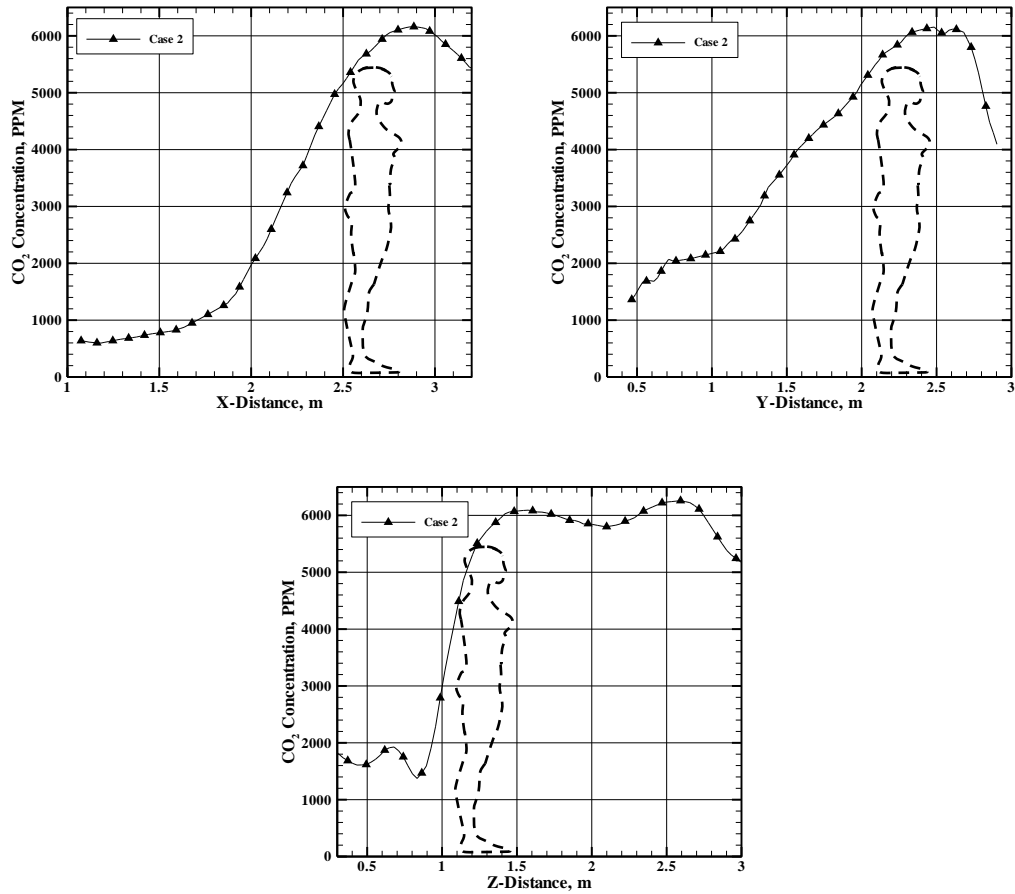


Fig. 4.25: CO₂ variations at X-Y & Z breath lines for Case 2 (natural ventilation).

The effect of the natural ventilation is evident in the Fig. 4.25 at all directions. Along the X direction, over 5000 PPM is observed at a distance 1.5 m and above. This high concentration zone is slightly narrowed as compared to Case 1 (See Fig. 4.22). Similar effect can also be noticed in Fig. 4.25, where 6000 PPM CO₂ achieved at a distance 1.25 m along the Z direction which is approximately 0.25m right shifted as compared to the Case 1. At a height of 1m along the z direction, the CO₂ is 3000 PPM which is 50% of Case 1 at the same location (see Fig. 4.22c). However, from 1.5m and above the concentration of CO₂ is still seen over 6000 PPM.

4.2.3.3. Forced Ventilation without Hood

For forced ventilated case, the exhaust velocity was set at 1.5 m/s. The effect of forced ventilation is significant on temperature variation as seen in Fig. 4.26. The temperature is moderately increased up to a distance of 2m and beyond, the temperature is increased by 1°C only. The direct effect of ventilation can be well understood from Fig. 4.26. The temperature fluctuates after a distance 1.5m, adjacent to the vent. The fluctuation may be caused by complex mixing of the suction air and the hot stream from the stove. Near the roof the heat accumulation zone got narrow as compared to Case 1 and the maximum temperature adjacent to the roof is reached 47 °C which is 5°C less than that of Case 1.

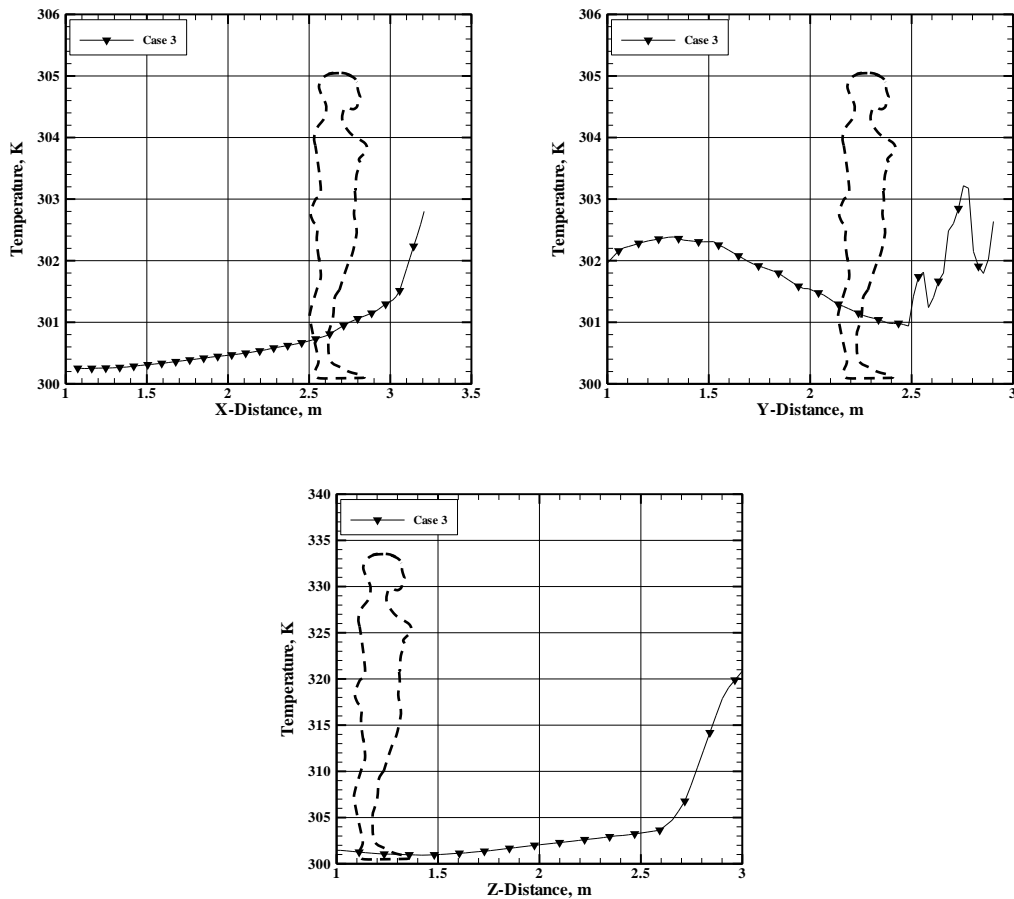


Fig. 4.26: Temperature variations at X-Y & Z breath lines for Case 3 (forced ventilation without hood).

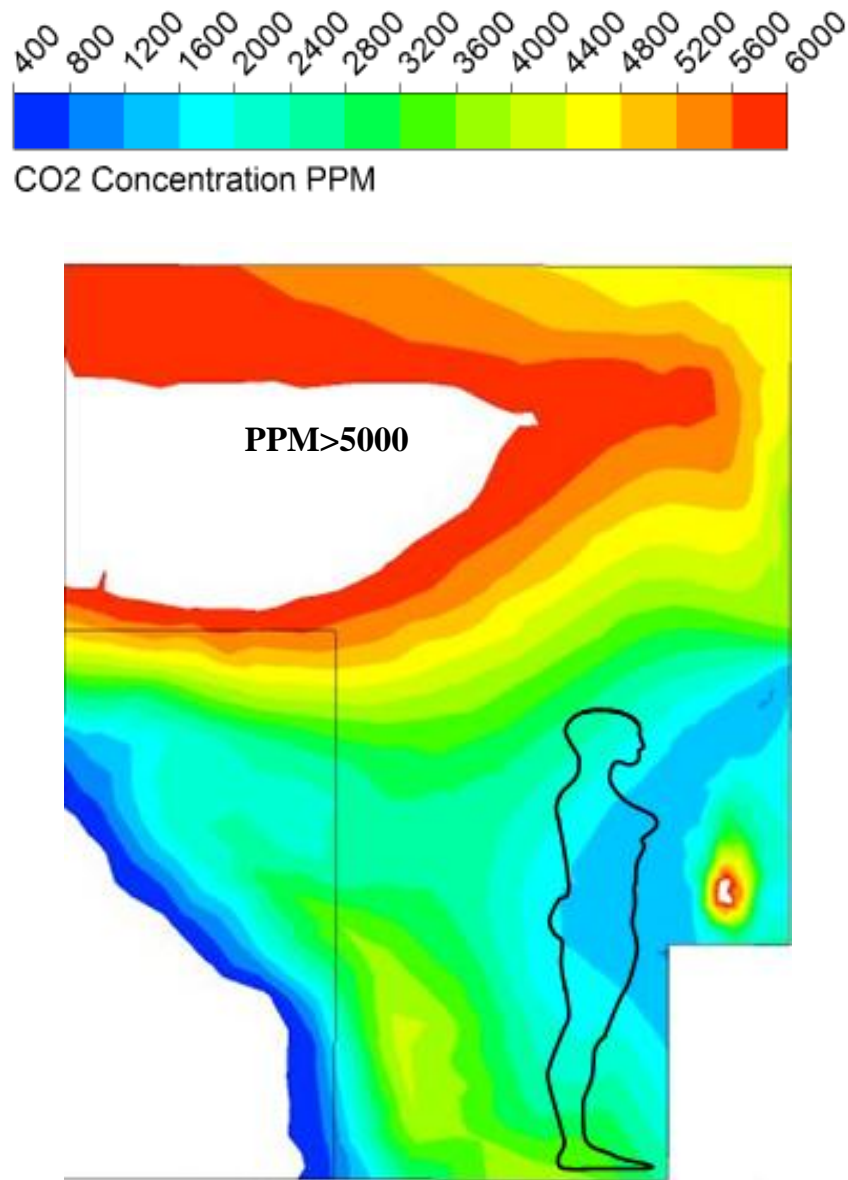


Fig. 4.27: CO₂ concentration contour at Y-breath plane. 1.5 m/s vent (Case 3).

Fig. 4.27 shows the contour of CO₂ distribution at the YZ breathing plane for an exhaust velocity of 1.5 m/s (Case 3). A significant improvement of the air quality in regard to CO₂ emission is observed around the cooking zone. Breathing zone shows CO₂ concentration within a range of 1600 PPM to 2000 PPM. Although the range is still higher but lower emission exposure is evident as compared to Case 1 and Case 2 air quality.

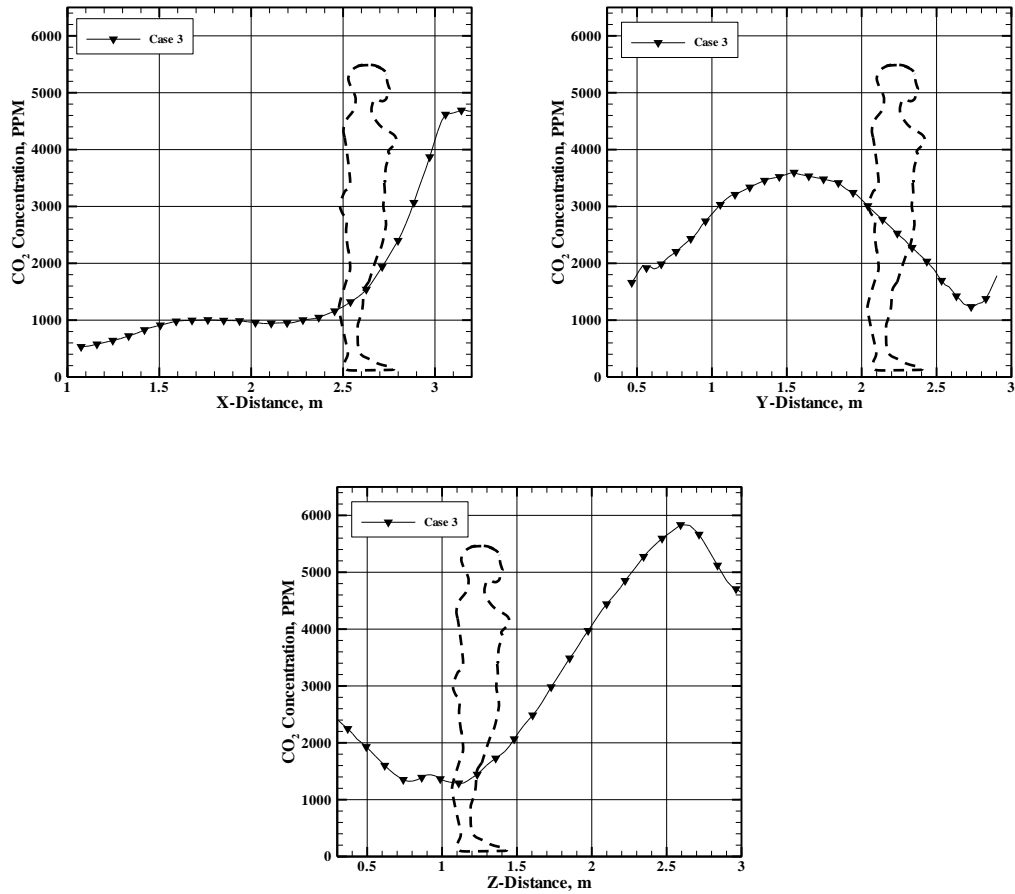


Fig. 4.28: CO₂ variations at X-Y & Z breathe lines for Case 3 (forced ventilation without hood).

In order to make quantitative analysis of the CO₂ distributions, Fig. 4.28 is presented at X, Y and Z breathe lines. In the x direction, up to a distance of 1.5 m from the left the CO₂ concentration remains about 1000 PPM. However, beyond this distance on the right, it increases in drastic manner from 1000 PPM to 4700 PPM. Along the Y direction, CO₂ reaches a maximum of 3500 PPM at 0.5 m distance and then decreases to 1200 PPM within 1m. The cause is attributed to the use of forced ventilation effect. In the vertical Z direction, at 1m and above distance the CO₂ goes higher than 4000 PPM.

4.2.3.4. Forced Ventilation with Hood

In the recent years the use of kitchen hood system has been increasing in the urban areas of developing countries. It becomes a part of the green building design by the developer companies due to its significant impact on emission dilution and controlled thermal environment. It is most commonly seen feature of the buildings designed for upper income group families since it adds extra cost and space for installation and setup. Middle and lower middle income group people are still left unattended with this special facility. The purpose of conducting study of Case 4 (forced ventilation with hood) is to analyze hoods effectiveness in controlling emission and temperature rise in the space.

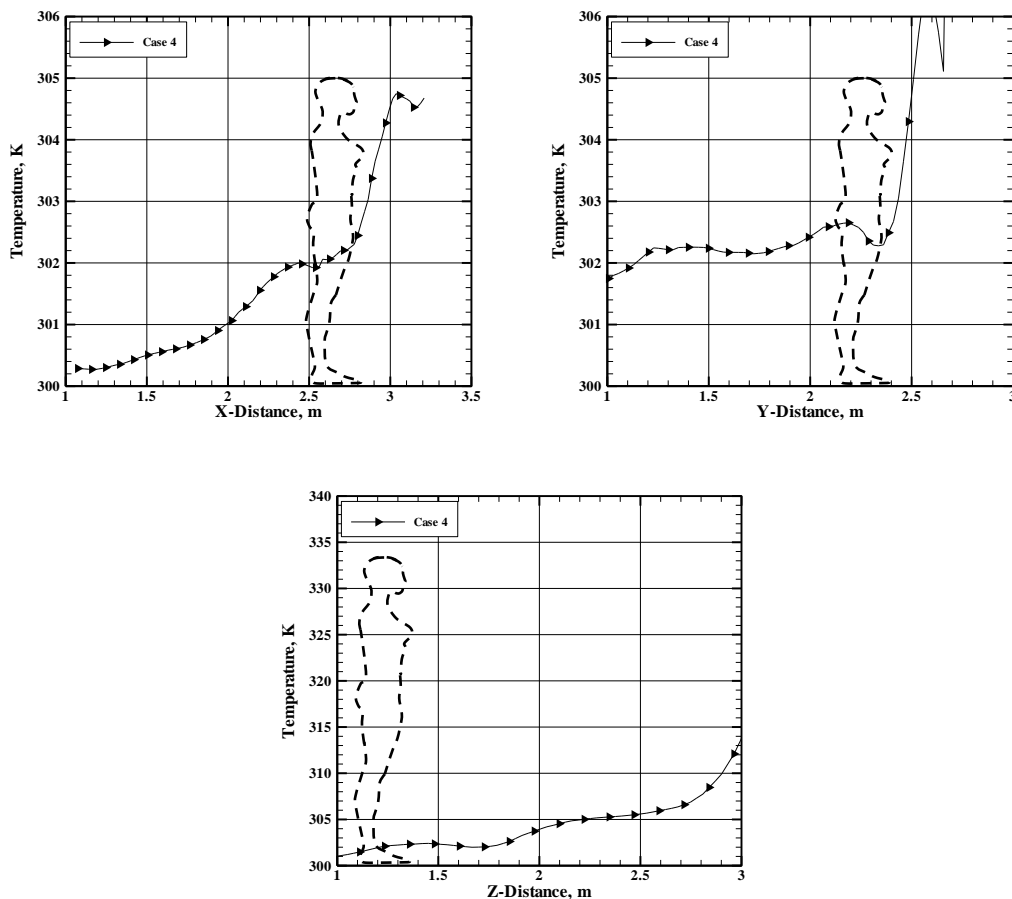


Fig. 4.29: Temperature variations at X-Y & Z breath lines for Case 4 (forced ventilation with hood).

Numerical study revealed that hood plays significant role when it comes with the kitchen to achieve thermal comfort and healthy environment. In order for study of the temperature field, Fig. 4.29 is presented to see the temperature variations at X, Y and Z breath lines. A sharp temperature rise of about 2.8°C can be seen at 2m distance on the right of the cook. Similar trend can also be noticed in Y distance where the temperature rise is about 4°C. It may be due to the use of hood which absorbs heat and thereby raising the temperature in adjacent region. However, comparison between Case 1, Case 2 and Case 3, Case 4 shows significant drop of temperature in the upper zone near the roof which was marked as the high heat accumulation zone. The peak temperature drop is from 27°C (see Fig. 4.20) to 14 °C in Case 4 (Fig. 4.29).

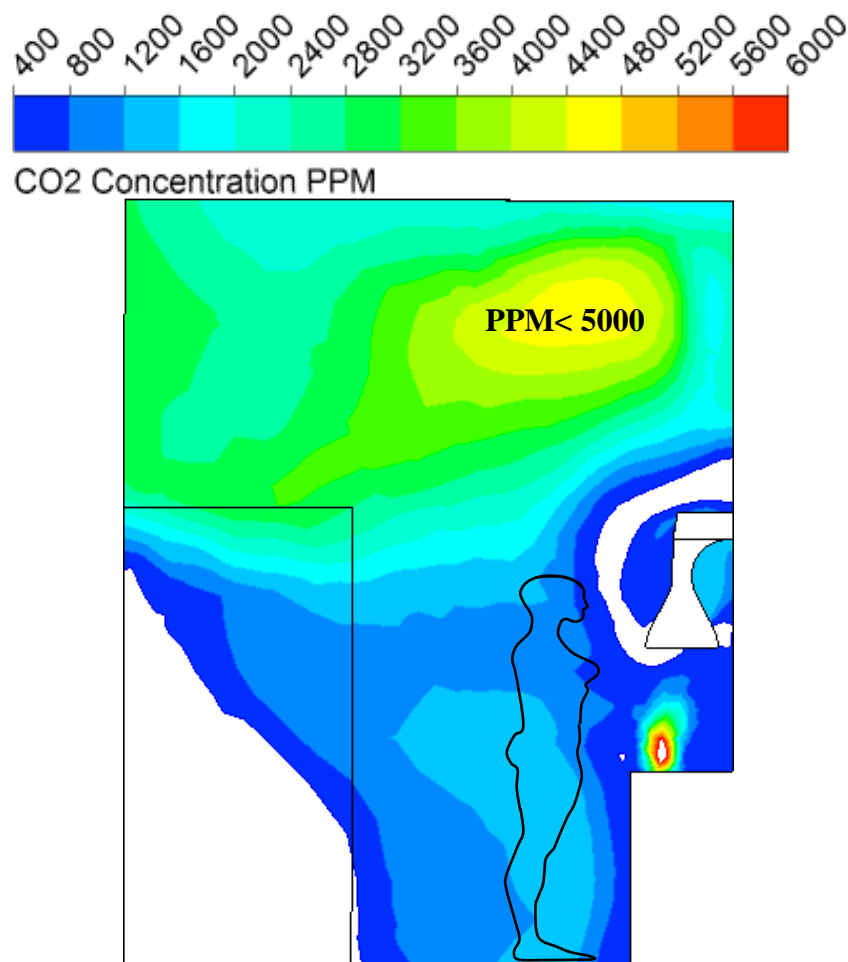


Fig. 4.30: CO₂ concentration contour at Y-breath plane. 1.5 m/s with hood (Case 4).

Fig. 4.30 is presented to signify the importance of using hood system in the kitchen. It basically explains the reason for choosing hood for healthy environment. In the contour plot of CO₂, it is seen that the entire breathing zone is safe for the cook as it reduces the emission at a considerable rate. The concentration in this zone ranges from 400 PPM to 1200 PPM. However, the trapped emission in the upper zone with concentration range of about 3000 PPM to 4400 PPM is still persisting. This phenomenon of the entrap emission is to be properly addressed by the engineers and the designers who will look into the matter for neutralizing the trapped space. An idea may be recommended in this regard to reassess such conditions by varying the suction hood position in space. This numerical study is also focused on the effect of position of suction vent in the subsequent section of this chapter.

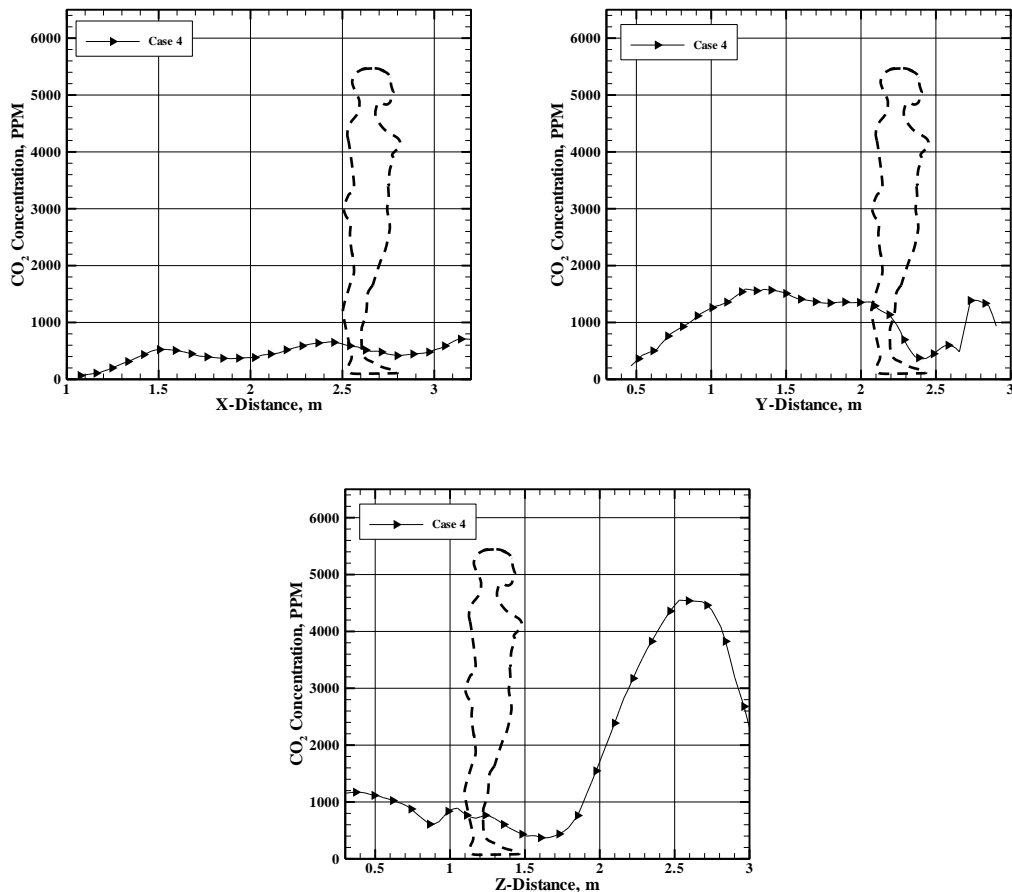


Fig. 4.31: CO₂ variations at X-Y & Z breath lines for Case 4 (forced ventilation with hood).

Fig. 4.31 quantifies the CO₂ concentration along the X, Y and Z breath lines. Along the X line the CO₂ is less than 1000 PPM which is below the safe limit of the contamination. Along the Y distance, concentration varies about 1400 to 1600 PPM from 1m to 2m distance behind the cook. The upper trapped zone is clearly visible in Fig. 4.31 where CO₂ has been plotted in Z direction. Above the breathing point CO₂ increases from 500 PPM to maximum 4500 PPM within a distance of 1m.

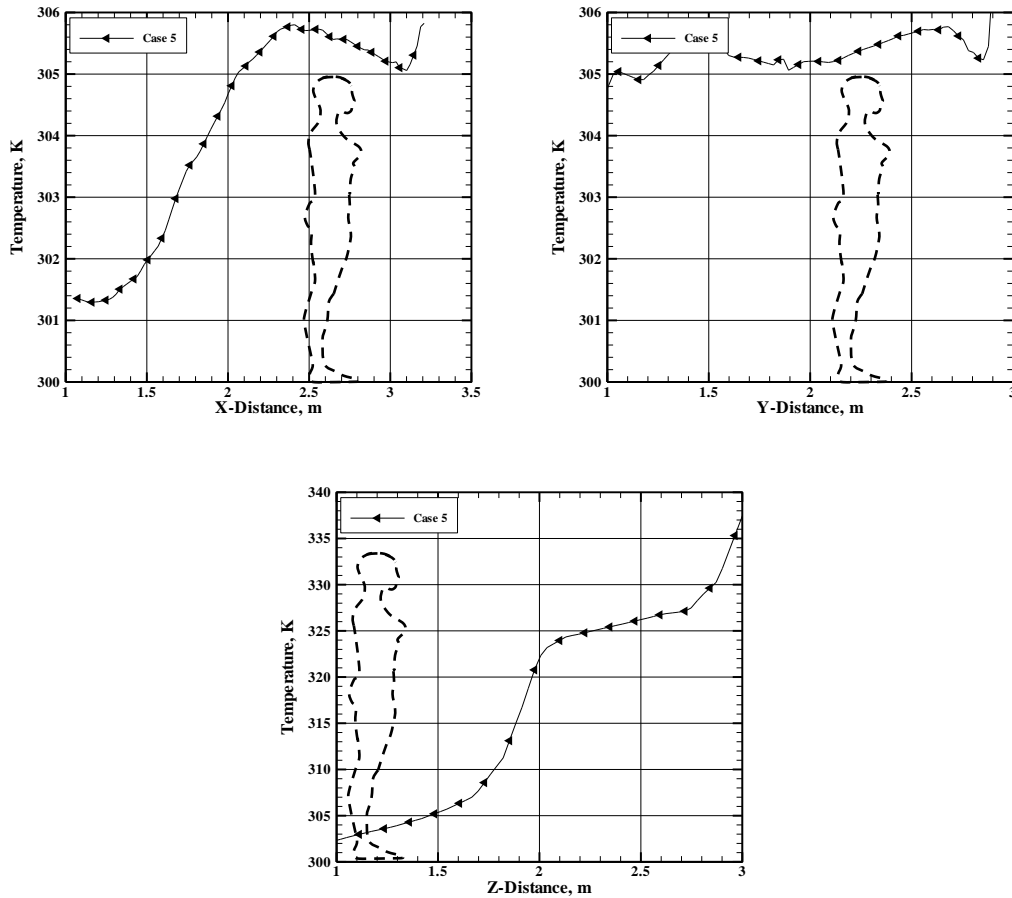


Fig. 4.32: Temperature variations at X-Y & Z breath lines for Case 5 (forced ventilation with front vent).

Position of the exhaust vent has been studied in this section. Two systems are adopted. In one system the location of the vent is just in front of the stove (see Fig. 4.4c). The vent is of circular cross-sections and two circular openings are used with a net area of flow of 0.082 m². Temperature distributions along the X, Y and Z breath lines are plotted in Fig. 4.32. This system does not satisfy the necessity of thermal comfort as it shows higher temperature distributions in all directions. There is about

4°C temperature difference along X direction. On the other hand, the temperature gradient in Y direction is less though magnitude shows higher which is closed to 36°C (see Fig. 4.32). In the high thermal zone the temperature is always higher than the other cases. The maximum temperature attained is 64°C adjacent to the roof (see Fig. 4.32).

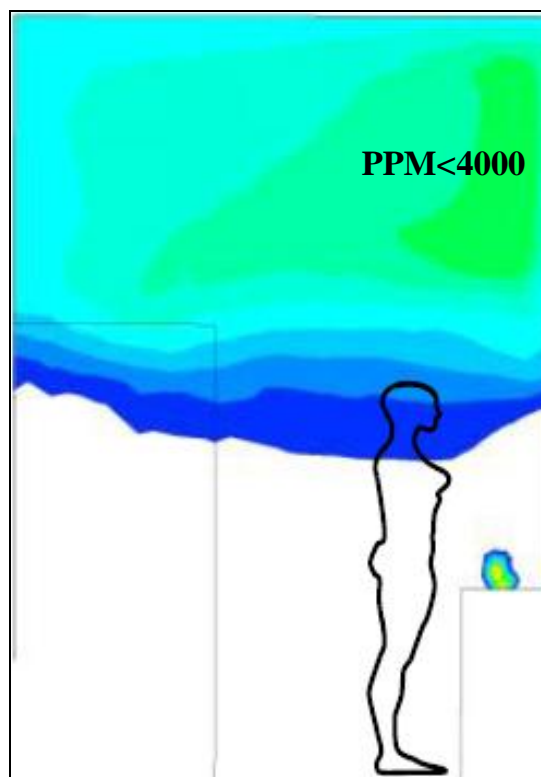
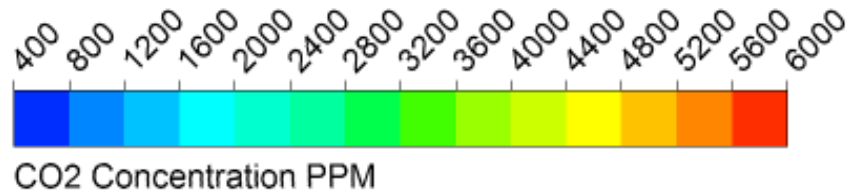


Fig. 4.33: CO₂ concentration contour at Y-breath plane. Front vent (Case 5).

Fig. 4.33 shows the CO₂ contour at the YZ breathing plane. Although the front suction vent is not proven to be effective on temperature control but it can quite effectively control CO₂ emission inside the kitchen. At the breathing zone the concentration remains below 1000 PPM which is safe for human health.

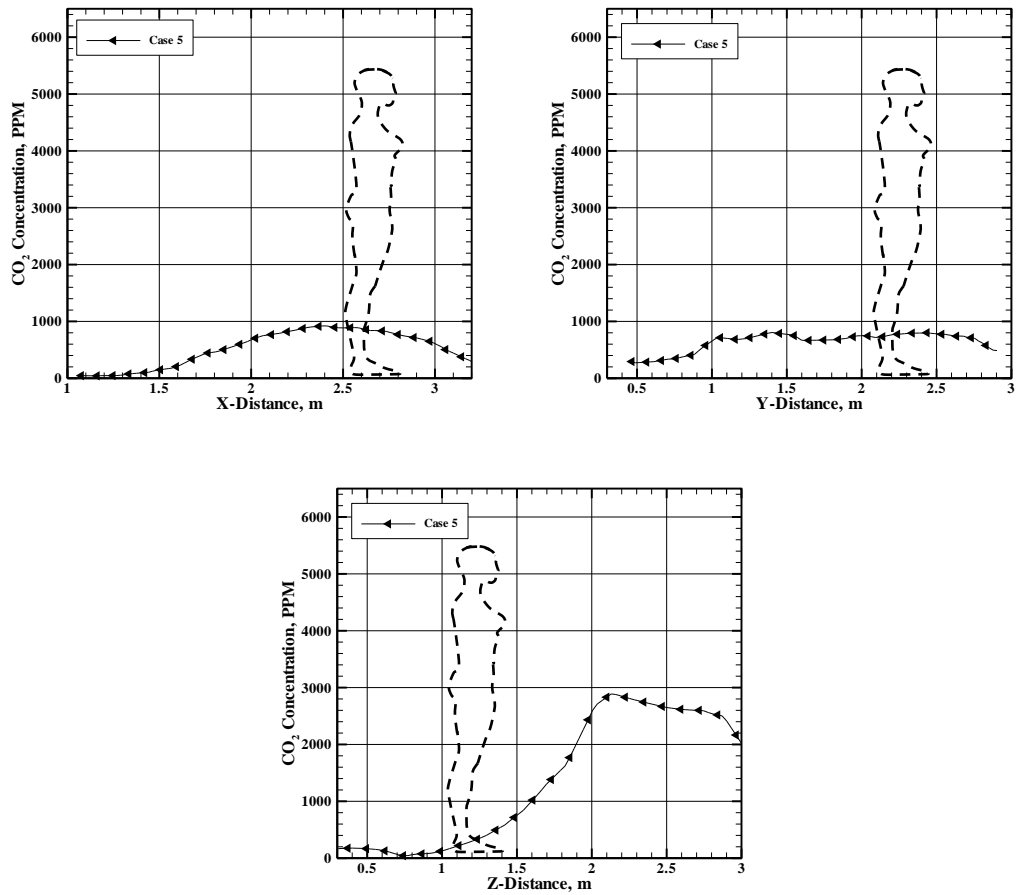


Fig. 4.34: CO₂ variations at X-Y & Z breath lines for Case 5 (forced ventilation with front vent).

In the quantitative plots of CO₂ as shown in Fig. 4.34, the concentrations are not exceeding 1000 PPM along the X and Y directions. However, in vertical direction the lower zone seems better in terms of concentration level but the upper zone shows the level higher than the safe and at 2.1m position it reaches a maximum value of 2800 PPM.

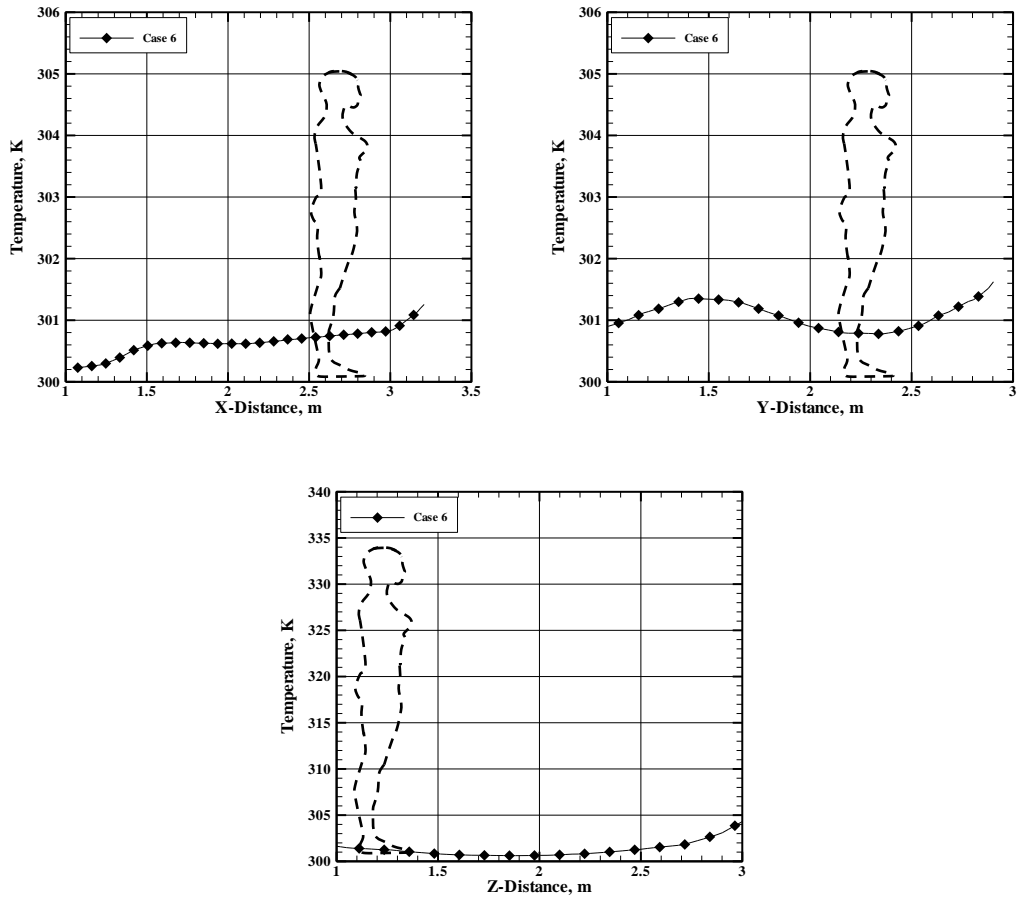


Fig. 4.35: Temperature variations at X-Y & Z breath lines for Case 6 (forced ventilation with base vent).

A significant improved thermal condition can be achieved for the Case 6 with base vent as seen in Fig. 4.35. In both X and Y directions the change of temperature is within 1 or 1.5 °C. Thermal gradients are very insignificant in all X, Y and Z directions. Maximum temperature rise in the upper zone is 7°C that ensures better thermal environment inside the kitchen space.

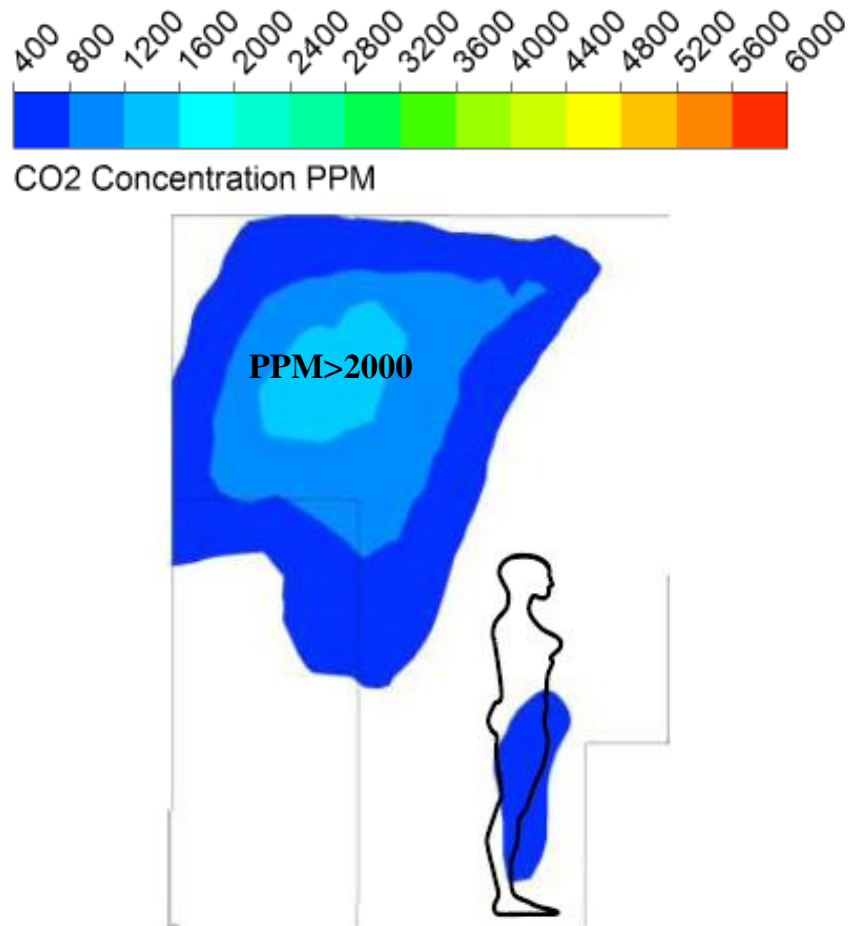


Fig. 4.36: 12 CO₂ concentration contour at Y-breath plane. Base vent (Case 6).

The base vent might probably be the best choice for the designer as it both satisfies the thermal comfort and healthy environment. However, it is beyond the capacity of the authors understanding whether it also satisfies the performance of the stoves. It is a matter of further investigations for the thermal efficiency of the stoves if such suction exhaust is added at the base. As seen in Fig. 4.36, the CO₂ concentration in the whole plane is well below 1200 PPM and the breathing zone is the safest zone in terms of comfort and health among all cases investigated in this study.

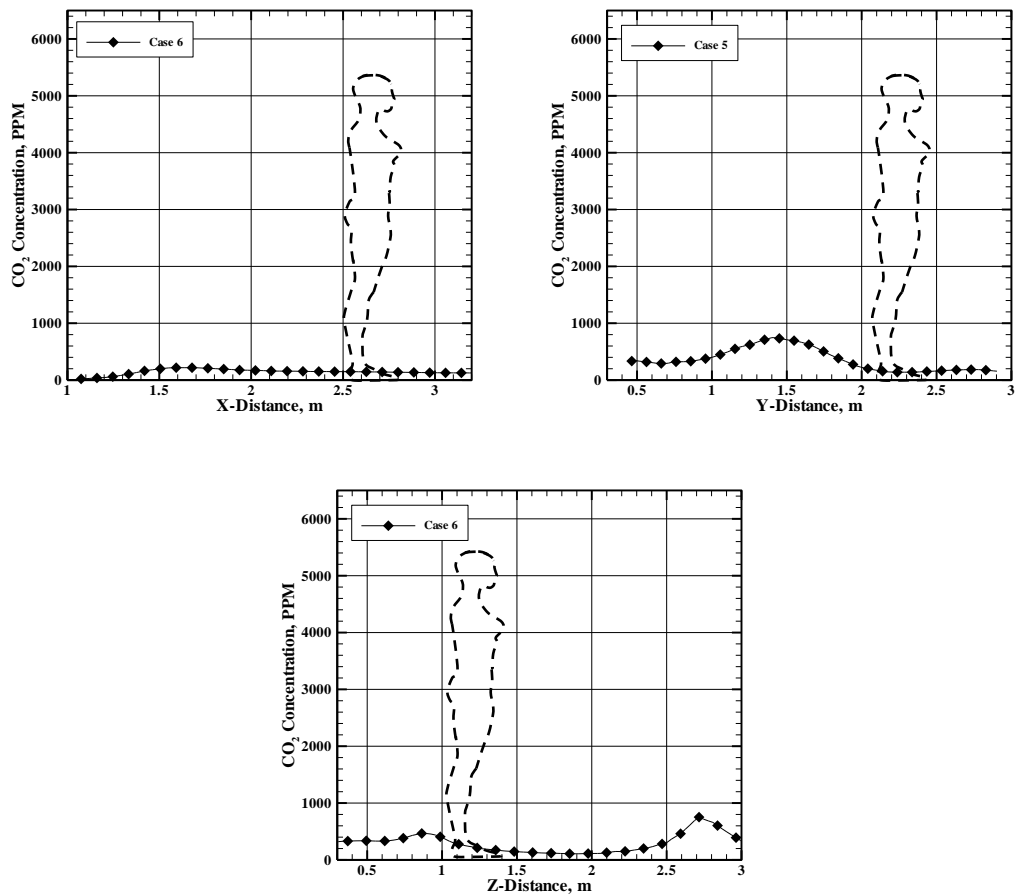


Fig. 4.37: CO₂ variations at X-Y & Z breath lines for Case 6 (forced ventilation with base vent).

Fig. 4.37 shows CO₂ distributions at all lines passing through the breathing point. Irrespective of the location in the space of the kitchen the level of concentration is always seen to be lower. It is a significant characteristic outcome of this research where Case 6 shows all attributes suitable for the designer's consideration.

4.3. Summary

Inhalation zone is the critical zone for the cook. It is important to eliminate any hazardous elements from the room that goes beyond the safe concentration level. The concern of this study was to investigate the emission characteristics of the breathing zone of urban kitchen. This zone is positioned at 0.33 m distance and 0.73

m height from the middle of the two source burner (see Fig. 4.38b). Cases are compared in Fig. 4.38. Based on the numerical results, CO₂ concentration at this zone was above 5000 PPM for Case1, 500 PPM for Case 4 (with kitchen hood), 800 PPM for Case 5 (with front suction vent) and 200 PPM for Case 6 (with base suction vent). This study will certainly be beneficial for kitchen ventilation design of green building structure. It will help the designers to find alternate methods or solutions for maintaining healthy environment for the room occupants.

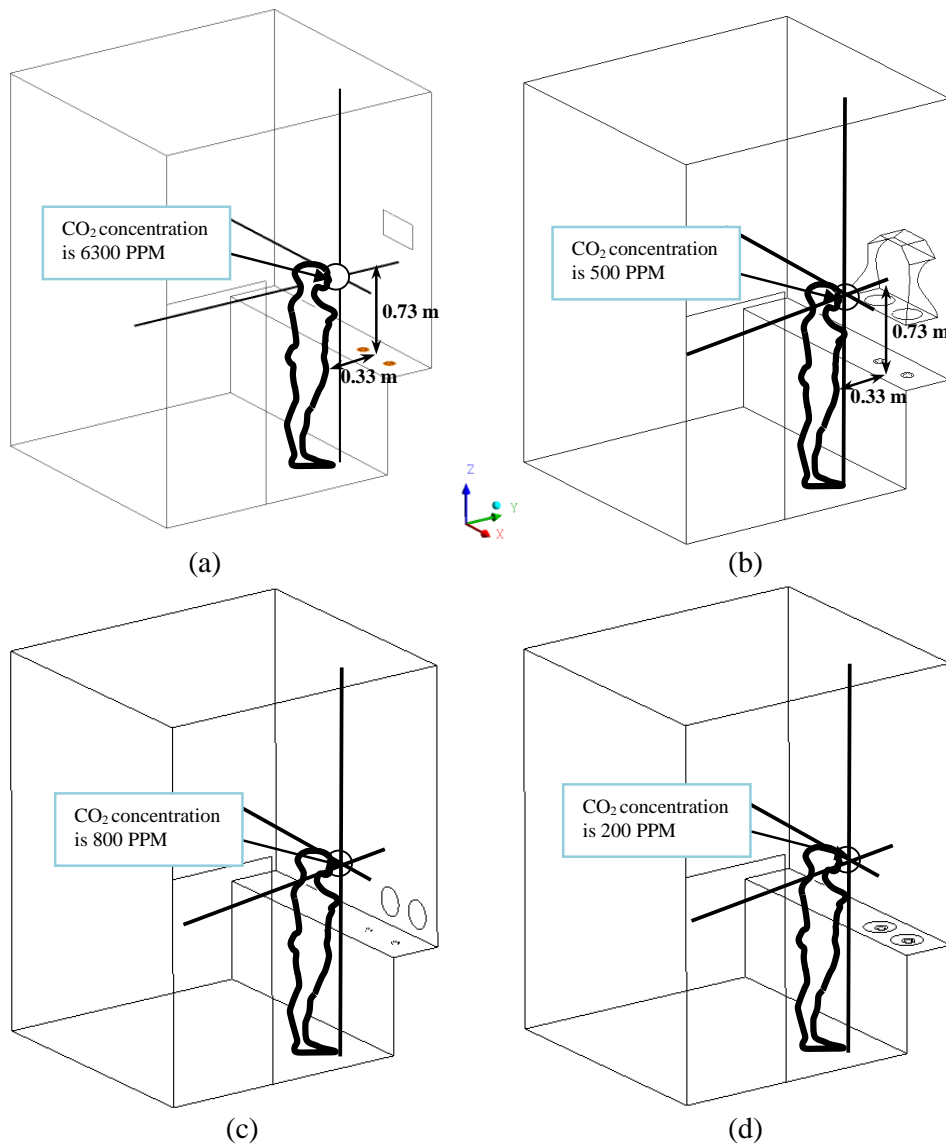


Fig. 4.38: CO₂ concentration at the breathing zone (a) Case 1, (b) Case 4, (c) Case 5 and (d) Case 6.

Table 4.5 is presented for breathing concentration exposure to CO₂ in connection with the possible cause of health problem with ventilation performance. As seen, Case 1 and Case 2 are the worst cases where CO₂ concentration is are much higher than safe value. This may create severe health related problems and may be fatal for long term exposure. Case 3 ventilation has been performing at moderated level. Some minor to moderate level of the health risk may occur. On the other hand, Case 4, Case 5 and Case 6 show the best ventilations cases that control the CO₂ concentration within the acceptable range inside the kitchen space.

Table 4.5: Findings of breathing point CO₂ concentration in connection with the possible health hazards

Test Cases	PPM	Possible Health Hazard	Remarks on ventilation
Case 1	6300	Oxygen deprivation, permanent brain damage, coma and even death.	Poor
Case 2	6000	Oxygen deprivation, permanent brain damage, coma and even death.	Poor
Case 3	1900	complaints of drowsiness	Moderate
Case 4	500	Typical level found with no health related complaints	Better
Case 5	800	Typical level found with no health related complaints	Good
Case 6	200	Completely safe for human health	Best

Chapter 5

5. Study of Rural Kitchen

In spite of dreadful consequences of the emission exposures in the kitchen the safety issues have been given little importance by the concerned authorities. Important health safety factors for the poor village people have always been ignored by the researchers as well as environmentalists. Rural families are suffering extreme health related issues due to indoor pollution exposures. The emission of CO₂ and CO from burning various conventional bio-fuels can reduce the quality life. In rural areas, the research on the structure of the kitchen, kitchen exhaust system and resulting health threats to the room occupants are practically unattended. Considering the fact of numerical limitations, a number of experiments were conducted for estimating source level concentrations of CO, CO₂ and Particulate Matter (PM).

A simple experiment has been conducted as a preliminary study of the emission from a conventional rural kitchen stove. In Fig. 5.1a, the position of the CO₂ and CO meters have been shown and Fig. 5.1b shows the single burner traditional kitchen stove with the instrumental setup. The study area is in a Village 1 km West of IUT campus. Measurements were taken for emission concentration of CO and CO₂ and are presented in Table 5.1. It is seen that the average CO and CO₂ concentration around the periphery are 400 PPM and 4089 PPM respectively. However, at the breathing point the concentrations are 132 PPM and 1500PPM which are about 2.7 and 1.5 times higher than the safe limit as directed by US Environmental Protection Agency (USEPA) and Wisconsin [2] respectively.

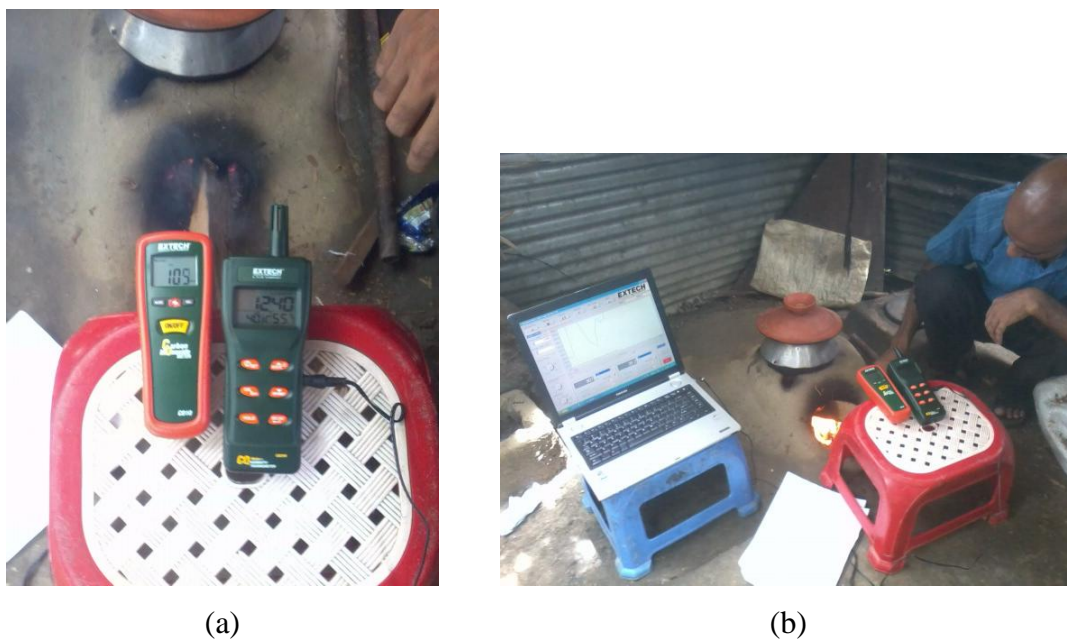


Fig. 5.1: (a) Digital CO / CO₂ meter at the breathing zone, (b) Traditional kitchen for experiment.

Table 5.1: CO and CO ₂ emission concentration				
Pollutants	At stove core (PPM)	Avg. around the stove periphery, PPM	At 1 m height from stove core (PPM)	Allowable safe limit (PPM)
CO	--	400	132	50*
CO ₂	--	4089	1500	1000**

*EPA (<http://www.epa.gov/iaq/co.html>)
 ** Wisconsin (<http://www.dhs.wisconsin.gov/eh/chemfs/fs/carbondioxide.htm>)

5.1. Estimation of Source Concentration

A kitchen of usual size has been used for pollutants sampling and the experiments have been conducted at IUT campus for measuring source emission concentration inside the stove. Single burner kitchen stove is used for burning different grades of bio-fuels such as Rice Husk, Cow dung and Firewood. Some major properties including the calorific values can be seen in the Appendix V. The kitchen stove is of concrete construction provided and installed by Grameen Shakti, Bangladesh and the schematic of the experimental setup is presented in Fig. 5.2a. For

data sampling, one CO₂ meter and one CO meter were used. A duct has been used to direct the flue gases to a point where the measurement is taken at suitable condition. Fig. 5.2b shows the exact position of CO and CO₂ meters at 0.457 m downstream of the flue gas exit. It ensures safety of the measuring devices from burning out of the sensors.

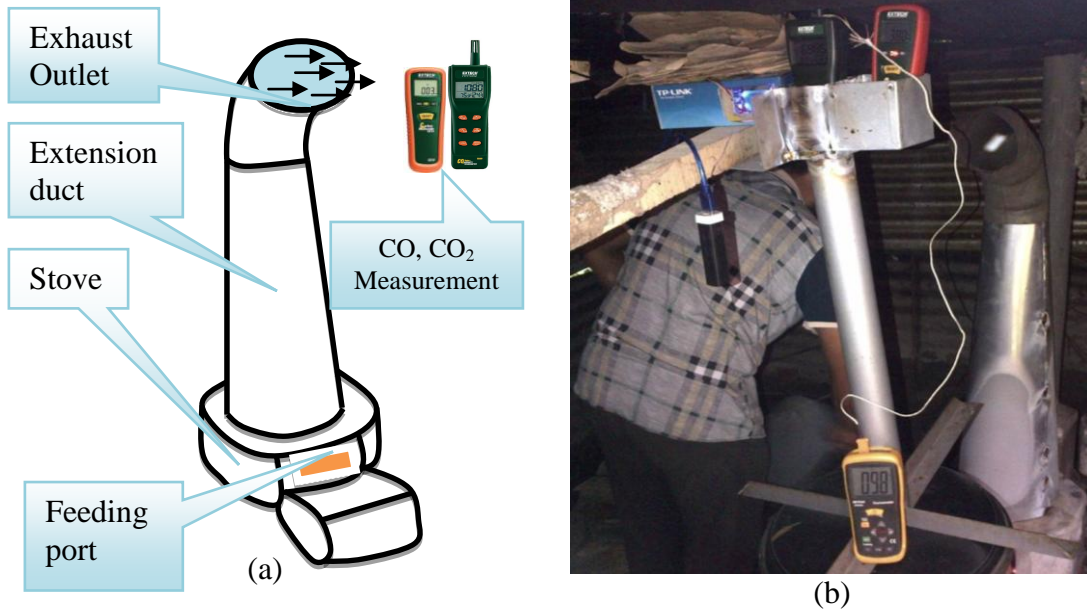
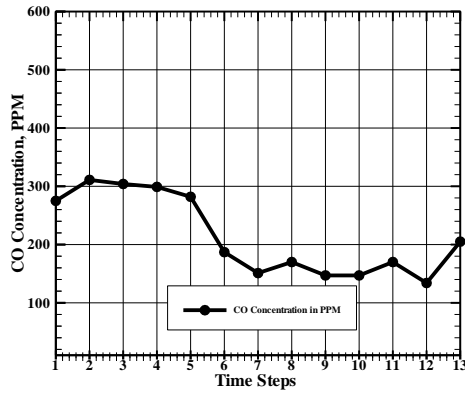


Fig. 5.2: Experimental setup at IUT Campus a) stove with duct and b) position of the measuring devices.

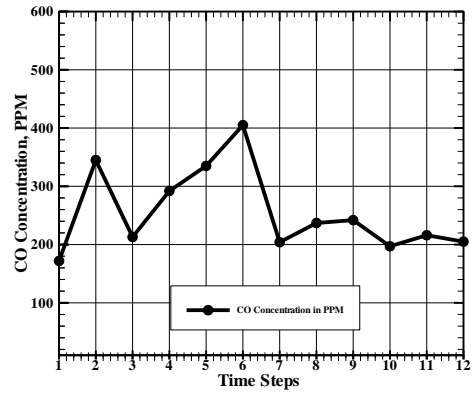
5.1.1. CO at source:

After the preliminary results as seen in Table 5.1, extensive experimentations have been conducted to keenly examine time behavior of the pollutants concentrations. It is as expected, turned out that the emissions are highly time dependent which might be the reasons of chaotic air circulations within the kitchen space and unsteady burning characteristics of the bio-fuels. Figure 5.2a shows source concentration of CO for Cowdung at different time steps. The data have been recorded at every 1 minute time interval. The maximum and minimum concentrations are 300 PPM and 140 PPM, respectively for Cowdung as the bio-fuel burnt. For the mixture of Cowdung and Rice husk (Fig. 5.3b) as the bio fuel, the maximum and minimum concentrations are observed 370 PPM and 180 PPM, respectively. On the other hand, Firewood and Cowdung mixture shows (Fig. 5.4a)

relatively uniform concentration of CO emission with average value of 200 PPM. However, when the firewood was burnt only as a fuel, the maximum and minimum concentrations were found to be 300 PPM and 160 PPM, respectively (see Fig. 5.4b).

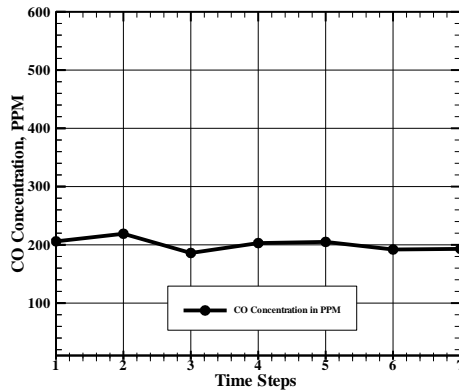


(a)

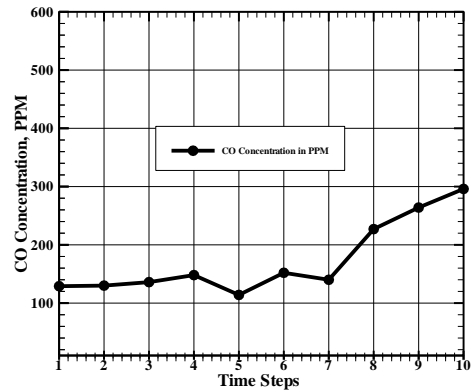


(b)

Fig. 5.3: CO concentration at source for (a) Cowdung and (b) Cowdung-Rice husk.



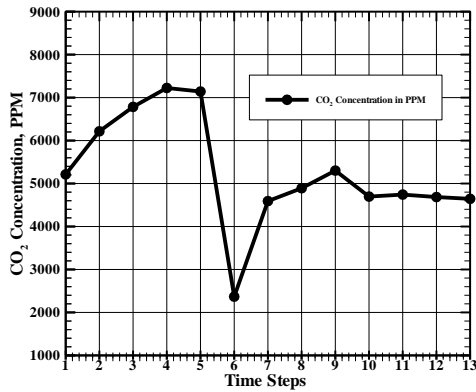
(a)



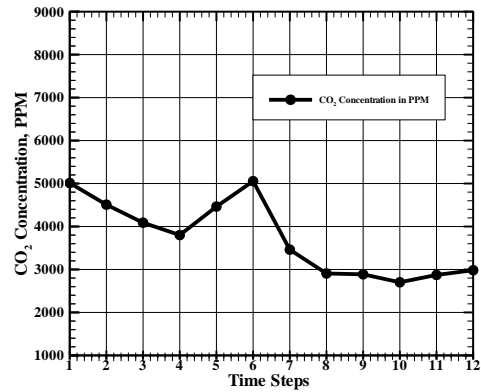
(b)

Fig. 5.4: CO concentration at source for (a) Firewood and Cowdung and (b) Firewood.

5.1.2. CO₂ at source:

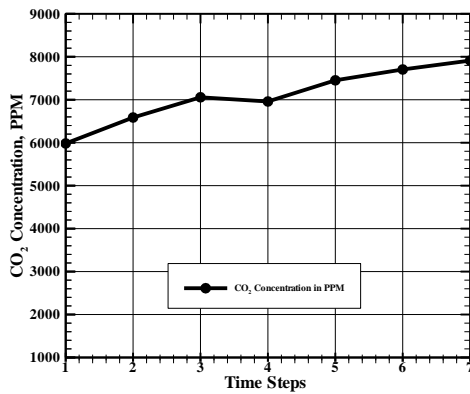


(a)

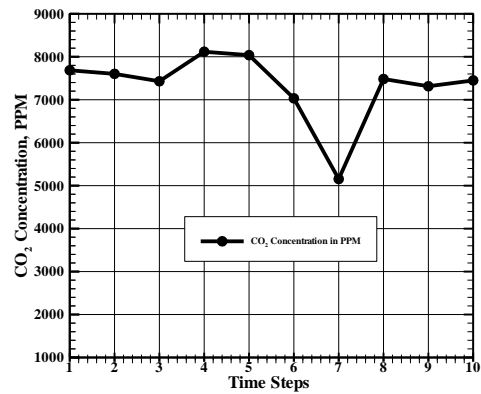


(b)

Fig. 5.5: CO₂ concentration at source for (a) Cowdung and (b) Cowdung and Rice husk.



(a)



(b)

Fig. 5.6: CO₂ concentration at source for (a) Firewood and Cowdung and (b) Firewood.

Fig. 5.5 shows CO₂ concentrations of the source for different bio-fuels. When the Cowdung is used as the fuel (Fig. 5.5a), the maximum concentration is seen 7000 PPM with a minimum of 2400 PPM. For the mixture of Cowdung and Rice husk (see Appendix V for their properties) burning, maximum CO₂ is 5200 PPM and minimum is 2800 PPM as seen in Fig. 5.5b. However, when the Firewood (see Appendix V for their properties) is burnt, the CO₂ concentration is over 8000 PPM with a minimum of 5000 PPM as seen in Fig. 5.6b. After adding Cowdung with the Firewood, the

trend is increasing with time. The maximum CO₂ attained is about 8000 PPM and the minimum is 6000 PPM (see Fig. 5.6a).

5.1.3. PM at source-by innovated inverted pitcher concept:

For measuring the particulate matter at source, a new experimental technique was adopted due to limitations of instrumental operating conditions. The PM device allows measurement to take at a maximum operating temperature of 35°C. However, at source the combustion temperature of the biomass is several hundred degrees which does not allow the instrument to measure directly from the source. An aluminium bucket of 0.0158 m³ volume was used to collect the PM sample directly from the source (see Fig. 5.7a). A certain procedure was maintained during the experiment. The bucket was drilled about 2.54 cm of diameter at four different locations at the bottom as shown in Fig. 5.7.

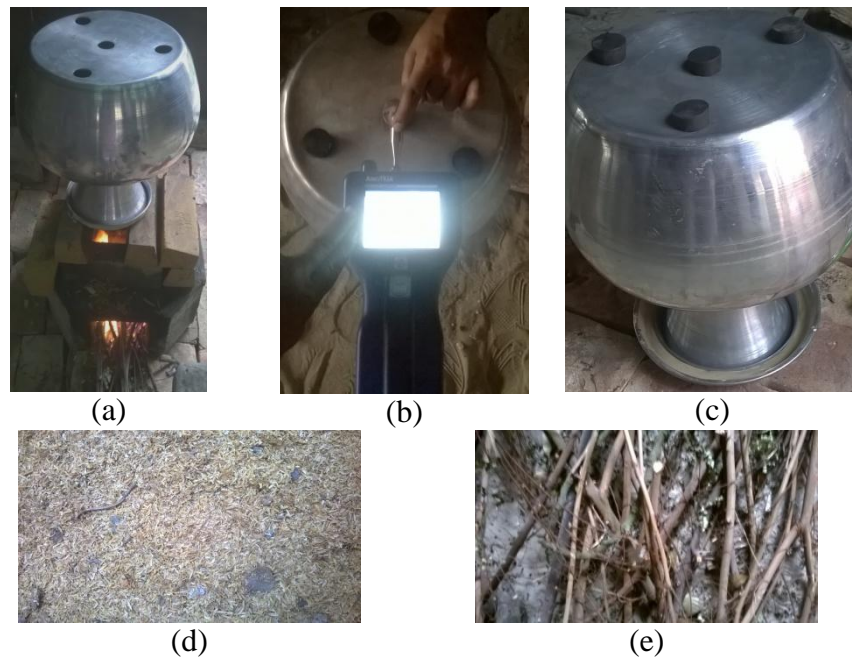


Fig. 5.7: Experiment of PM source concentration measurement.

All these four holes were then sealed with the removable rubber pad. During the sample collections, the bucket was placed upside down on the stove in which the biomass is burned. All four holes were then opened for a while to allow escaping trapped air and filling by the burning exhaust. After a while all holes were properly sealed and bucket was then placed on the floor for natural cooling. The measurement

was then taken by replacing the rubber seal of the center hole with another rubber seal with a 90° elbow which allow passage for PM source sample. The suction probe of the PM meter was placed at the outlet of the elbow for source concentration measurement (see Fig. 5.7b). Fig. 5.7 d and e shows the biomass sample of rice husk and dry leaves with branches.

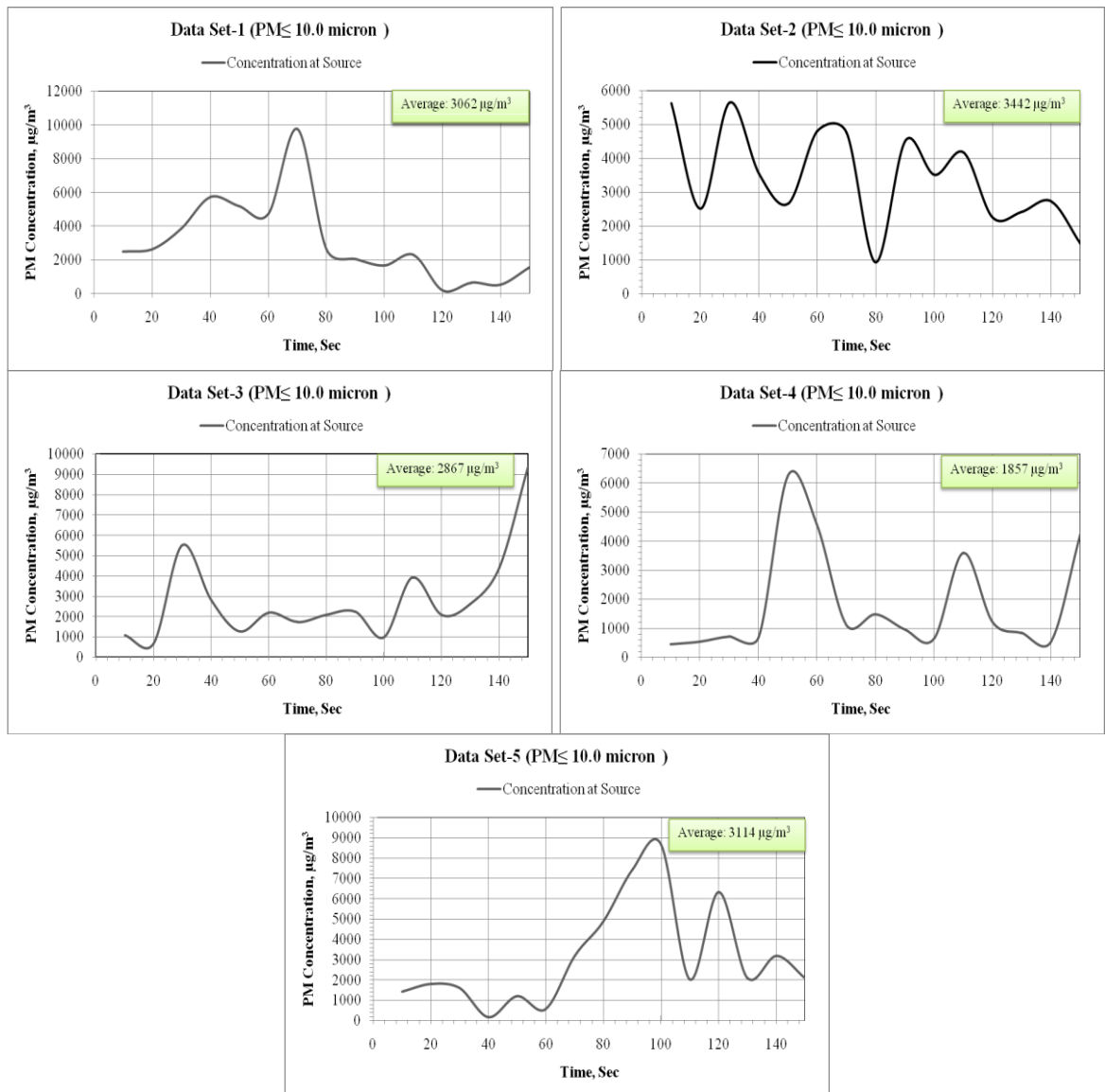


Fig. 5.8: Different data set of PM concentration at source of rural kitchen stove.

The measured source concentration of the PM, having $\leq 10 \mu\text{m}$ size is presented in Fig. 5.8. There are five set of readings taken. For each observation the data were collected for 150s. It is observed that the PM at source is highly unsteady

in nature. In data set 1, the average value of the particulate matter over the 150s time period is calculated as $3062 \mu\text{g}/\text{m}^3$, data set 2 shows $3442 \mu\text{g}/\text{m}^3$, data set 3 shows $2867 \mu\text{g}/\text{m}^3$, data set 4 shows $1857 \mu\text{g}/\text{m}^3$ and data set 5 shows $3114 \mu\text{g}/\text{m}^3$. Since the numerical simulation of this study is based on steady condition, an average value of $2867 \mu\text{g}/\text{m}^3$ was used as the source input of the numerical model.

5.2. Measurement of Temperature and Emission

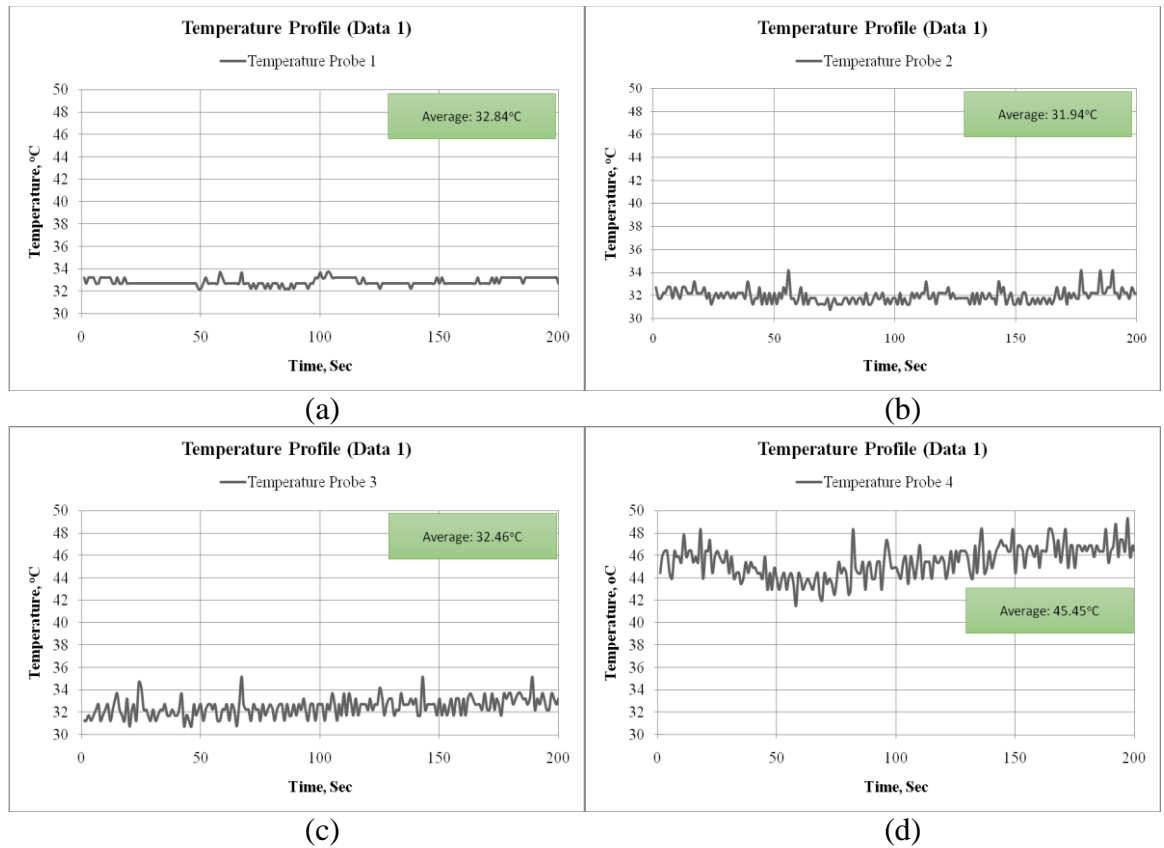


Fig. 5.9: Temperature profile with time along Z direction for rural kitchen 1 at (a) probe 1, (b) probe 2, (c) probe 3 and (d) probe 4.

Time dependent indoor temperature variations of rural kitchen are presented in Fig. 5.9, 5.10 and 5.11. There are four temperature sensors connected with 4ft vertical stand at 1ft equal length interval from the ground to the roof of the kitchen. The stand positioned at breathing point and probe 2 is basically measured the breathing point temperature. At probe 1, the temperature fluctuations with time are smaller than the other probes (see Fig. 5.9a). In this position steady temperature of

about 33°C is maintained. Probe 2 temperature maintains steady fluctuation between 31°C to 34°C (see Fig. 5.9b). Temperature at probe 3 also shows similar fluctuating trend with a magnitude slightly higher than 34°C (see Fig. 5.9c). On the other hand, at probe 4 temperatures fluctuates between minimum 42°C to maximum 48°C (see Fig. 5.9d).

Fig. 5.10 is presented for temperature distributions at four distinct positions of the sensors. Temperature distributions are found to be relatively steady over time with a average of 33.48°C (Fig. 5.10a). The average temperature at the breathing point surprisingly found less than probe 1 temperature which is about 32.37°C (see Fig. 5.10b). Probe 3 recorded slightly higher average temperature of 33.89°C. However, at the upper probe 4 near the roof the temperature is 38.38°C.

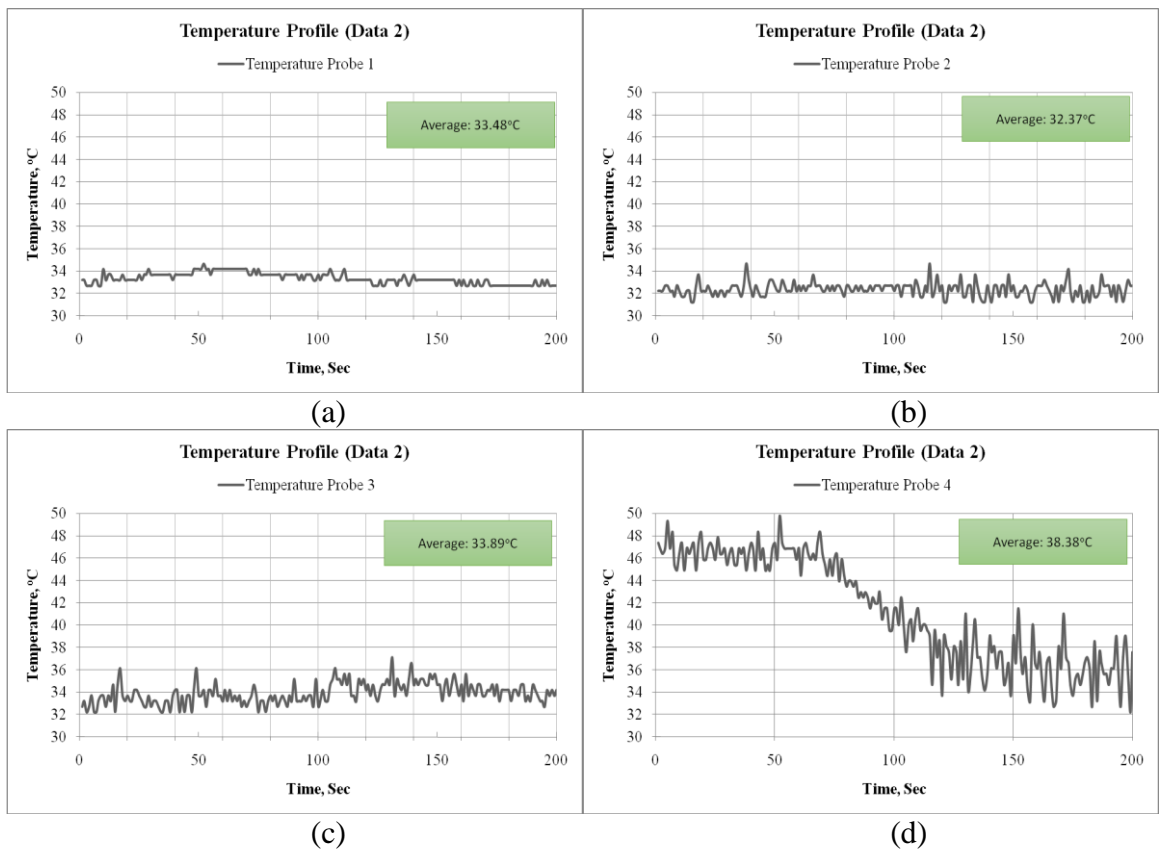


Fig. 5.10: Temperature profile with time along Z direction for rural kitchen 1 at (a) probe 1, (b) probe 2, (c) probe 3 and (d) probe 4.

Temperature variations also monitored for rural kitchen 2 at Gazipur district and presented in Fig. 5.11. Temperature unsteadiness captured similar pattern as seen in kitchen 1 experiment. The average temperature at probe 1 recorded as 33.94°C where probe 2 showed 32.57°C . Probe 3 shows average of 33.63°C . At all these three locations the temperature is exceeding 36°C within 150s to 200s times. Probe 4 recorded fluctuations of 32°C to 42°C temperature at different times of data collections. At this point the average temperature is seen 35.82°C which is comparatively less than recorded temperature for kitchen 1.

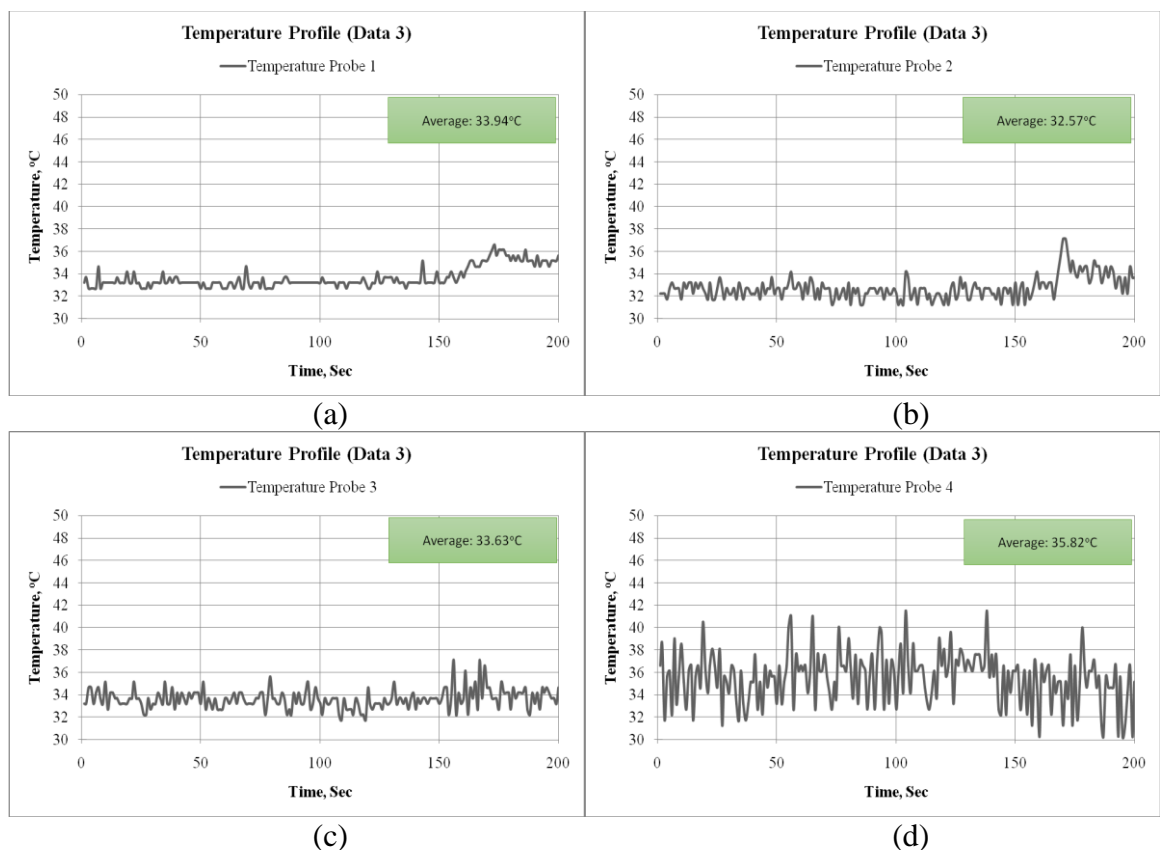


Fig. 5.11: Temperature profile with time along Z direction for rural kitchen 2 at (a) probe 1, (b) probe 2, (c) probe 3 and (d) probe 4.

Unsteady nature of the CO_2 emission at the breathing point for kitchen 1 is observed and presented in Fig. 5.12. One set of reading shows fluctuations in time with a range from 1000 PPM to a maximum of 5500 PPM with an average value of 2253 PPM. In another set of data, the variations with time are observed in between 600 PPM to 3500 PPM with an average of 1448 PPM. Rate of production of CO_2 is

found to be highly time dependent as the burning process of the biomass is irregular and uneven. Unsteady dispersion and dilution with the flow field might also be the cause of fluctuating characteristics of CO₂ concentration at the breathing zone.

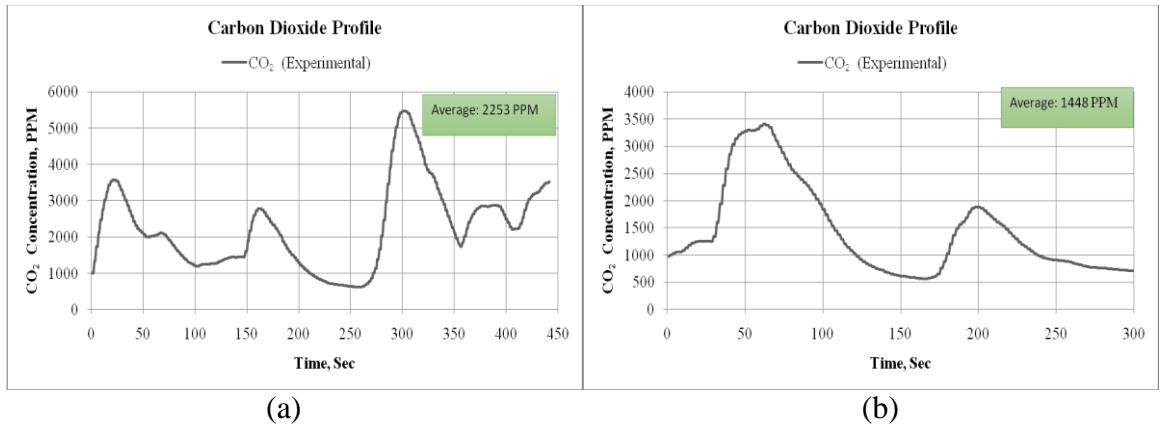


Fig. 5.12: CO₂ profile with time at the breathing point for rural kitchen 1 (a) data set 1 and (b) data set 2.

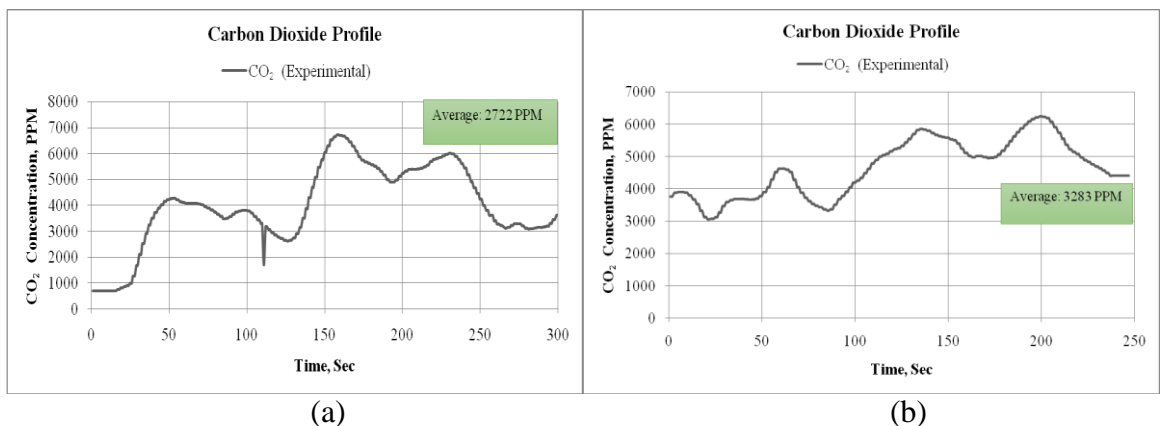


Fig. 5.13: CO₂ profile with time at the breathing point for rural kitchen 2 (a) data set 1 and (b) data set 2.

The experiment for CO₂ emission was also carried out in kitchen 2 at different place and the variations are presented in Fig. 5.13. In this case also the time variations of CO₂ concentrations are well captured in both data set 1 and 2. In data set 1, variations can be seen minimum of 500 PPM to a maximum of 6800 PPM. At different time interval some peaks are evident in both data sets. Data set 2 shows variations from 3000 PPM to 6000 PPM of CO₂ concentration. The average values are calculated as 2722 PPM and 3283 PPM respectively for data set 1 and 2.

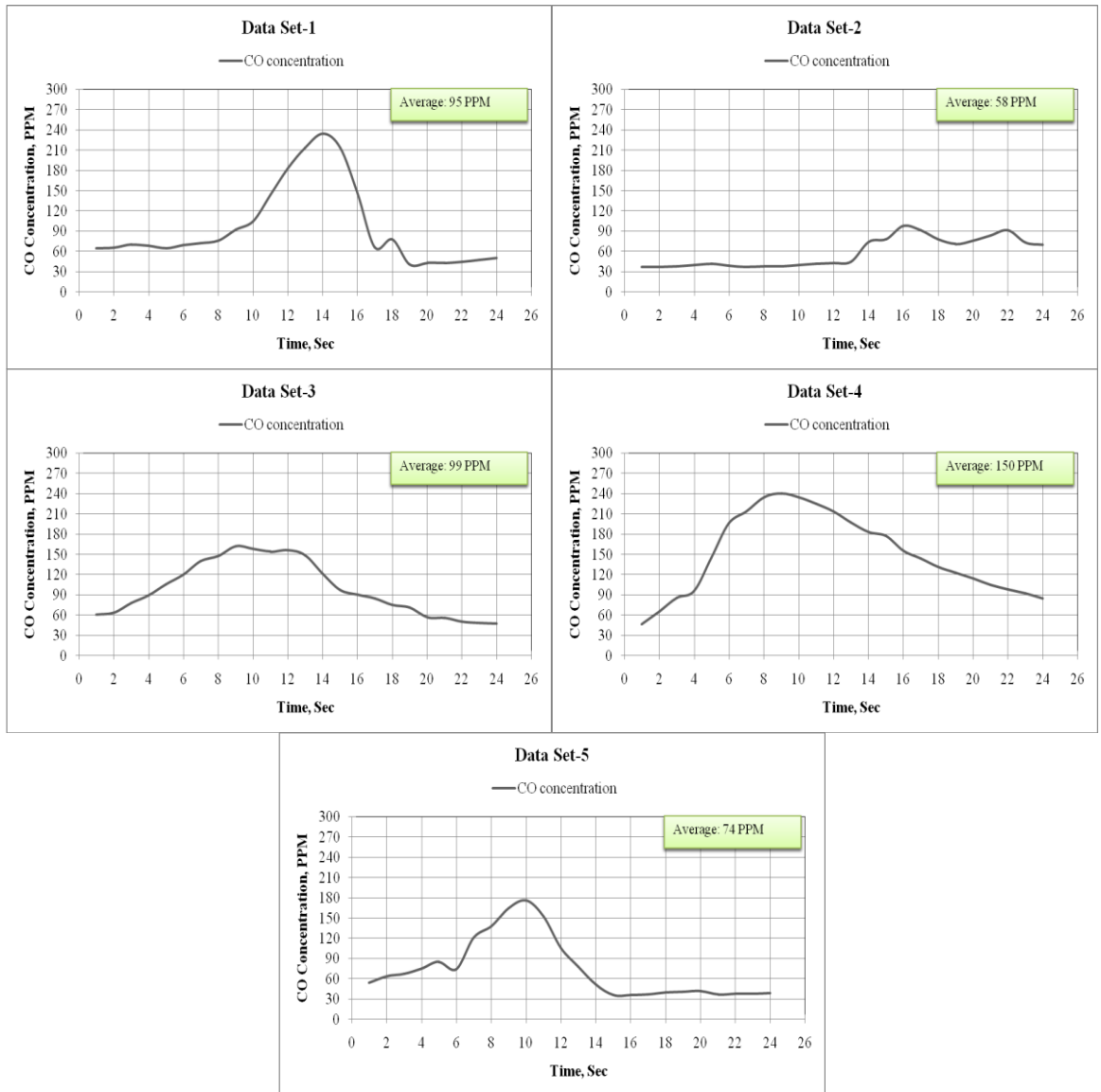


Fig. 5.14: CO concentration with time at the breathing point for rural kitchen 2.

Biomass combustion produces significant CO emission at a higher concentration rate. In order to see the concentration level following Fig. 5.14 is presented. In data set 1, CO varies with time from 60 PPM rising to 240 PPM at the middle and then again decreases. The average of the CO concentration is 95 PPM. At this level of CO exposure for short or long term can reduce oxygen carrying capacity of the human organ. At different time interval (data set 2) a steady lower emission of below 40 PPM observed for a while and after a while it increases to 90 PPM with average of 58 PPM. Data set 3 shows a maximum emission of 150 PPM at the

middle of the time with an average of 99 PPM. A maximum average emission observed in data set 4 with 150 PPM and data set 5 showed 74 PPM of average. This experiment certainly confirms that at the breathing point concentration remains significantly higher. At such exposure to CO will cause severe health damage to the occupant as the long term consequences.

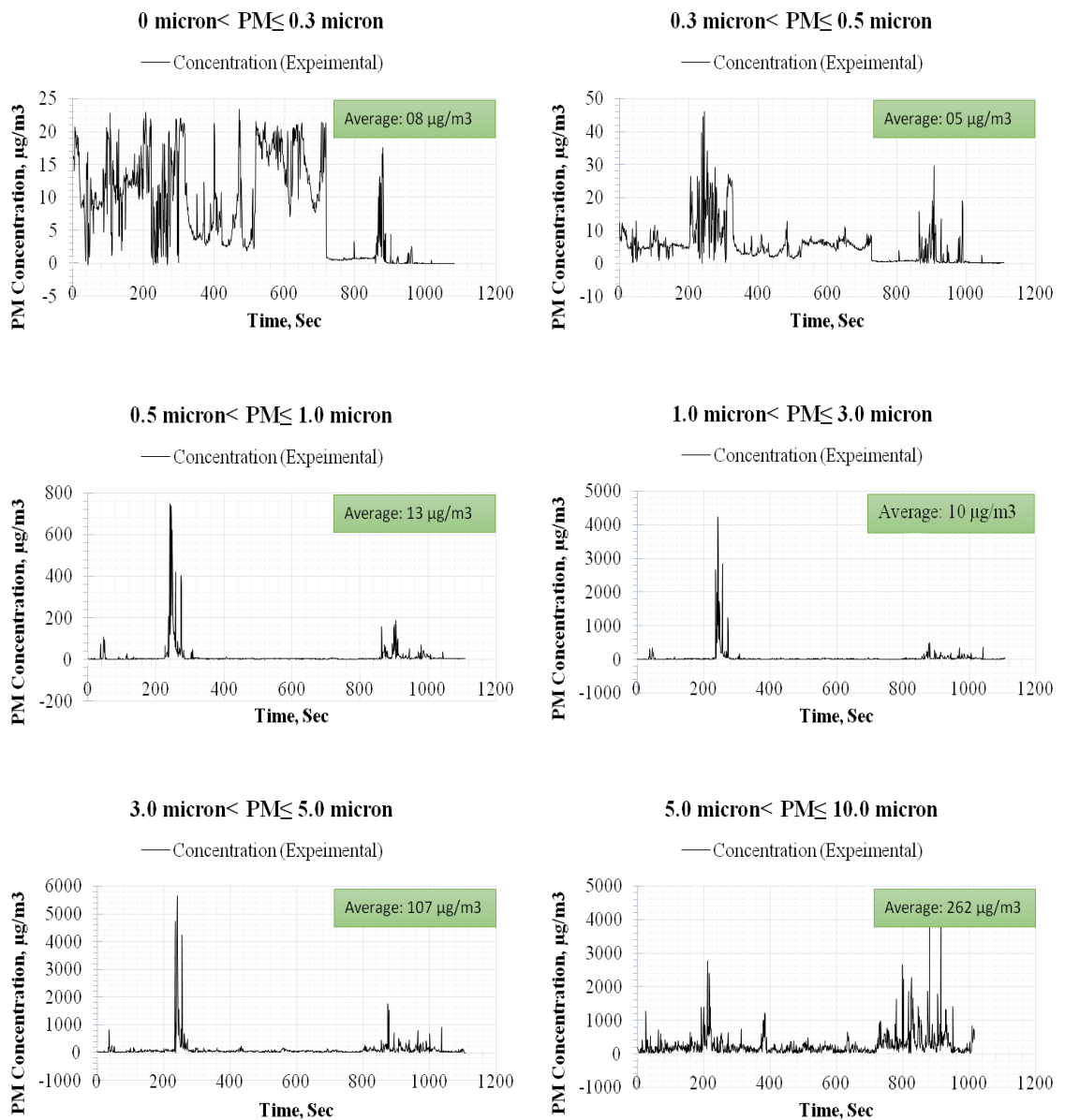


Fig. 5.15: PM concentration with time at the breathing point for rural kitchen 1.

Particulate matter, is also known as PM or soot, consists of microscopically small solid particles or liquid droplets suspended in the air. The smaller the particles, the deeper they can penetrate into the respiratory system and the more hazardous they are to breathe. Long-term exposure to PM concentrations inside the kitchen may lead to a marked reduction in life expectancy. It is primarily due to increased cardio-pulmonary and lung cancer mortality. Severe health problem may be seen with lower respiratory symptoms and reduced lung function in children and adults. PM may be classified as fine particles ranges from 0 to 3 μm size and coarse particles ranges from 3 to 10 μm . Fig. 5.15 is presented for particle size concentration at the breathing point of kitchen 1. Consistent incidence of PM size $\leq 0.3\mu\text{m}$ at the breathing point can be seen in Fig. 5.15a. It shows highly unsteady characteristics with a concentration range of 0 to 23 $\mu\text{g}/\text{m}^3$ and a mean value of 8 $\mu\text{g}/\text{m}^3$. Irregular fluctuations of PM size between $0.3\mu\text{m} < \text{PM} \leq 0.5\mu\text{m}$ are observed with a range of 0 to 40 $\mu\text{g}/\text{m}^3$ and a mean value of 5 $\mu\text{g}/\text{m}^3$. For the sizes of $0.5\mu\text{m} < \text{PM} \leq 1.0\mu\text{m}$ and $1.0\mu\text{m} < \text{PM} \leq 3.0\mu\text{m}$ the mean values are seen 13 $\mu\text{g}/\text{m}^3$ and 10 $\mu\text{g}/\text{m}^3$ respectively. Therefore, the total mean concentration of the fine particles is 36 $\mu\text{g}/\text{m}^3$ which is three times higher than the USEPA standard for fine particles. On the other hand for the particulate matter of coarse particle size from $3.0\mu\text{m} < \text{PM} \leq 10.0\mu\text{m}$, the total mean concentration count is calculated as 369 $\mu\text{g}/\text{m}^3$ whereas the USEPA standard concentration is 150 $\mu\text{g}/\text{m}^3$.

Similar experiments were conducted in rural kitchen 2 and presented in Fig. 5.16. The mean concentrations of PM of sizes $\leq 0.3\mu\text{m}$, $0.3\mu\text{m} < \text{PM} \leq 0.5\mu\text{m}$, $0.5\mu\text{m} < \text{PM} \leq 1.0\mu\text{m}$, $1.0\mu\text{m} < \text{PM} \leq 3\text{m}$. and $3.0\mu\text{m} < \text{PM} \leq 10.0\mu\text{m}$ are 9 $\mu\text{g}/\text{m}^3$, 20 $\mu\text{g}/\text{m}^3$, 85 $\mu\text{g}/\text{m}^3$, 113 $\mu\text{g}/\text{m}^3$, 100 $\mu\text{g}/\text{m}^3$ and 139 $\mu\text{g}/\text{m}^3$ respectively. The total concentration of fine and course particles are 114 $\mu\text{g}/\text{m}^3$ and 352 $\mu\text{g}/\text{m}^3$, respectively.

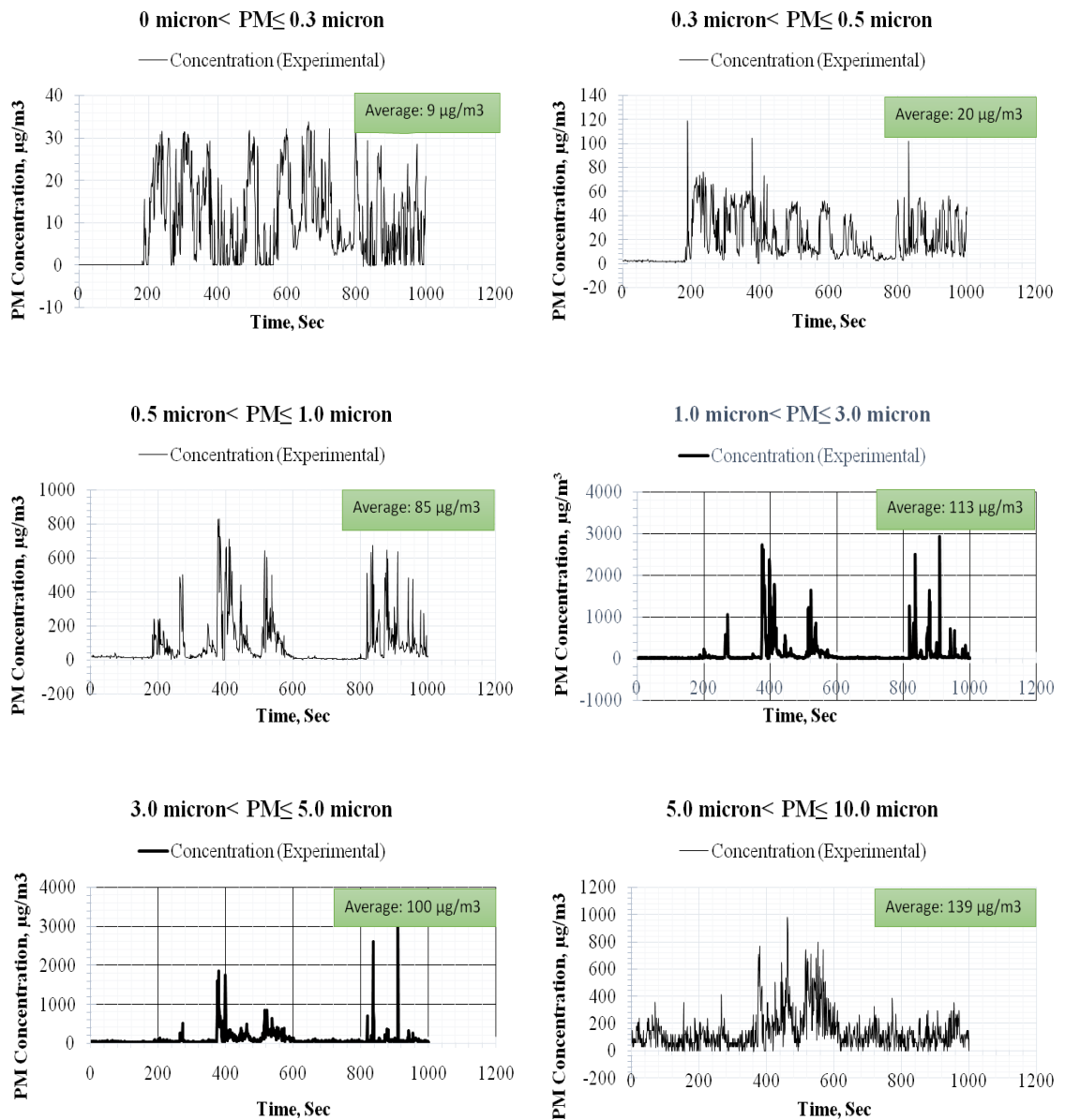


Fig. 5.16: PM concentration with time at the breathing point for rural kitchen 2.

5.3. Numerical study of Rural Kitchen

The results have been presented here for CO , CO_2 and PM_{10} concentration at three different planes as shown in Fig. 5.17. One plane named as longitudinal plane which is passing the mid-section of the stove in the X-Z plane. Second plane is named as lateral plane passing the breathing point in Y-Z plane. Finally, the third plane is called longitudinal plane which is parallel to the X axis and passing the breathing point of the cook.

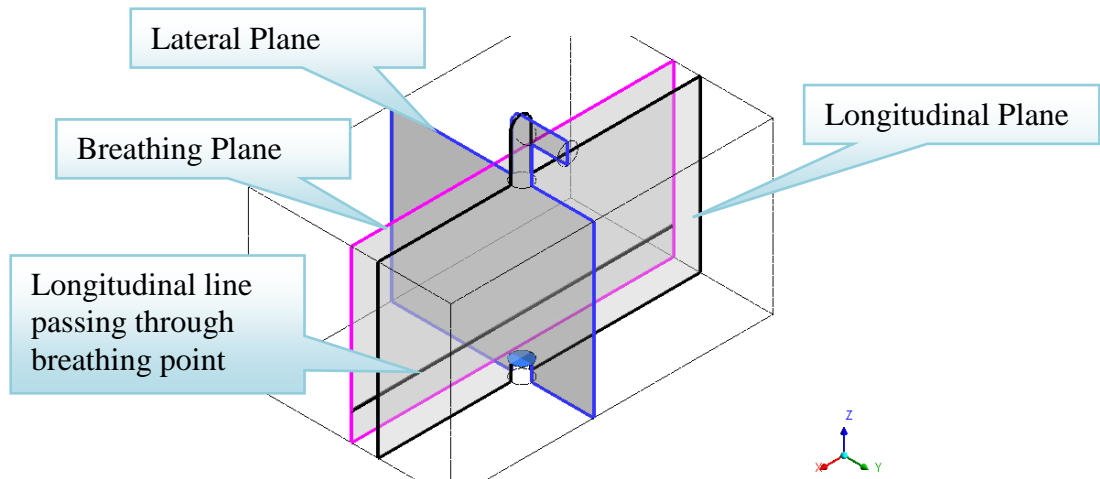


Fig. 5.17: Kitchen model with different planes and line.

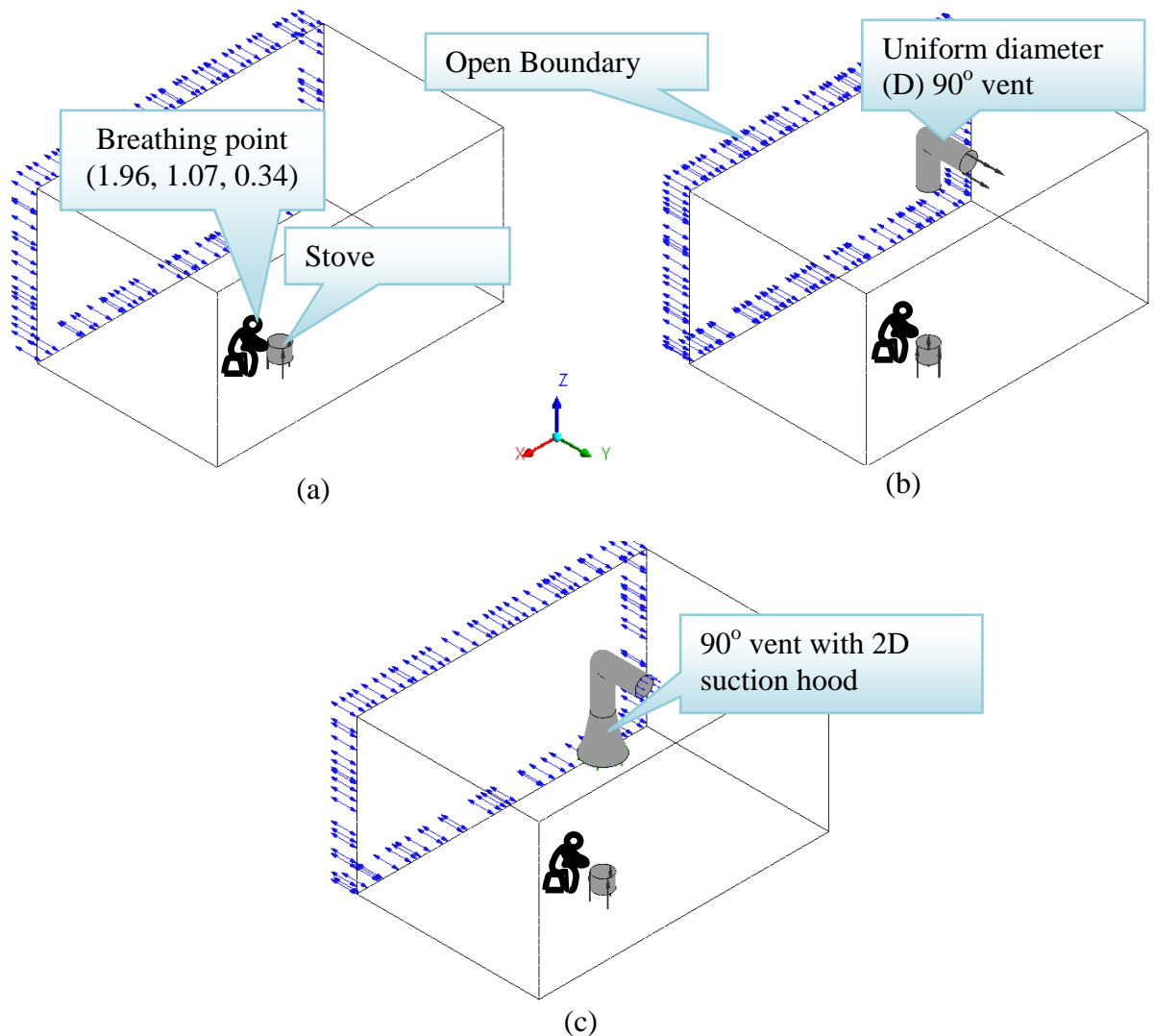


Fig. 5.18: Computational domain with boundary conditions (a) without vent (b) vent without hood and (c) vent with suction hood diameter 2D. (All dimensions are in m)

Several ventilation techniques have been adopted for the rural kitchen study. Fig. 5.18 shows computational domain with the boundary conditions and different ventilation cases. An open type boundary condition was employed in all cases as indicated with the double sided blue arrows. The breathing point location is at $x=1.8\text{m}$, $y=1.07\text{m}$ and $z=0.34\text{m}$. A single point source is used for CO , CO_2 and PM_{10} emissions. First of all a conventional rural kitchen was modeled and simulated (Fig. 5.18a) with three sides closed and one side open. Secondly, a roof top 90° vent (or chimney) is used with uniform suction to discharge diameter (D) of 22 cm. In the third technique, a hood is considered with a suction diameter of $2D$ and is extended to two times of the diameter, D from the roof. The third technique was then specially designed and modified based on the results of other techniques for the best desirable outcomes.

5.3.1. Numerical grid and code validation

Computational grid for rural kitchen was generated using ICEM CFD V12.1 software. Figs. 5.19 and 5.20 shows computational grids at two different planes. Complete tetrahedral cells were used for the domain with some refinement in the hood, vent and source regions. In order to perform computational validation, the experimental work was considered. In this study, a kitchen was modeled similar to the experimental setup. The test conditions were imposed to simulate same kitchen as a validation case of the present study. Fig. 5.21 shows timely variations of CO_2 and comparison between average numerical and experimental data for conventional rural kitchen. It is seen that the time averaged experimental and numerical results are in reasonable agreement.

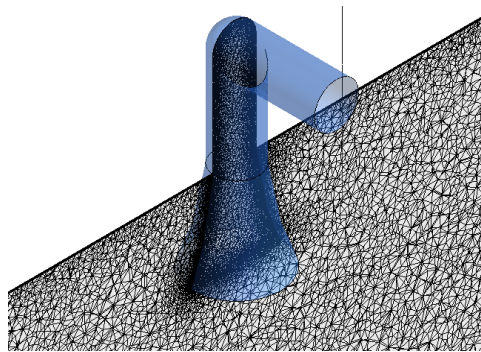


Fig. 5.19: Computational grid at X-Z and Y-Z plane.

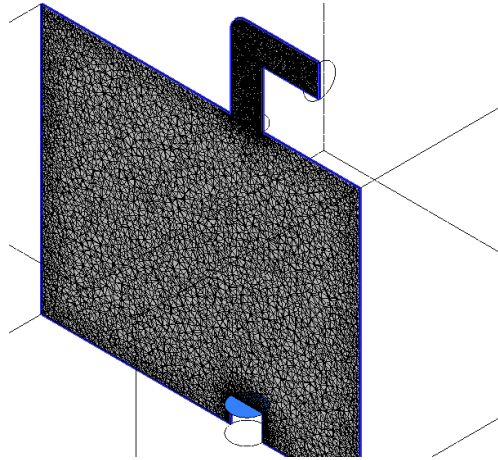


Fig. 5.20: Computational grid at Y-Z plane with Chimney.

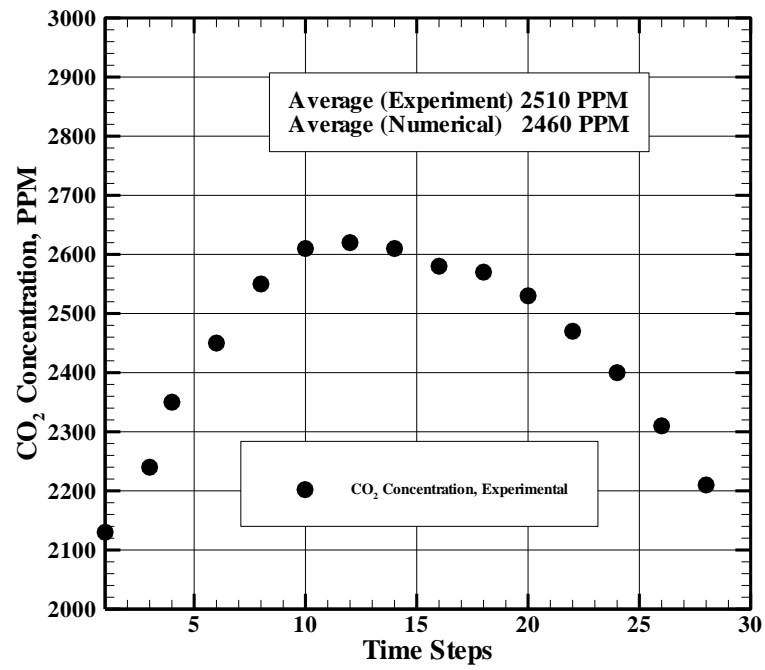


Fig. 5.21: Comparisons between Experiment and Prediction.

5.3.2. Without Ventilation

In this section, the distributions of CO, CO₂ and PM₁₀ at all three planes have been investigated for a typical rural kitchen without ventilation which is commonly seen in the villages of the developing countries. Fig. 5.22 is presented for the CO concentration at three different planes with a source concentration of 338 PPM. It is seen that for the close vent case, left lower portion has higher concentration of about 121 PPM to 148 PPM range with more dispersion than the right lower portion (see Fig. 5.22a). On the other hand, rear side of the stove in Fig. 5.22b shows relatively higher concentration than the front side. More importantly, at the whole breathing zone the CO concentration varies within a range of 66 PPM to 121 PPM.

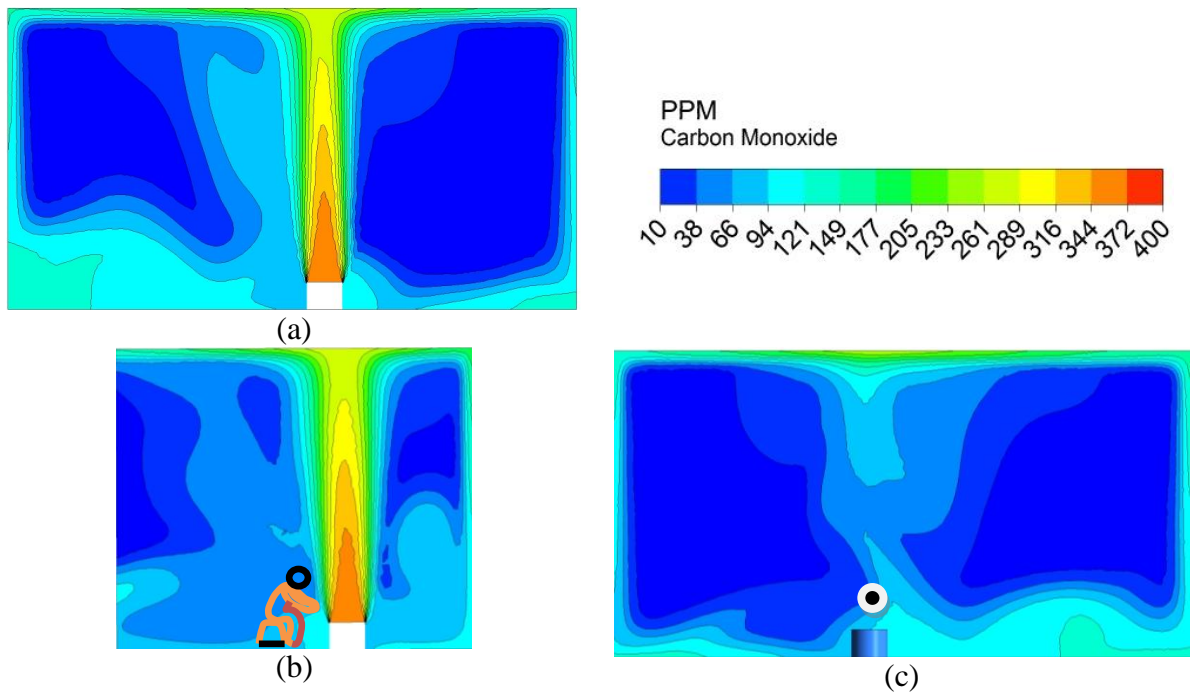


Fig. 5.22: Carbon Monoxide concentration (source 338 PPM) at (a) longitudinal plane, (b) lateral plane and (c) breathing plane with close vent.

Fig. 5.23 is plotted to quantify the CO distributions at the line passing the breathing point in the longitudinal distance (X-direction). It appears in the figure that CO varies over the X distance. The maximum concentration of 116 PPM can be seen at 0.8m distance. It is then followed by two other peaks with relatively lower concentrations of 95 PPM at 1.8m and 35 PPM at 2.5m distances respectively. The breathing point concentration is indicated with a value of 90 PPM. So it is very clear

that in the rural kitchen occupants are exposed to 8 to 9 times higher CO emission than the limit when left unventilated.

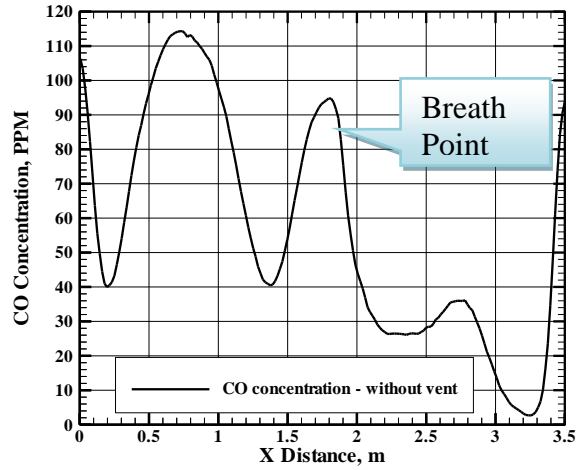


Fig. 5.23: CO concentration at a line passing the breathing point for source 338 PPM.

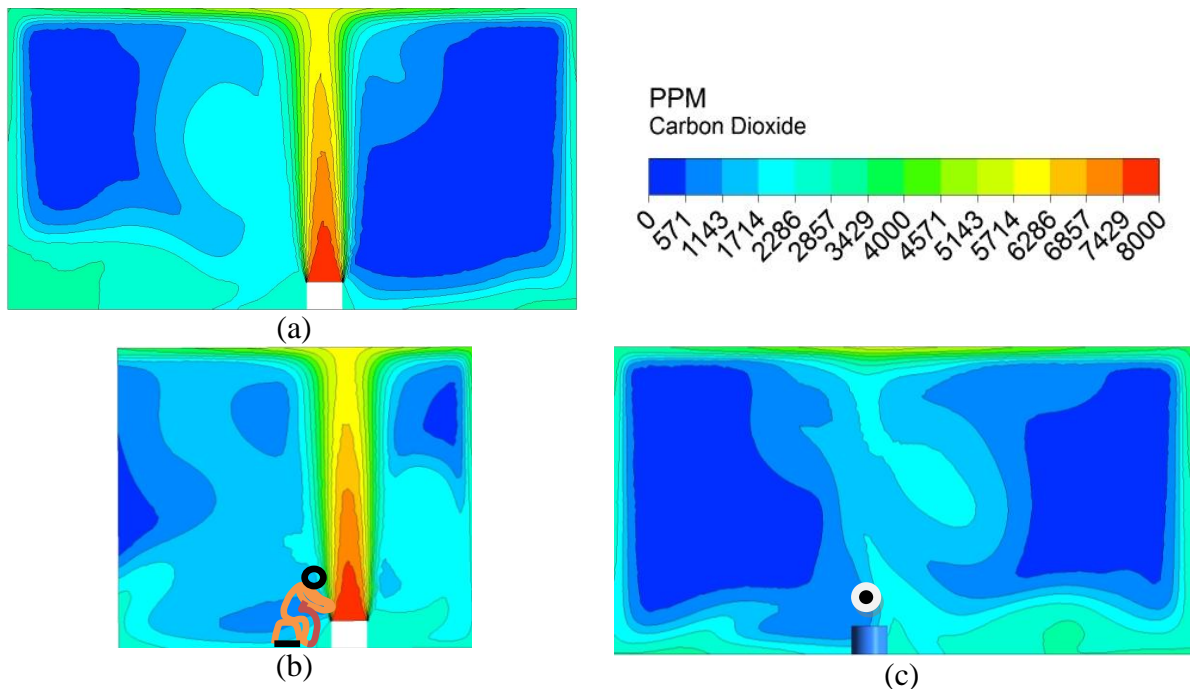


Fig. 5.24: Carbon Dioxide concentration (source 7100 PPM) at (a) longitudinal plane, (b) lateral plane and (c) breathing plane with close vent.

To examine CO₂ emission contour at different planes Fig. 5.24 is presented for closed vent condition. At the plane passing the mid stove in the longitudinal direction (see Fig. 5.24a), the emission concentration shows vertical dispersion within a range of 571 PPM to 2286 PPM. Adjacent to the breathing zone the maximum emission is seen on the left side. However on the right the emission is lower than the standard limit. Fig. 5.24b shows lateral dispersion of the CO₂ and can be seen significant on the fore side. At the longitudinal plane passing the breathing point right section shows higher emission.

Similar pattern as of CO distribution can be seen in the breathing line for CO₂ as well (see Fig. 5.25). The breathing point value of CO₂ emission is about 1800 PPM as indicated. Three peaks are evident with maximum concentration of 2300 PPM at a distance of 0.8m and minimum of 1250 PPM at a distance of 2.7m.

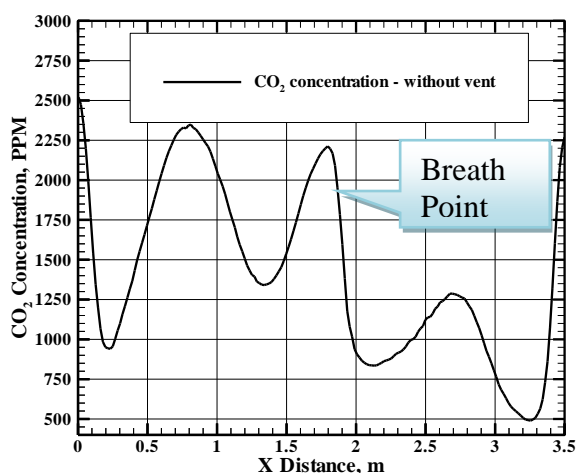


Fig. 5.25: CO₂ concentration at a line passing the breathing point for source 7100 PPM.

Biomass burning is a major source for Particulate Matter emission. It was also intended to investigate the level of PM₁₀ emission at different planes. An identical trend is also captured for PM₁₀ as like CO and CO₂ emissions. It is desirable properties for safe breathing in the rural kitchen that the PM₁₀ should be bellow 150 µg/m³. However, Fig. 5.26 shows that the PM₁₀ concentration is about 600 µg/m³ at all sides of the breathing zone.

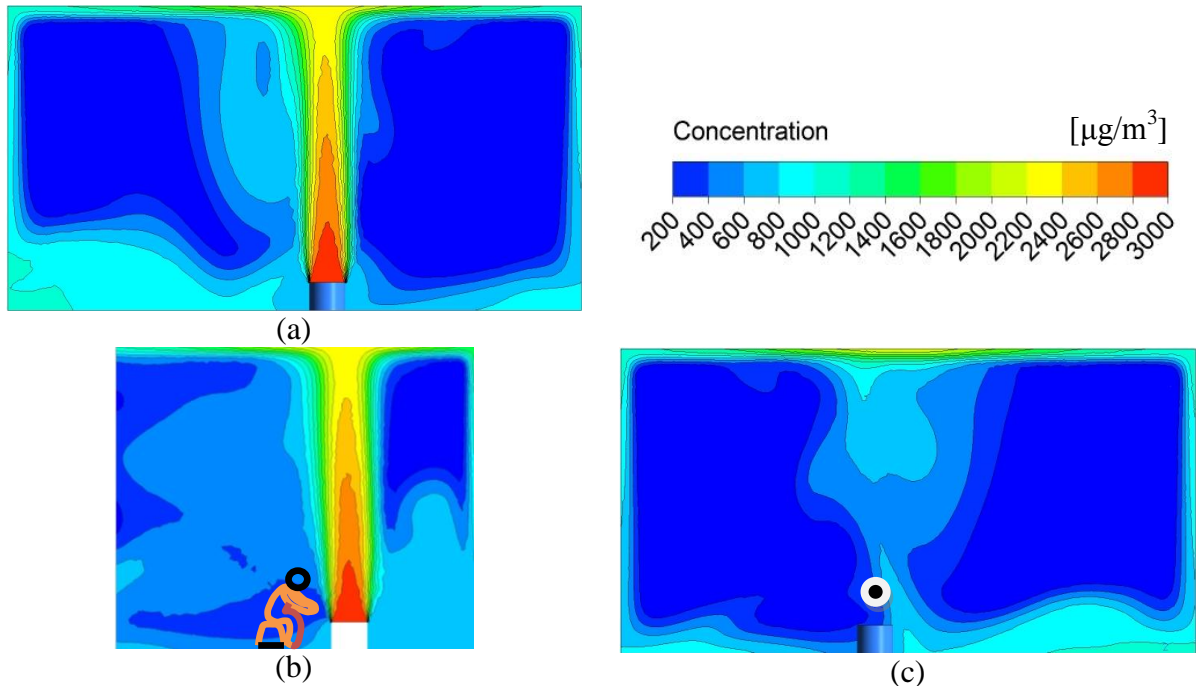


Fig. 5.26: Particulate Matter concentration (source $2867 \mu\text{g}/\text{m}^3$) at (a) longitudinal plane, (b) lateral plane and (c) breathing plane with close vent.

Figure 5.27 illustrates the local values of PM_{10} along the X-breath line in the longitudinal direction. The concentration is fluctuating between $50 \mu\text{g}/\text{m}^3$ to $800 \mu\text{g}/\text{m}^3$ at different sections. The maximum PM_{10} is $800 \mu\text{g}/\text{m}^3$ at a distance of 0.6m with a sharp peak of $750 \mu\text{g}/\text{m}^3$ near the breathing zone. Far from this zone another peak is observed with a concentration level of $260 \mu\text{g}/\text{m}^3$ at the 2.8m distance.

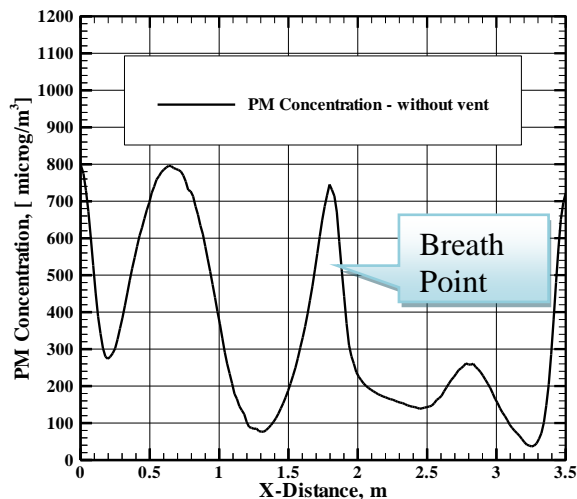


Fig. 5.27: Particulate Matter concentration at a line passing the breathing point for source of $2867 \mu\text{g}/\text{m}^3$.

5.3.3. With Natural Ventilation

It is apparent from the above study that the rural kitchen environment is highly polluted and hazardous. Thus poor people working in that environment are inadvertently prone to the immeasurable sufferings. This research undoubtedly a novel step for them to give a better environment and better life at a minimum cost possibly no cost as the rural people are in fact avoiding the things that cause them to pay. Keeping that in mind the following sections are dedicated for investigating the control methods of the pollution. In the first step a simple chimney with 22 cm uniform diameter and 90° bend is introduced at the roof top of the modeled kitchen. The natural suction hole was intentionally placed right at the top of the stove. It ensures that high emission enters directly in to the chimney suction. The added advantage of having suction directly on top of the stove is that after burning the exhaust gas is heated and become lighter which always tend to lift up and get some momentum to enter the chimney section. However, as a matter of fact, any arbitrary size and shape of the chimney does not signify the improvement. It requires study of the dispersion mechanism for various conditions.

Fig. 5.28 is presented for CO distribution at different planes with chimney opened to atmosphere. Natural ventilation will take place under such condition. Though the improvement is not significant in compared to the close vent condition but it still gives an idea for further improvement. High concentration zone of 94 PPM around the main stream flow becomes narrower. However, in close vent system (Fig. 5.26) the concentration coverage area is more. On the other hand for lateral plane, a small zone of 121 PPM is disappeared and drops to 94 PPM near the left proximity to the stove. On the other hand in the breathing plane 121 PPM concentration zone shifts towards the right with controlled spreading which signify a promising improvement of using a simple natural vent.

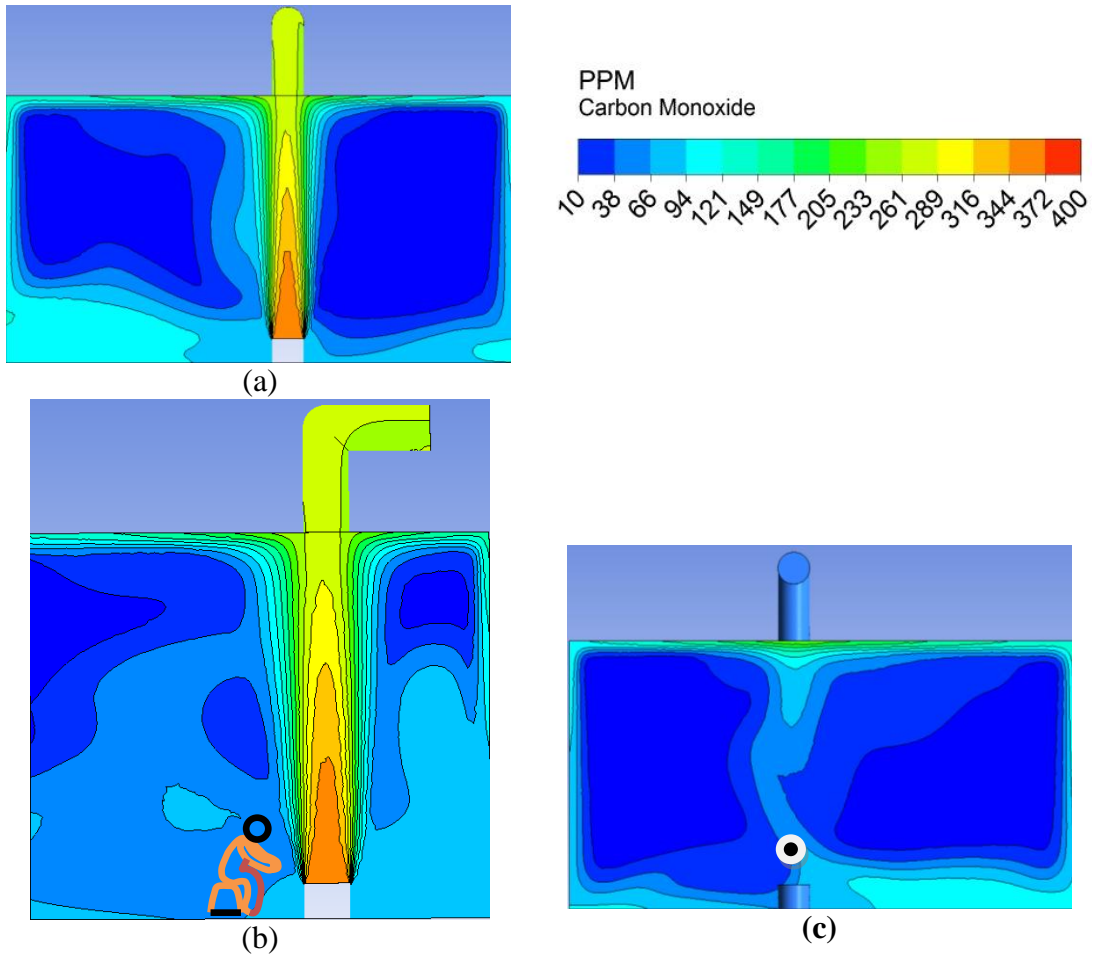


Fig. 5.28: Carbon Monoxide concentration (source 338 PPM) at (a) longitudinal plane, (b) lateral plane and (c) breathing plane with open vent.

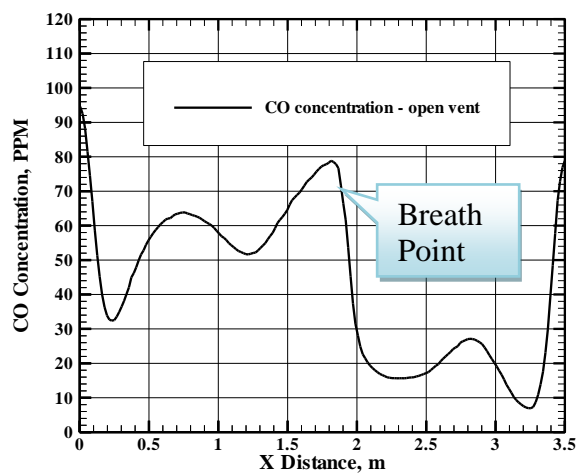


Fig. 5.29: CO concentration at a line passing the breathing point for source of 338 PPM.

Fig. 5.29 shows CO variations at the X-breath line along longitudinal distance. Emission reaches maximum concentration of about 80 PPM and right at the breathing point (indicated in Fig. 5.29) CO is 60 PPM which is a reduction of about 33% compared to close vent case.

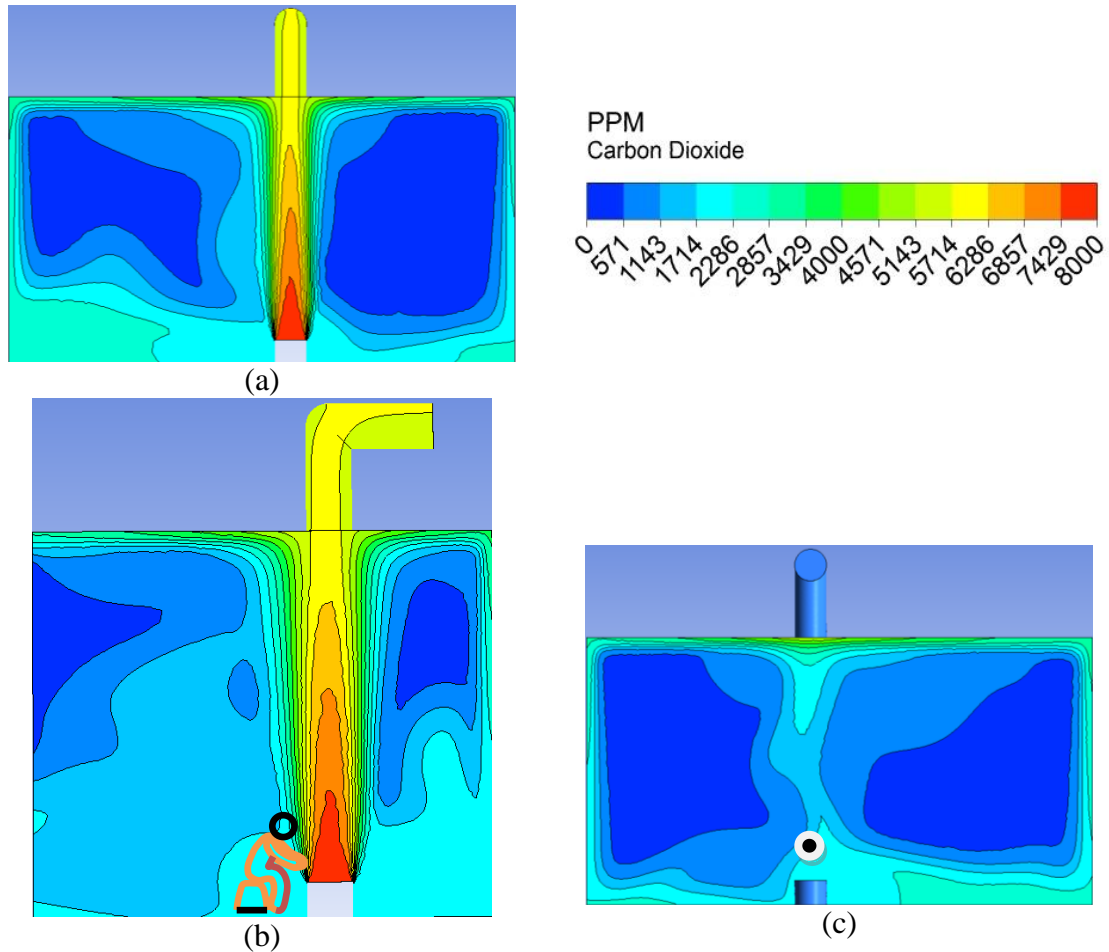


Fig. 5.30: Carbon Dioxide concentration (source 7100 PPM) at (a) longitudinal plane, (b) lateral plane and (c) breathing plane with open vent.

In the contour of CO₂ concentration (Fig. 5.30a), low emission coverage is more on the left as compared to close vent case. Longitudinal spreading becomes narrower about the high emission stream when compared to close vent case. Figure 5.30c shows relatively higher concentration appeared on the left of the stove where a small zone of low emission is disappeared (as seen in Fig. 5.20b of close vent case). At the breathing plane (Fig. 5.30c), upper zone shows lower dispersions and the lower zone concentration is appeared to be less when compared to close vent case.

Fig. 5.31 is presented for CO₂ distribution along the X breath line under open vent condition. A flat peak is appeared at the middle zone even though the breathing point concentration is about 2000 PPM which is about 10% greater than the close vent case. However, two other low concentration peaks are of 1100 PPM and 950 PPM appeared at the left and right zone respectively.

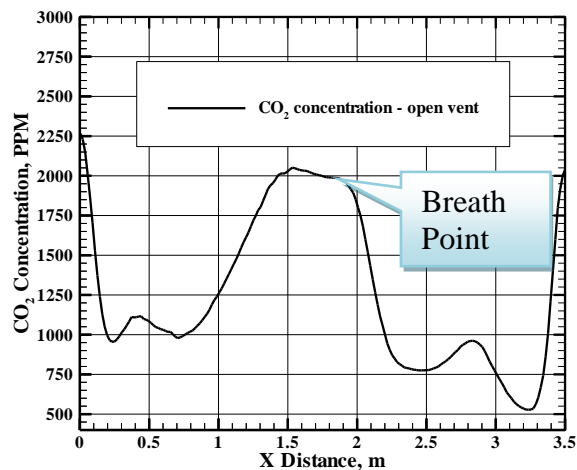


Fig. 5.31: CO₂ concentration at a line passing the breathing point for source of 7100 PPM.

PM₁₀ concentration is visualized at different planes in Fig. 5.32. The emission lower than 200 µg/m³ is appeared on both left and right zone with significant coverage area. Lower left and right zone seems to have concentration range from 400 µg/m³ to 800 µg/m³. In the lateral plane (Fig. 5.32b) a small zone of over 800 µg/m³ is detected at the lower left of the stove which may also be seen in the Fig. 5.32c. The overall concentration seems better compared to close vent condition in the fore and left upper region. Much improved conditions can be noticed at the breathing plane as well. Low concentration coverage is more on either side of the stove and around the stove concentration drops from 800 µg/m³ to 600 µg/m³.

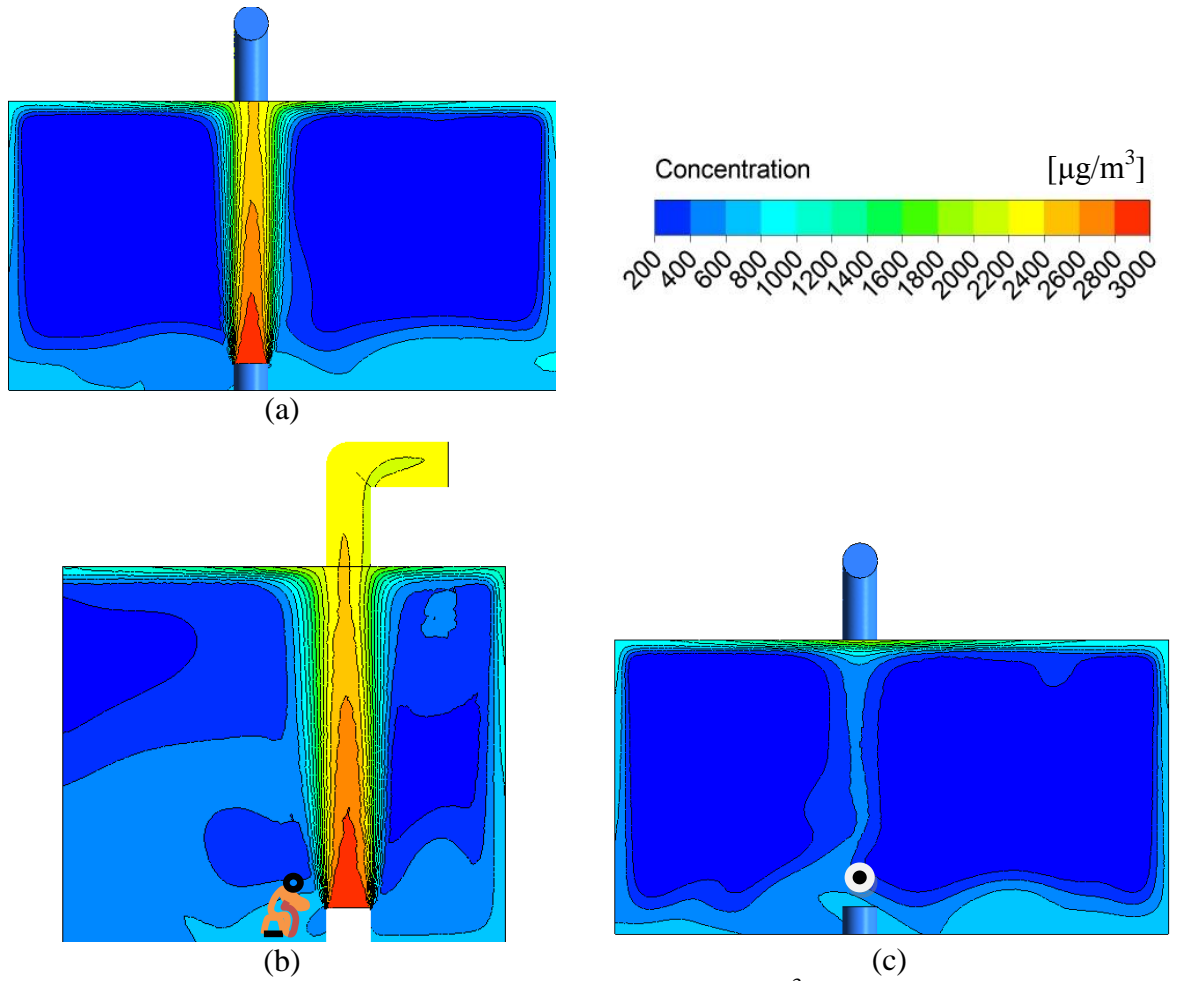


Fig. 5.32: Particulate Matter concentration (source $2867 \mu\text{g}/\text{m}^3$) at (a) longitudinal plane, (b) lateral plane and (c) breathing plane with open vent.

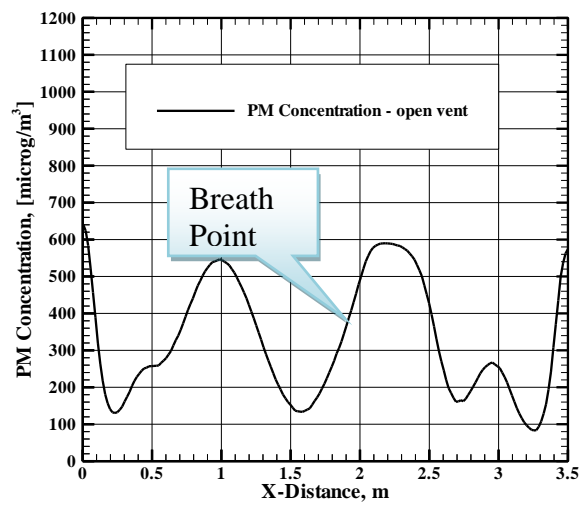


Fig. 5.33: Particulate Matter concentration at a line passing the breathing point for source of $2867 \mu\text{g}/\text{m}^3$.

Two peaks of similar PM₁₀ distribution pattern are observed in Fig. 5.33 at a distance of 1m and 2.25m respectively. The PM₁₀ concentrations remained below 600 $\mu\text{g}/\text{m}^3$ where the close vent case showed over 700 $\mu\text{g}/\text{m}^3$ at the peaks. At the breathing point the PM₁₀ concentration is seen about 380 $\mu\text{g}/\text{m}^3$.

5.3.4. Natural Ventilation with Hood

Further investigations have been conducted for emission using hood under natural ventilation. Instead of considering the suction plane at the roof, a new suction plane has been taken at 2D distance down from the roof and the suction hood diameter is doubled (i.e. 2D). It allows high discharge capacity of the emission to the atmosphere and thus expected to have lower emission pattern at the planes. Very promising results have been observed for all emission in all planes with compared to all other cases.

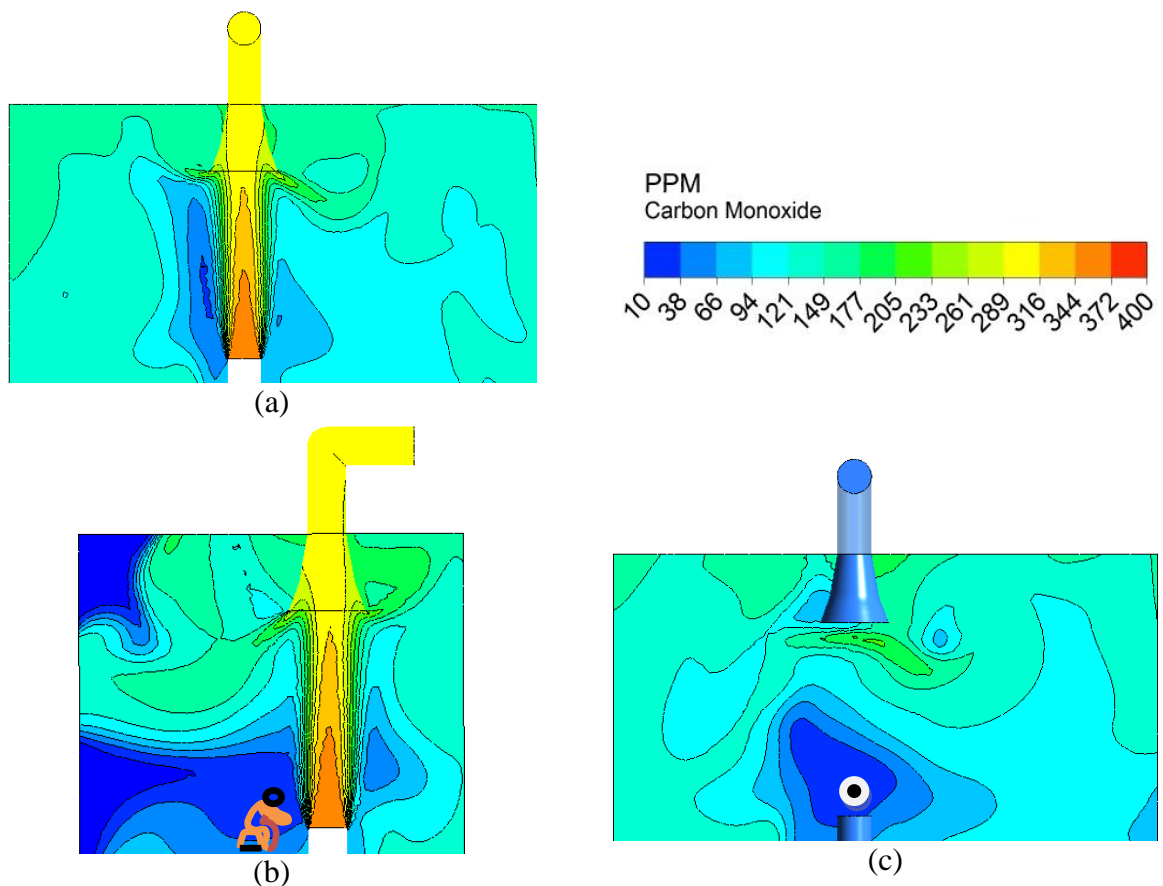


Fig. 5.34: CO concentration (source 338 PPM) at (a) longitudinal plane, (b) lateral plane and (c) breathing plane with open hood.

Fig. 5.34 is presented for CO contour at all three planes. A very remarkable phenomenon is observed at the far zone from the stove on either side (see Fig. 5.34a) where emissions are comparatively increased. Similar phenomenon can be observed at breathing plane as well. This is may be due to the reverse circulation of the emission deflected by the hood. On the contrary, this phenomenon becomes a blessing for the breathing zone where more fresh air (Fig. 5.34b) enters to fill the gap in the zone. A significant lower emission zone is evident in Fig. 5.34c, where CO dropped to 10 PPM or slightly higher.

Quantitatively the CO emission level can be well understood by the Fig. 5.35. Concentration is drastically reduced to 25 PPM at the breathing point and then increased to over 120 PPM near the right wall of the kitchen. Though the breathing point is not fully satisfying the maximum limit (10 PPM) but the improvement is compelling.

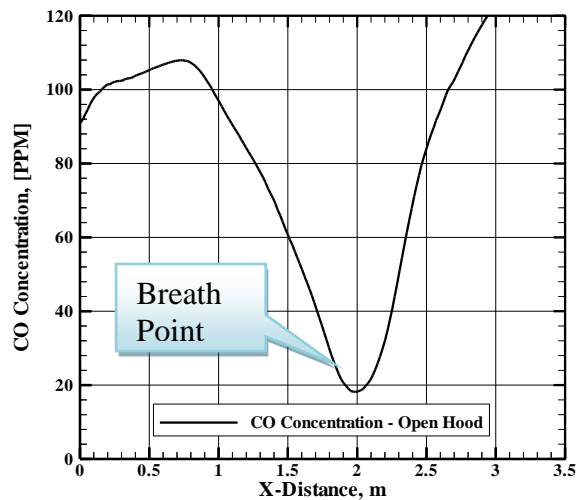


Fig. 5.35: CO concentration at a line passing the breathing point with open hood for source of 338 PPM.

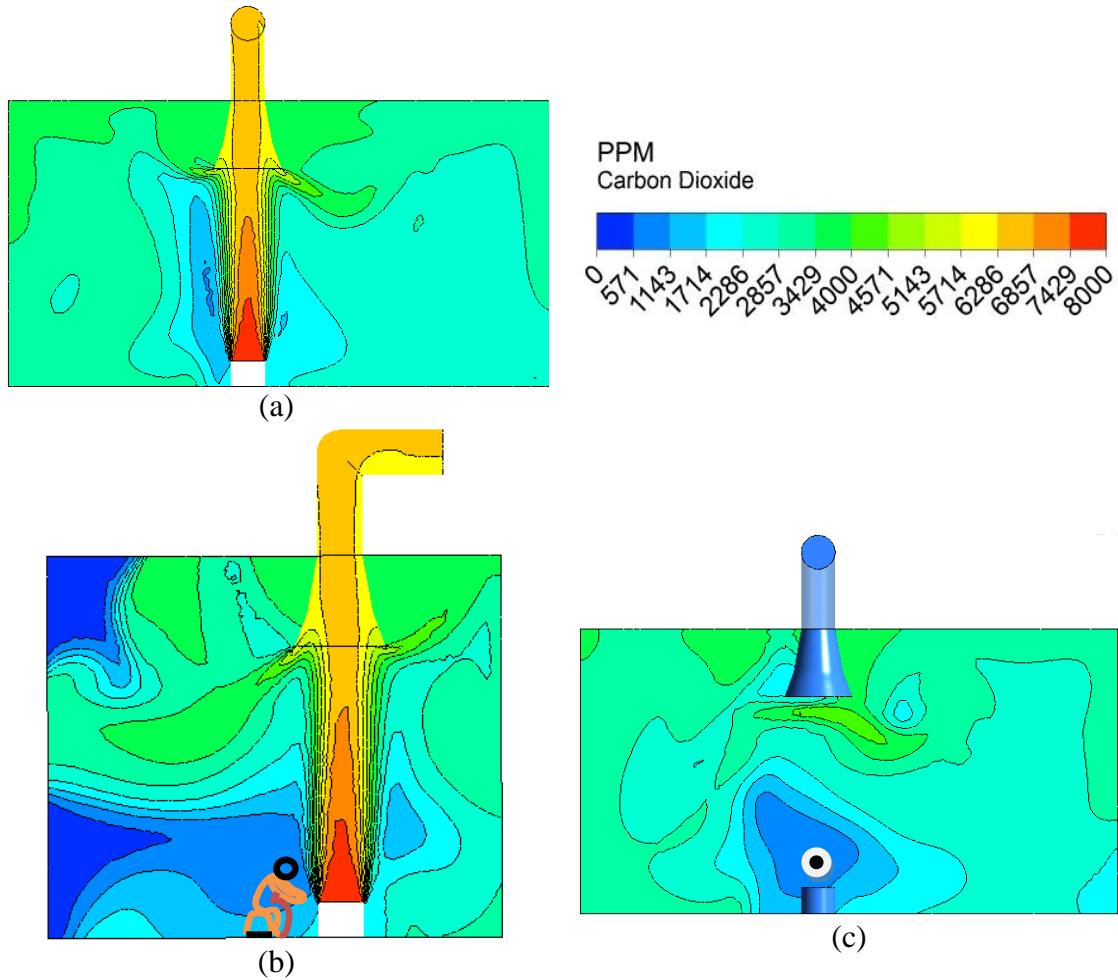


Fig. 5.36: CO₂ concentration (source 7100 PPM) at (a) longitudinal plane, (b) lateral plane and (c) breathing plane with open hood.

Similar to CO distributions, CO₂ also revealed the same. Around the main stream flow, CO₂ is well below 1100 PPM (See Fig. 5.36). In the lateral plane the entrainment of the fresh air is evident and keeps the concentration below 1000 PPM (Fig. 5.36b).

Fig. 5.37 is adopted to make a quantitative distribution of CO₂ in the breathing line. As seen earlier the left and right regions are having higher concentrations of 2500 PPM and over 3000 PPM respectively. However, at the breathing point the CO₂ concentration exhibits safe value of 1000 PPM.

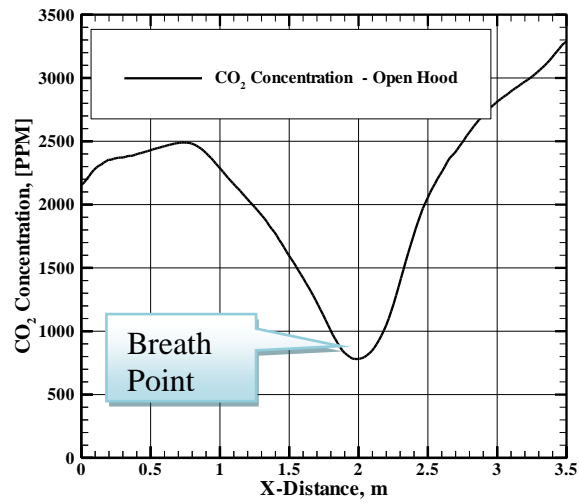


Fig. 5.37: CO₂ concentration at a line passing the breathing point with open hood for source 7100 PPM.

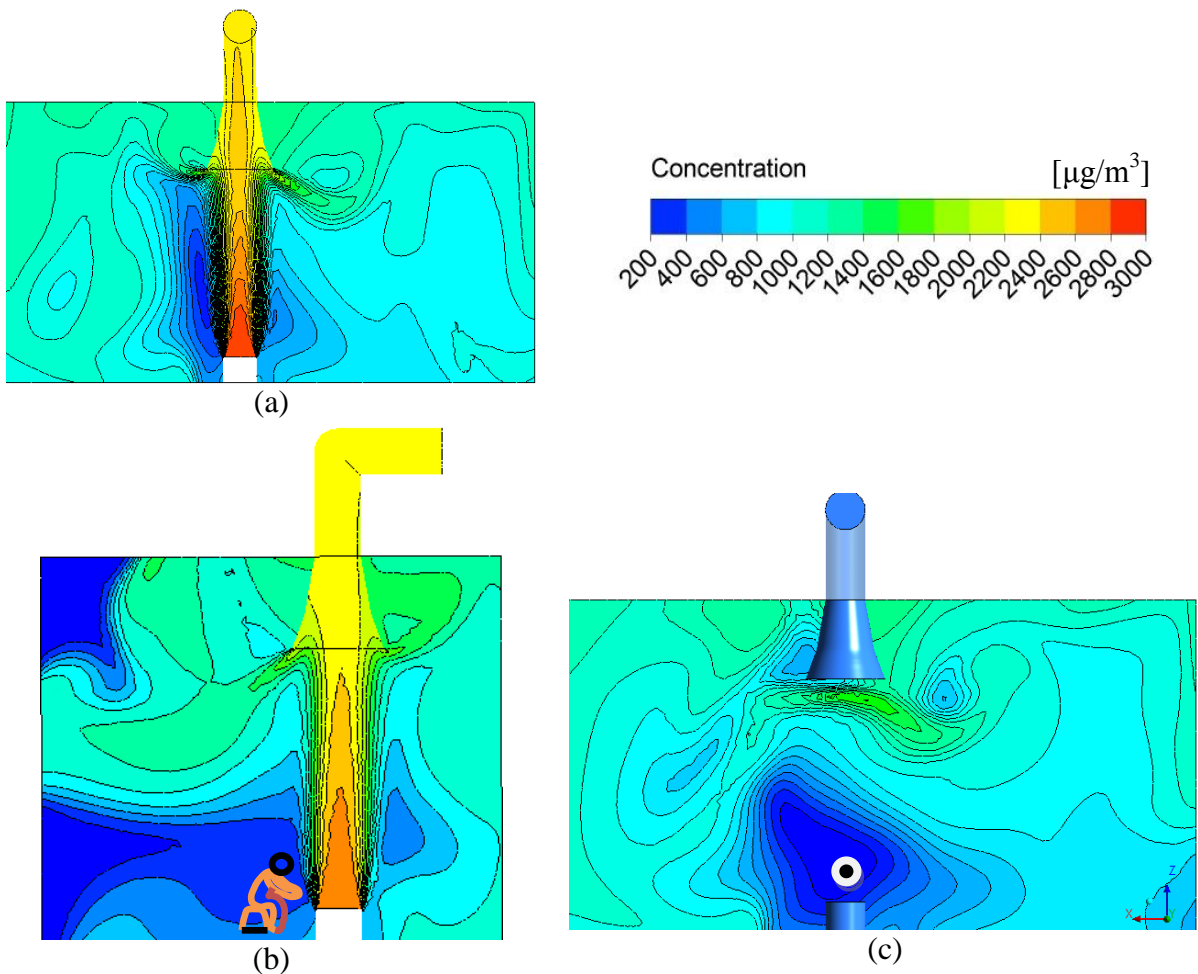


Fig. 5.38: Particulate Matter concentration (source 2867 µg/m³) at (a) longitudinal plane, (b) lateral plane and (c) breathing plane with open hood.

PM₁₀ concentrations are also investigated for the effect of using hood in the kitchen and presented in Fig. 5.38. Adjacent to the main stream zone of PM₁₀, on either side low concentrations are apparent where far zone exhibits significantly higher concentration (see Fig. 5.38a). The incoming fresh air takes the place of entire breathing zone which is a very desirable phenomenon as discussed earlier. However the upper zone still remains at a very higher concentration level. The coverage area of low emission boundary zone can be well understood from Fig. 5.38c where the cook seems to be in a healthier environment.

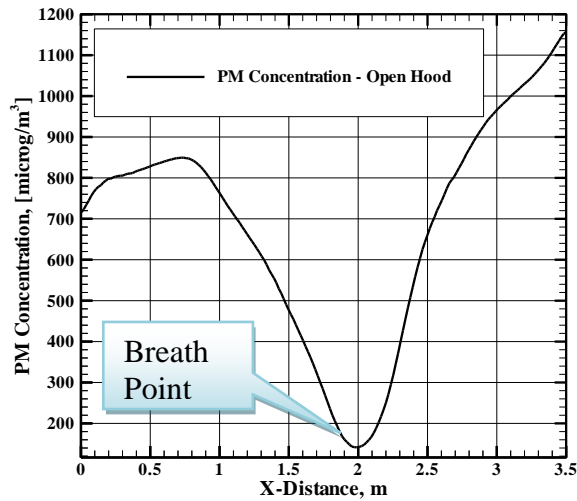


Fig. 5.39: Particulate Matter concentration at a line passing the breathing point for source of 2867 $\mu\text{g}/\text{m}^3$.

The PM₁₀ drops to 180 $\mu\text{g}/\text{m}^3$ at the breathing point which is still exceeding the limit of 150 $\mu\text{g}/\text{m}^3$ as per USEPA. However, kitchen with hood results in significant improvement as compared to other cases. Far zone in Fig. 5.39, shows over 800 $\mu\text{g}/\text{m}^3$ on the left and over 1100 $\mu\text{g}/\text{m}^3$ on the right.

5.4. Summary

In this part of the study, rural kitchens were both experimentally and numerically investigated for emissions such as CO, CO₂ and PM₁₀. Two typical rural kitchens were examined. Emission concentrations at source were recorded and used for numerical simulations.

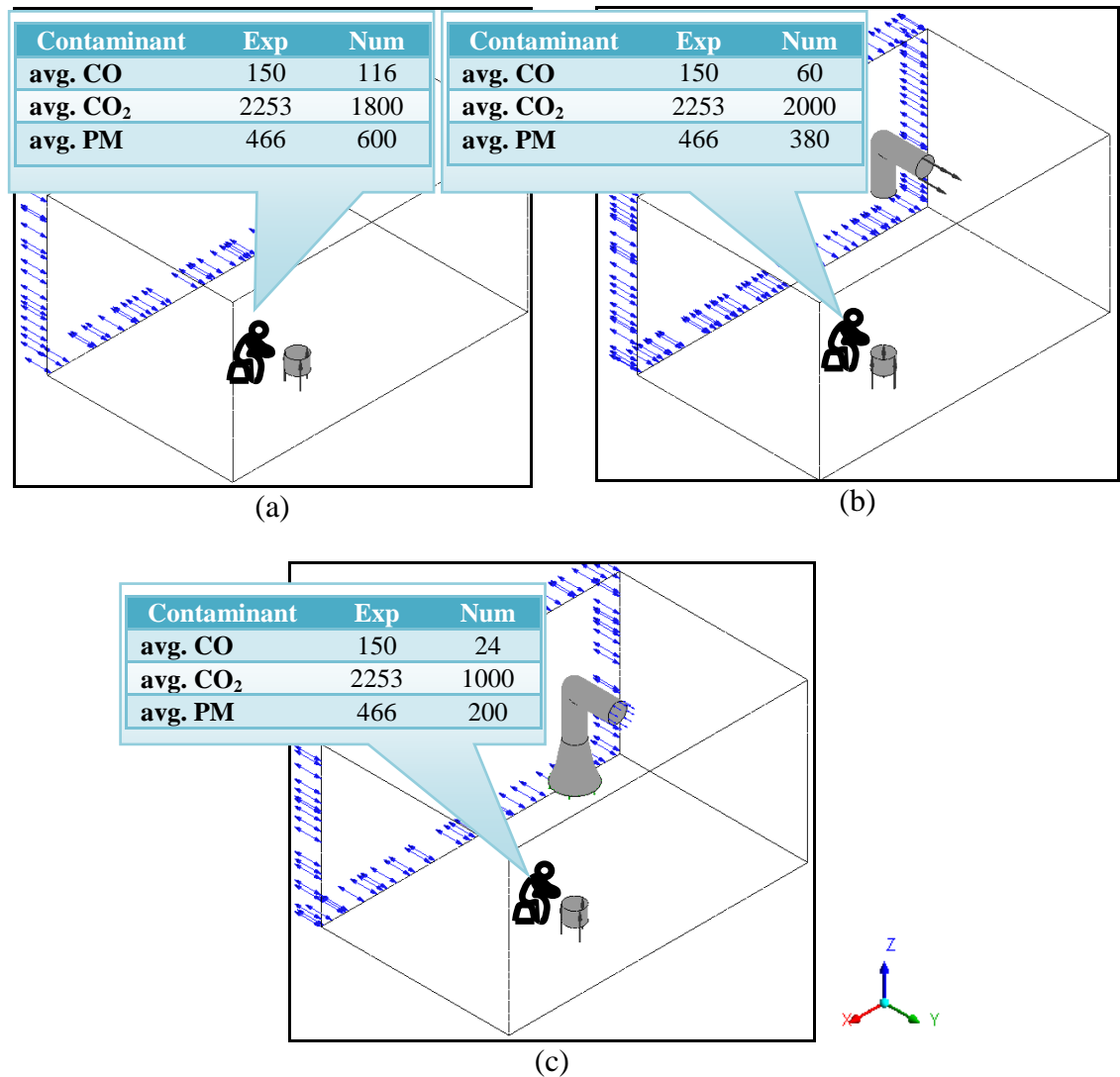


Fig. 5.40: Comparison between average experimental and numerical concentrations for (a) without vent (b) vent without hood and (c) vent with suction hood diameter 2D.

Breathing point concentrations were measured for bio-fuel burning and the numerical predictions were compared and analyzed at some pre-specified planes and lines with more attention to the breathing point. Fig. 5.40 might help to make comparative discussions among the cases for emission study and findings. At close ventilated conditions (Fig. 5.40a) the average CO is slightly under predicted (116 PPM) than the experiment (150 PPM). The predicted CO₂ was found as 1800 PPM which is again under predicted the experimental value (2253 PPM). However, the PM concentration is over predicted (600 $\mu\text{g}/\text{m}^3$) than the experiment (466 $\mu\text{g}/\text{m}^3$).

The main outcome of this study was to have controlled emissions from natural ventilation (Fig. 5.40b) and natural ventilation using hood (Fig. 5.40c). The predicted CO and PM are reduced by 48% and 37% respectively by introducing natural ventilation only (Fig. 5.40b). However, the average CO₂ is slightly increased. Furthermore, a significant improvement was observed when a hood was added. Under this condition, the predicted CO, CO₂ and PM₁₀ are greatly reduced by 79%, 45% and 67% respectively (Fig. 5.40c).

The following Table 5.2 is presented for association of different contaminant exposures with the possible health related consequences. As seen that the close ventilation of the rural kitchen causes high risk health related problem such as seizures, coma, respiratory failure, and death, lung cancer. A moderate level of health risk has been observed for case with chimney which is still not satisfying the air quality demand. However, a chimney with extension hood is found to be very effective in controlling the hazardous pollutants even under natural ventilation system.

Table 5.2: Findings of breathing point concentrations of different contaminants in connection with the possible health hazards

Test Cases	CO (PPM)	CO₂ (PPM)	PM (µg/m³)	Possible Health Hazard	Remarks on ventilation
Without vent	116	1800	600	High risk for seizures, coma, respiratory failure, and death, lung cancer.	Poor
With chimney	60	2000	380	Moderate risk for seizures, coma, respiratory failure, and death, lung cancer.	Moderate
With chimney and hood	24	1000	200	No health risk	Good

Chapter 6

6. Conclusions and Future Recommendations

A typical urban kitchen has been modeled and simulated using 3-dimensional CFD code ANSYS CFX-12.1. Two heat sources were used similar to the standard double burner gas stoves. The results were tested for grid independence to obtain an optimum grid resolution. The results are presented for temperature field, velocity field and CO₂ concentration level. The predictions are discussed under the effect of ventilation (natural and forced) and no ventilation system. The following conclusions can be drawn from this study-

1. For the gas stoves located in the kitchen corner, the flow tends to shift towards the corner side wall and exhibits high temperature zone all above the burners. Flow structure within the kitchen space is observed almost identical at all cases. The inhalation zone is acting like a source in Case 1, Case 2 and Case 3. However, in Case 4 it does not exist. More air circulates through the door in Case 1 (Close vent) as compared to other cases.
2. High temperature stream spreads from the kitchen roof adjacent to the door side wall and this phenomenon is observed in Case 1 and Case 3. Forced ventilation system can lower the temperature by a maximum of 8°C far from the stoves and near the stoves; the temperature reduction is about 12 °C. Within the breathing zone, the temperature is about 6°C higher than the comfort level of temperature.
3. CO₂ concentration between Case 1 and Case 4 can be reduced by 68.3% through increasing air vent velocity. At the breathing zone the predicted CO₂ concentration is greater than 5000 PPM which is far above the limiting standard values. However, forced ventilation with sufficient air exchange rate can reduce the CO₂ level significantly below the safe threshold.
4. Flow structure is seen different for hood system and air turbulence is higher. But there is no existence of the source like point. The hood system reduces

the thermal spreading in the kitchen room. It can confine the thermal uncomfortable zone effectively. CO₂ concentration (@ 1.5 m/s hood system Vs close vent) can be reduced by 10 times through use of efficient hood system. At breathing zone the hood system can reduce the CO₂ level to as low as 500 PPM only which is much lower than the safe threshold. If World Health Organization (WHO) or United Nations (UN) recommends kitchen construction with a mandatory hood system, it could substantially improve respiratory health and lifespan of the kitchen room occupants especially of the south Asian, African peoples who are more vulnerable.

5. Among the all cases hood suction below the stove (Case 6) shows better performance as long as the thermal comfort and health safety are concerned. This system can significantly keep CO₂ concentration as low as 800 PPM. Case 5 can also be a recommended system as it shows low CO₂ concentration.
6. For the front suction hood (Case 5) roof top heat accumulation is seen as high as 32.8 °C. However, base suction system can provide better thermal comfort.

A typical rural kitchen has been experimented for emissions and then modeled to perform 3-dimensional CFD simulation using ANSYS CFX-12. The experiments were conducted for capturing concentration of CO, CO₂ and PM at the source of the stove. Emissions were recorded for different bio-fuels such as Firewood, Cowdung, Rice husk and their mixtures. The concentration of CO, CO₂ and PM at the source, were used as input in the numerical cases. Predicted results were then tested for grid independence to obtain an optimum grid resolution and validated with the experimental data. The predictions have been discussed under the effect of without ventilation, open vent conditions and open vent with hood. The following conclusions can be drawn from this study.

1. Based on the predicted results, it is evident that simple natural ventilation is not enough to keep down the concentration below the safe limit. At the breathing point for without ventilation case, the CO and CO₂ concentrations are

predicted as 70 PPM and 2050 PPM respectively which are far above the limiting threshold.

2. The predicted CO and PM₁₀ are reduced by 48% and 37% respectively by introducing natural ventilation only through the chimney. Furthermore, a significant improvement observed when a hood was added. Under this condition, the predicted CO, CO₂ and PM₁₀ are greatly reduced by 79%, 45% and 67% respectively. Therefore, to overcome the long term effect of exposure to all deadly hazardous emissions, it is recommended for any rural kitchen to use efficient exhaust system with forced ventilation duct if affordable or an advanced natural ventilation design.

Indoor air pollution has been the major interest for both the researchers and the designers who work for implementations of the technology. In the recent years, the increasing demand for comfort and healthy living, people becoming aware of improving the indoor environments. However, no universal methods have been recommended that could reach the target level of safety and comfort of living. This current study can be further extended by implementing intensive simulations of whole apartment to see how the pollutants disperse in to other rooms. Different cases may be adopted for finding the best suitable positions of the kitchen within the apartment layout as it is the major source of indoor pollution. The study may further be extended for the emission of liquefied petroleum gas (LPG) burning as because in the near future there is a possibility that the domestic gas supplies in the urban kitchen will be replaced in Bangladesh.

For the rural kitchen, there is a wide scope for improving the stove exhausts design. Experimental and numerical studies might also be considered for further development of the exhaust size, pattern and shapes.

References

- [1] Posner, J.D., Buchanan, C.R. and Dunn-Ranking, D., 2003, "Measurement and Prediction of Indoor Air Flow in a Model Room", *Journal of Energy and Building*, Issue no. 35, pp. 515-526.
- [2] Wisconsin Department of Health Services, USA, 2012.
<http://www.dhs.wisconsin.gov/eh/chemfs/fs/carbondioxide.htm>
- [3] ANSYS CFX-12.1 Documentation Release 12.1, 2009 by ANSYS, Inc., USA.
- [4] Kirkwood, B., Gove, S., Rogers, S., LobLevyt, J., Arthur, P. and Campbell, H., 1995, "Potential interventions for the prevention of childhood pneumonia in developing countries: a systematic review", *Bull. World Health Organ.* , 73, 793–798.
- [5] Bruce, N., 1999, "Lowering Exposure of Children to Indoor Air Pollution to Prevent ARI: the Need for Information and Action", *Capsule Report (3)*, Arlington, VA, Environmental Health Project.
- [6] WHO, 2001, "Informal Consultation on Epidemiologic Estimates for Child Health", Geneva, Department of Child and Adolescent Health Development, WHO. Available at: [http:// www.who.int/child-adolescent-health/ NewPublications/CHILD_HEALTH/ Report-of-CHERG-meeting.html](http://www.who.int/child-adolescent-health/NewPublications/CHILD_HEALTH/Report-of-CHERG-meeting.html).
- [7] Murray, C. and Lopez, A., 1996, "The Global Burden of Disease", Cambridge, MA, Harvard School of Public Health, WHO, World Bank.
- [8] Smith, K., 1993, "Fuel combustion, air pollution exposure, and health: the situation in developing countries", *Annual. Rev. Environ. Energy*, 18 , 526–566.
- [9] Smith, K. and Metha, S., 2000, "The Global Burden of Disease from Indoor Air Pollution in Developing Countries: Comparison of Estimates", Prepared for the WHO/ USAID Global Technical Consultation on Health Impacts of Indoor Air Pollution in Developing Countries.
- [10] Awbi, H. B., and Allwinkle, S. J., 1986, "Domestic Ventilation with Heat Recovery to Improve Indoor Air Quality", *Energy and Buildings*, 9, 305–312.

- [11] Kondo, Y., Akabayashi, S., Nagase, O. and Matsuda, A., 1998, “Numerical Simulation of Ventilation Efficiency in Commercial Kitchen”, proceedings of Roomvent 98: 6th International Conference on Air Distribution in Rooms, Stockholm, Sweden,
- [12] Park M., Lee D., Kim K., and Lee J., 2000, “Prediction of the Ventilation Performance in a Kitchen with Various Locations of Gas Range and Window”, PHOENICS User Conference Proceedings.
- [13] Chi-ming Lai, 2005, “Assessment of Side Exhaust Systems for Residential Kitchens in Taiwan”, Building Services Engineering Research and Technology, Vol. 26, No. 2, 157-166.
- [14] Nantka M., B., 2006, “Indoor Conditions in Silesian Buildings with Natural Ventilation”, Indoor Built Environ;15;6:571–582.
- [15] Kajtar, L., and Leitner, A., 2007, “CFD Modeling of Indoor Air Quality and Thermal Comfort”, Proceedings of the 2nd IASME / WSEAS International Conference on Continuum Mechanics, Portoroz, Slovenia.
- [16] [16] Odunze N., Mishra R., and Reed J., 2007, “The CFD analysis of the effects of the size and location of an Air-Inlet in domestic kitchen extraction”, School of Computing and Engineering Researchers Conference, University of Huddersfield.
- [17] Panagopoulos, I., Karayannis, A., Kassomenos, P., and Aravossis, K., 2009, “A CFD Simulation Study of VOC and Formaldehyde Indoor Air Pollution Dispersion in an Apartment as Part of an Indoor Pollution Management Plan”, Proceedings of the 2nd International CEMEPE, SECOTOX Conference, Mykonos, ISBN 978-960-6865-09-1.
- [18] Villi G., Pasut W., and Carli M., D., 2009, “Computational Aspects of Modeling Different Strategies For Kitchen Ventilation: A Comparison Between The Multi-Zone Approach And CFD Modeling With Reference To Predicted Indoor Pollutant Concentrations”, Eleventh International IBPSA Conference Glasgow, Scotland, July 27-30, - 1574.
- [19] Zhou, J. and Kim, C., 2010, “Numerical investigation of indoor CO₂ concentration distribution in an apartment”, 3rd International Symposium on Sustainable Healthy Buildings; Seoul, Korea. 27 May.

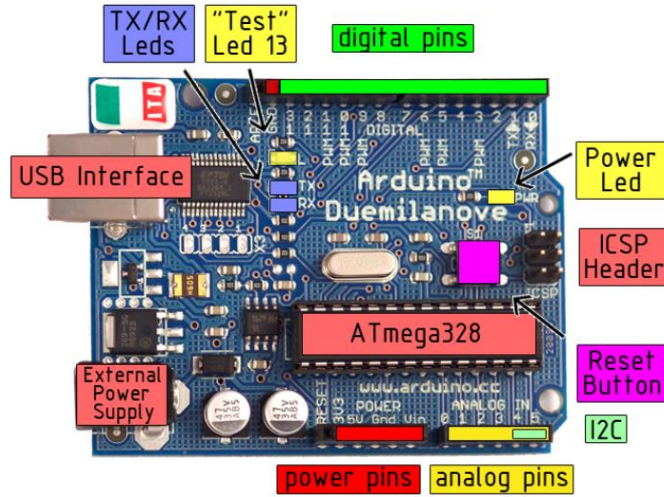
- [20] Mohammed, R., 2013, “Numerical Investigation of Indoor Air Quality and Thermal Comfort in a Ventilated Room”, World Academy of Science, Engineering and Technology International Journal of Environmental, Ecological, Geological and Marine Engineering Vol:7 No:12.
- [21] Brohard, G., Swierczyna, R., Sobiski, P., And Smith, V., Fisher, D., 2002, “Makeup Air Effects On Commercial Kitchen Exhaust System Performance” California Energy Commission, P500-03-007.
- [22] Pandey, M.R., Neupane, R.P., Gautam, A., and Shrestha, I.B., 1989, “Domestic Smoke Pollution and Acute Respiratory Infections in a Rural Community of the Hill Region of Nepal”, Environment International, Vol. 15, pp. 337-340.
- [23] Albalak, R., Frisancho, A.R., and Keeler, G.J., 1999, “Domestic Biomass Fuel Combustion and Chronic Bronchitis in Two Rural Bolivian Villages”, Thorax;54:1004–1008.
- [24] Zhang, J. and Smith, K. R., 1999, “Emissions of Carbonyl Compounds from Various Cook stoves in China”, Environmental Science and Technology, 33 (14), pp 2311–2320.
- [25] Ravi, M.R. ,Kohli, S. , and Ray, A., 2002, “Use of CFD Simulation as a Design Tool for Biomass Stoves”, Energy for Sustainable Development, Volume VI, No. 2.
- [26] Mishra, V., 2003, “Indoor air pollution from biomass combustion and acute respiratory illness in preschool age children in Zimbabwe”, International Journal of Epidemiology; 32:847–853, DOI: 10.1093/ije/dyg240.
- [27] Schei, M.A., Hessen, J.O., Smith, K.R., Bruce, N., McCracken, J., and Lopez, V., 2004, “Childhood Asthma and Indoor Woodsmoke from Cooking in Guatemala”, Journal of Exposure Analysis and Environmental Epidemiology 14, S110–S117.
- [28] Dasgupta, S., Huq, M., Khaliquzzaman, M., Pandey, K. and Wheeler D., 2006, “Indoor air quality for poor families: new evidence from Bangladesh” published in Indoor Air; 16: 426–444.
- [29] Smith, K. R., 2002, “Indoor air pollution in developing countries: recommendations for research” published in Indoor Air; 12: 198–207.

- [30] Kilabuko, H., James, Matsuki, Hidieki, and Nakai, Satoshi, 2007, “Air Quality and Acute Respiratory Illness in Biomass Fuel using homes in Bagamoyo, Tanzania”, *Int. J. Environ. Res. Public Health*, 4(1), 39-44.
- [31] Kumar R.,Nagar J., Raj N., Kumar P., Kushwah A., Meena M. and Gaur S.N., 2008, “Impact of Domestic Air Pollution from Cooking Fuel on Respiratory Allergies in Children in India”, *Asian Pacific Journal of Allergy and Immunology*, 26: 213-222.
- [32] Padhi B. and Padhy P., Domestic Fuels, 2008, “Indoor Air Pollution, and Children’s Health, The Case of Rural India”, *Annals of the New York Academy of Sciences*, Volume 1140, Environmental Challenges in the Pacific Basin.
- [33] Gurley, E., Shohel M., Abdullah, S. and Luby, B. S., 2008, “Measuring The Health Effects of A Pilot Indoor Air Pollution Intervention In Bangladesh”, Draft protocol, ICDDR,B study team.
- [34] Kao, H. M., Chang, T.J., Hsieh, Y.F., Wang, C.H., and Hsieh. C.I., 2009, “Comparison of Airflow and Particulate Matter Transport in Multi-Room Buildings for Different Natural Ventilation Patterns”, *Energy and Buildings* 41, 966–974.
- [35] Kumie, A., Emmelin, A., Wahlberg, S., Berhane, Y., Ali, A., Mekonnen, E., Brandstrom, D., 2009, “Magnitude of indoor NO₂ from biomass fuels in rural settings of Ethiopia”, published in *Indoor Air*; 19: 14–21.
- [36] Khalequzzaman, M., Kamijima, M., Sakai, K., Hoque, B. A. and Nakajim, T., 2010, “Indoor air pollution and the health of children in biomass- and fossil-fuel users of Bangladesh situation in two different seasons” published in the *Japanese Society for Hygiene*.
- [37] Adefeso, I., Sonibare, J., Akeredolu, J., and Rabiu, J., 2012, “Environmental Impact of Portable Power Generator on Indoor Air Quality”, *International Conference on Environment, Energy and Biotechnology IPCBEE vol.33*.
- [38] Grabow, K., Still, D, and Bentson, S., 2013, “Test Kitchen Studies of Indoor Air Pollution from Biomass Cook Stoves”, *Energy for Sustainable Development*, Volume 17, Issue 5, Pages 458–462.

- [39] Agarwall S. B., Sukhsohale N. D., Narlawar U. W., Phatak M. S., and Ughade S. N., 2013, “Effect Of Indoor Air Pollution During Cooking On Peak Expiratory Flow Rate And Its Association With Exposure Index In Rural Women”, *Indian J Physiologic Pharmacology*; 57(2) : 184–188.
- [40] Joshi, S., M., “The sick building syndrome”, *Indian Journal of Occupational Environment and Medicine*, 2008, 12(2), pp: 61–64. doi: 10.4103/0019-5278.43262
- [41] Kline, S. J. and McClintock, F. A., 1953, “Describing the uncertainties in single sample experiments”, *Mechanical Engineering*, pages 3–8.
- [42] Birch, K., *Estimating Uncertainties in Testing*, 2003, “An Intermediate Guide to Estimating and Reporting Uncertainty of Measurement in Testing”, British Measurement and Testing Association, March, Teddington, Middlesex, United Kingdom, TW110NQ.

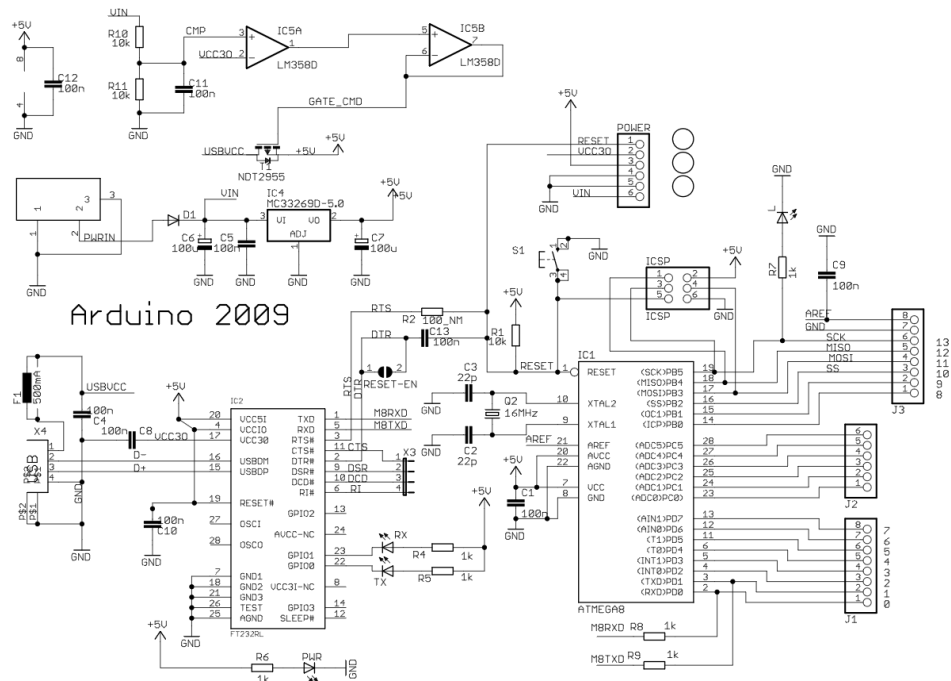
Appendix I

Arduino Microcontroller and Circuit Diagram



Arduino Duemilanove microcontroller board.

*Source: <http://digital.csic.es/bitstream/10261/127788/7/D-c-%20Arduino%20uno.pdf>



Arduino Duemilanove microcontroller Circuit Diagram.

*Source: <http://www.next.gr/meter-counter/thermometer-circuits/index9.html>

Appendix II

Uncertainty analysis

The estimation of the uncertainty of a measurement allows meaningful comparison of equivalent results from different laboratories or within the same laboratory, or comparison of the result with reference values given in specifications or standards. Availability of this information can allow the equivalence of results to be judged by the user and avoid unnecessary repetition of tests if differences are not significant.

The commonly used method for calculating uncertainties in any experiment is given by Kline and McClintock [41]. The total uncertainty propagation for $r = f(v_{j=1...n})$ is expressed in equation 1.

$$u(r) = \sqrt{\sum_{j=1}^n \left[\frac{\partial r}{\partial v_j} u(v_j) \right]^2} \dots\dots\dots (1)$$

Where, u stands for the standard uncertainty, which is equivalent to the standard deviation, and v_j stands for variables that contribute to the uncertainty in the results r that resolves any data reduction equations. A correction factor [42] is to be used to the standard deviation for the number of measurement as per following table.

Correction Factor			
n	k=1	k=2	k=3
3	1.32	2.27	-
4	1.20	1.66	3.07
5	1.14	1.44	2.21
6	1.11	1.33	1.84
7	1.09	1.26	1.63
8	1.08	1.22	1.51
9	1.07	1.19	1.43
10	1.06	1.16	1.36
11	1.05	1.14	1.32
12	1.05	1.13	1.28
13	1.04	1.12	1.25
14	1.04	1.11	1.23

15	1.04	1.10	1.21
16	1.03	1.09	1.20
17	1.03	1.09	1.18
18	1.03	1.08	1.17
19	1.03	1.08	1.16
20	1.03	1.07	1.15

In most instances of reporting the measurement result of a test to a third party an expanded uncertainty at a specified confidence level is quoted, the interpretation is that the true value lies within the confidence interval given by the stated uncertainty and level of confidence. The combined standard uncertainty is therefore multiplied by an appropriate coverage factor. This reflect the confidence level required and, in the majority of cases, the probability distribution of the combined standard uncertainty is assumed to be normal, and that a value of the coverage factor (*k*) defines an interval having a confidence level of approximately 95%.


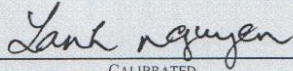
Expanded uncertainty is calculated by combining the coverage factor and standard uncertainty by using the following equation.

$$U = k \cdot u(r) \dots \dots \dots (2)$$

Where *U* is the expanded uncertainty and *k* is the coverage factor.

Appendix III

Calibration Certificate

		<h2 style="margin: 0;">CERTIFICATE OF CALIBRATION</h2> <p style="margin: 0; font-size: small;">TSI Incorporated, 500 Cardigan Road, Shoreview, MN 55126 USA Tel: 1-800-874-2811 1-651-490-2811 Fax: 1-651-490-3824 http://www.tsi.com</p>																																				
<table border="1" style="width: 100%; border-collapse: collapse;"> <tr> <th colspan="3" style="text-align: left; padding: 2px;">ENVIRONMENT CONDITION</th> </tr> <tr> <td style="width: 30%; padding: 2px;">TEMPERATURE</td> <td style="width: 30%; padding: 2px;">73.98 (23.3)</td> <td style="width: 40%; padding: 2px;">°F (°C)</td> </tr> <tr> <td style="padding: 2px;">RELATIVE HUMIDITY</td> <td style="padding: 2px;">53</td> <td style="padding: 2px;">%RH</td> </tr> <tr> <td style="padding: 2px;">BAROMETRIC PRESSURE</td> <td style="padding: 2px;">28.77 (974.3)</td> <td style="padding: 2px;">inHg (hPa)</td> </tr> </table>		ENVIRONMENT CONDITION			TEMPERATURE	73.98 (23.3)	°F (°C)	RELATIVE HUMIDITY	53	%RH	BAROMETRIC PRESSURE	28.77 (974.3)	inHg (hPa)	<table border="1" style="width: 100%; border-collapse: collapse;"> <tr> <td style="width: 50%; padding: 2px;">MODEL</td> <td style="padding: 2px;">9306-V2</td> </tr> <tr> <td style="padding: 2px;">SERIAL NUMBER</td> <td style="padding: 2px;">93061538013</td> </tr> </table>		MODEL	9306-V2	SERIAL NUMBER	93061538013																			
ENVIRONMENT CONDITION																																						
TEMPERATURE	73.98 (23.3)	°F (°C)																																				
RELATIVE HUMIDITY	53	%RH																																				
BAROMETRIC PRESSURE	28.77 (974.3)	inHg (hPa)																																				
MODEL	9306-V2																																					
SERIAL NUMBER	93061538013																																					
<input checked="" type="checkbox"/> AS LEFT <input type="checkbox"/> AS FOUND		<input checked="" type="checkbox"/> IN TOLERANCE <input type="checkbox"/> OUT OF TOLERANCE																																				
AEROtrak CALIBRATION BENCH																																						
<table border="1" style="width: 100%; border-collapse: collapse;"> <thead> <tr> <th style="width: 35%;">MEASUREMENT VARIABLE</th> <th style="width: 15%;">SYSTEM ID</th> <th style="width: 20%;">DATE LAST CALIBRATED</th> <th style="width: 30%;">CALIBRATION DUE DATE</th> </tr> </thead> <tbody> <tr> <td style="text-align: center;">CONCENTRATION</td> <td style="text-align: center;">E003254</td> <td style="text-align: center;">01-09-15</td> <td style="text-align: center;">01-09-16</td> </tr> <tr> <td style="text-align: center;">PARTICLE SIZE</td> <td style="text-align: center;">E003259</td> <td style="text-align: center;">08-10-15</td> <td style="text-align: center;">08-10-16</td> </tr> <tr> <td style="text-align: center;">PARTICLE SIZE</td> <td style="text-align: center;">E003260</td> <td style="text-align: center;">08-10-15</td> <td style="text-align: center;">08-10-16</td> </tr> <tr> <td style="text-align: center;">FLOW</td> <td style="text-align: center;">E003256</td> <td style="text-align: center;">08-05-15</td> <td style="text-align: center;">08-05-16</td> </tr> <tr> <td style="text-align: center;">FLOW</td> <td style="text-align: center;">E003533</td> <td style="text-align: center;">08-05-15</td> <td style="text-align: center;">08-05-16</td> </tr> <tr> <td style="text-align: center;">FLOW</td> <td style="text-align: center;">E002475</td> <td style="text-align: center;">01-09-15</td> <td style="text-align: center;">01-09-16</td> </tr> </tbody> </table>				MEASUREMENT VARIABLE	SYSTEM ID	DATE LAST CALIBRATED	CALIBRATION DUE DATE	CONCENTRATION	E003254	01-09-15	01-09-16	PARTICLE SIZE	E003259	08-10-15	08-10-16	PARTICLE SIZE	E003260	08-10-15	08-10-16	FLOW	E003256	08-05-15	08-05-16	FLOW	E003533	08-05-15	08-05-16	FLOW	E002475	01-09-15	01-09-16							
MEASUREMENT VARIABLE	SYSTEM ID	DATE LAST CALIBRATED	CALIBRATION DUE DATE																																			
CONCENTRATION	E003254	01-09-15	01-09-16																																			
PARTICLE SIZE	E003259	08-10-15	08-10-16																																			
PARTICLE SIZE	E003260	08-10-15	08-10-16																																			
FLOW	E003256	08-05-15	08-05-16																																			
FLOW	E003533	08-05-15	08-05-16																																			
FLOW	E002475	01-09-15	01-09-16																																			
PARTICLE STANDARDS																																						
<table border="1" style="width: 100%; border-collapse: collapse;"> <thead> <tr> <th style="width: 20%;">PARTICLE SIZE</th> <th style="width: 15%;">STANDARD UNCERTAINTY</th> <th style="width: 15%;">STANDARD DEVIATION</th> <th style="width: 15%;">LOT NO.</th> <th style="width: 35%;">EXPIRATION DATE</th> </tr> </thead> <tbody> <tr> <td style="text-align: center;">0.296 µm</td> <td style="text-align: center;">0.003 µm</td> <td style="text-align: center;">0.0053 µm</td> <td style="text-align: center;">41479</td> <td style="text-align: center;">12-31-15</td> </tr> <tr> <td style="text-align: center;">0.498 µm</td> <td style="text-align: center;">0.0045 µm</td> <td style="text-align: center;">0.0079 µm</td> <td style="text-align: center;">41529</td> <td style="text-align: center;">12-31-15</td> </tr> <tr> <td style="text-align: center;">0.994 µm</td> <td style="text-align: center;">0.0075 µm</td> <td style="text-align: center;">0.010 µm</td> <td style="text-align: center;">44399</td> <td style="text-align: center;">03-31-18</td> </tr> <tr> <td style="text-align: center;">3.06 µm</td> <td style="text-align: center;">0.01 µm</td> <td style="text-align: center;">0.030 µm</td> <td style="text-align: center;">42788</td> <td style="text-align: center;">12-31-16</td> </tr> <tr> <td style="text-align: center;">5.02 µm</td> <td style="text-align: center;">0.015 µm</td> <td style="text-align: center;">0.060 µm</td> <td style="text-align: center;">43593</td> <td style="text-align: center;">07-31-17</td> </tr> <tr> <td style="text-align: center;">10.2 µm</td> <td style="text-align: center;">0.95 µm</td> <td style="text-align: center;">0.200 µm</td> <td style="text-align: center;">44466</td> <td style="text-align: center;">04-30-18</td> </tr> </tbody> </table>				PARTICLE SIZE	STANDARD UNCERTAINTY	STANDARD DEVIATION	LOT NO.	EXPIRATION DATE	0.296 µm	0.003 µm	0.0053 µm	41479	12-31-15	0.498 µm	0.0045 µm	0.0079 µm	41529	12-31-15	0.994 µm	0.0075 µm	0.010 µm	44399	03-31-18	3.06 µm	0.01 µm	0.030 µm	42788	12-31-16	5.02 µm	0.015 µm	0.060 µm	43593	07-31-17	10.2 µm	0.95 µm	0.200 µm	44466	04-30-18
PARTICLE SIZE	STANDARD UNCERTAINTY	STANDARD DEVIATION	LOT NO.	EXPIRATION DATE																																		
0.296 µm	0.003 µm	0.0053 µm	41479	12-31-15																																		
0.498 µm	0.0045 µm	0.0079 µm	41529	12-31-15																																		
0.994 µm	0.0075 µm	0.010 µm	44399	03-31-18																																		
3.06 µm	0.01 µm	0.030 µm	42788	12-31-16																																		
5.02 µm	0.015 µm	0.060 µm	43593	07-31-17																																		
10.2 µm	0.95 µm	0.200 µm	44466	04-30-18																																		
<p style="font-size: x-small;">TSI does hereby certify that the calibration performed on the above described instrument meets the requirements of ISO 21501-4. TSI does hereby certify that the above described instrument conforms to the original manufacturer's specification (not applicable to As Found data) and has been calibrated using standards whose accuracies are traceable to the United States National Institute of Standards and Technology (NIST) or has been verified with respect to instrumentation whose accuracy is traceable to NIST, or is derived from accepted values of physical constants. TSI is registered to ISO-9001:2008 and complies with ISO 10012:2003, Quality Assurance Requirements for Measuring Equipment.</p>																																						
 _____ CALIBRATED		September 17, 2015 _____ DATE																																				
<p style="font-size: x-small;">Document Number: CERT_CCAPC_ISO</p>																																						
<p style="font-size: x-small;">Model 9306-V2 SN 93061538013 September 17, 2015</p>			<p style="font-size: x-small;">Page 1 of 2</p>																																			



CERTIFICATE OF CALIBRATION

TSI Incorporated, 500 Cardigan Road, Shoreview, MN 55126 USA
Tel: 1-800-874-2811 1-651-490-2811 Fax: 1-651-490-3824 http://www.tsi.com

SIZE CALIBRATION AND VERIFICATION OF SIZE SETTING

NOMINAL PARTICLE SIZE	GAIN STAGE	DIGITAL CUTPOINT	EXPANDED UNCERTAINTY
0.3 μm	A	19	3.9%
0.5 μm	A	304	3.9%
1 μm	B	6	3.9%
3 μm	B	68	3.8%
5 μm	B	166	3.8%
10 μm	B	543	3.8%

COUNTING EFFICIENCY

PARTICLE SIZE	ACTUAL	ALLOWABLE RANGE	PASS/FAIL
0.3 μm	52%	50% \pm 10	Pass
1.0 μm	90%	100% \pm 10	Pass

SIZE RESOLUTION

PARTICLE SIZE	MEASURED	ALLOWABLE RANGE	PASS/FAIL
0.5 μm	7.3%	\leq 15 %	Pass

FALSE COUNT RATE

SAMPLE TIME (MIN)	SAMPLED (L)	MEASURED COUNTS (#)	CONCENTRATION ($\#/M^3$)	95% UCL ($\#/M^3$)	ALLOWABLE RANGE ($\#/M^3$)	PASS/FAIL
15	42	0	0.00	71.2	\leq 71.2	Pass

SAMPLING FLOW RATE (L/MIN)

NOMINAL	ACTUAL	ERROR	ALLOWABLE RANGE	PASS/FAIL
2.83	2.81	-0.7 %	\pm 5%	Pass

SAMPLING TIME ACCURACY †

MEASURED	ALLOWABLE RANGE	PASS/FAIL
$< \pm$ 0.1%	\pm 1%	Pass

RESPONSE RATE †

MEASURED	ALLOWABLE RANGE	PASS/FAIL
0.08 %	\leq 0.5%	Pass

MAXIMUM PARTICLE CONCENTRATION †

210000000 $\#/m^3$ @10% Coincidence Loss
--

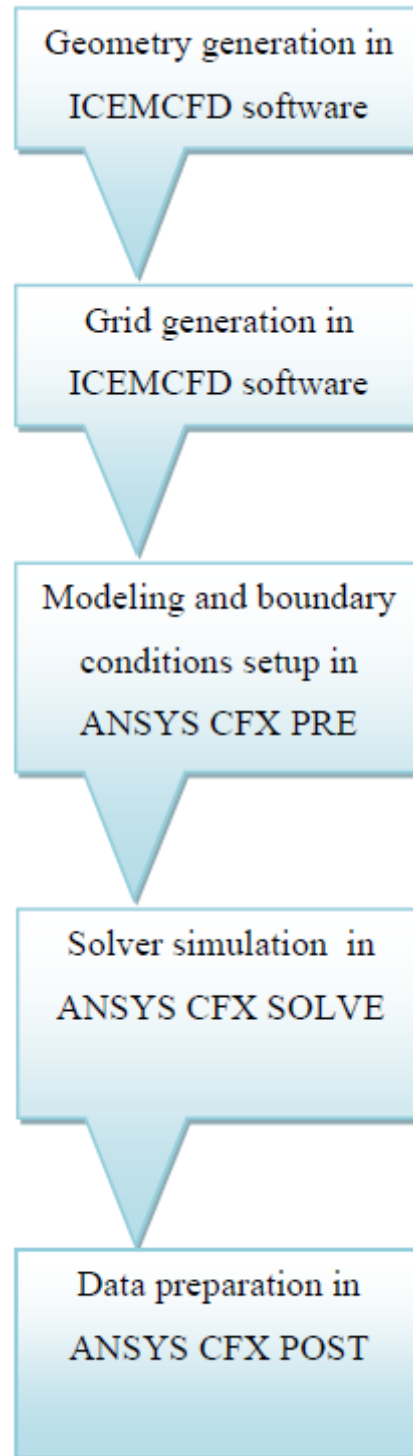
† Tested and verified during product development

CALIBRATION INTERVAL

CALIBRATION DATE	EXPIRATION DATE
September 17, 2015	September 17, 2016

Appendix IV

Simulation Process Flow Diagram



Appendix V

Typical Analysis of Biomass

Typical analysis of Rice Husk

Property	Range
Bulk density (kg/m ³)	96-160
Hardness(Mohr's scale)	5-6
Ash,%	22-29
Carbon, %	≈ 35
Hydrogen,%	4-5
Oxygen,%	31-37
Nitrogen,%	0.23-0.32
Sulphur,%	0.04-0.08
Moisture	8-9
Heating Value	7.07 MJ/Kg

*Source: "Properties and Industrial Applications of Rice husk: A review" International Journal of Emerging Technology and Advanced Engineering, ISSN 2250-2459, Volume 2, Issue 10, October 2012.

<http://www.ces.iisc.ernet.in/energy/paper/alternative/calorific.html>

Typical analysis of Cow Dung

Property	Range
Nitrogen (N)	0.27%
Ammonia Nitrogen	0.14%
Organic Nitrogen	0.13%
Phosphorus (P)	0.04%
Phosphate Equivalent (P205)	0.09%
Potassium (K)	0.18%
Potash Equivalent (K20)	0.22%
Total Solids	5.71%
Density	0.99 kg/l
Heating Value	7.65 MJ/Kg

*Source:

http://dairyone.com/wp-content/uploads/2013/11/Manure_Analysis_Report_Example.pdf

<http://www.ces.iisc.ernet.in/energy/paper/alternative/calorific.html>

Typical analysis of Firewood

Property	Range
Carbon	50%
Oxygen	44%
Hydrogen	06%
Higher Heating Value	18.86 MJ/kg

*Source: http://ecen.com/eee57/eee57e/carbon_content_in_biomass_fuel.htm

Appendix VI

List of Published Papers

Journals:

- [1] M. Hamidur Rahman, A.K.M. Sadrul Islam , "*Effects of the Position of Kitchen Hood Suction on thermal Comfort and Carbon Dioxide Gas Emission from an Urban Residential Kitchen in Developing Countries*", Applied Mechanics and Materials Vol. 819 (2016) pp 117-121 © (2016) Trans Tech Publications, Switzerland. DOI: 10.4028/www.scientific.net/AMM.819.117.
- [2] M. Hamidur Rahman, A. K. M. Sadrul Islam and M. Ruhul Amin, "*Numerical Study of Carbon Dioxide Gas Emission From an Urban Residential Kitchen In Developing Countries*" published in the Journal of Thermal Science and Engineering Applications, a transaction of ASME, Vol:07, Issue:04, June 2015.

Conferences:

- [1] M. Hamidur Rahman, A. K. M. Sadrul Islam and M. Ruhul Amin,, "*Numerical Study of CO and CO₂ Emissions from Rural Kitchen in Developing Countries*" published in the proceedings of ASME 2015 International Mechanical Engineering Congress & Exposition, November 13-19, 2015, Houston, Texas, USA.
- [2] M. Hamidur Rahman, A. K. M. Sadrul Islam and M. Ruhul Amin,, "*Effects of Kitchen Hood System on Thermal Comfort and Carbon Dioxide Gas Emission from an Urban Residential Kitchen in Developing Countries*" published in the proceedings of International Mechanical Engineering Congress & Exposition, November 14-20, 2014, Montreal, Canada.

- [3] M. Hamidur Rahman, A. K. M. Sadrul Islam and M. Ruhul Amin,, “*Numerical Study of Carbon Dioxide Gas Emission From an Urban Residential Kitchen In Developing Countries*” published in the proceedings of ASME 2012 International Mechanical Engineering Congress & Exposition, November 9-15, 2012, Houston, Texas, USA.
- [4] M. Hamidur Rahman, A.K.M. Sadrul Islam, “*CFD Modeling of Natural and Forced Ventilation System in a Conventional Kitchen in Bangladesh*” published in the 13th Asian Congress of Fluid Mechanics, 17-21 December, 2010, Dhaka, Bangladesh.